Interdiffusion along grain boundaries – Diffusion Induced Grain Boundary Migration, low temperature homogenization and reactions in nanostructured thin films

D.L. Beke, Yu. Kaganovskii, G.L. Katona

PII: S0079-6425(18)30069-0
DOI: https://doi.org/10.1016/j.pmatsci.2018.07.001
Reference: JPMS 523

To appear in: *Progress in Materials Science*

Received Date: 16 January 2018
Revised Date: 21 June 2018
Accepted Date: 1 July 2018

Please cite this article as: Beke, D.L., Kaganovskii, Yu., Katona, G.L., Interdiffusion along grain boundaries – Diffusion Induced Grain Boundary Migration, low temperature homogenization and reactions in nanostructured thin films, *Progress in Materials Science* (2018), doi: https://doi.org/10.1016/j.pmatsci.2018.07.001

Interdiffusion along grain boundaries – Diffusion Induced Grain Boundary Migration, low temperature homogenization and reactions in nanostructured thin films

D. L. Beke[a], *Yu. Kaganovskii*[b], *G. L. Katona*[a]

[a]*Department of Solid State Physics, University of Debrecen, H-4002, Debrecen, P.O.Box 400, Hungary*

[b] *Department of Physics, Bar-Ilan University, Ramat-Gan 52900, Israel*

Abstract

Interdiffusion along grain boundaries can lead to shift of grain boundaries in form of Grain Boundary Diffusion Induced Grain Boundary Migration, DIGM, in systems forming wide range solid solutions, and to the Grain Boundary Diffusion Induced Solid State Reactions, in systems containing intermetallic phases. If, during above processes, the grain size of the sample is smaller than the double of the migration distance complete homogenization can also be reached (cold homogenization). Atomic mechanisms and phenomenological description of such alloying are reviewed. The main driving force, at low temperatures where the bulk diffusion is completely frozen out, arises from the unequality of the grain boundary atomic fluxes, leading to stress accumulations. The cold homogenization is the manifestation of such stress relaxations. Reviewing experimental data, we illustrate that DIGM takes place on both sides of a binary AB thin film and the solute content in the DIGM zone is higher on the side of the component of higher melting point (i.e. in the slower component). In binary systems containing intermetallic compounds the cold homogenization can lead, either to the formation of a given stoichiometric compound, or to two phase equilibrium, in

accordance with the phase diagram. Different possible applications are likewise surveyed.

Contents

1. Introduction

Diffusion induced grain boundary migration, DIGM, which was discovered and identified in 1972 by den Broeder [1], happens if interdiffusion of two chemically different species along a grain boundary, GB, induces a transverse shift of the GB. This effect is observed at temperatures typically below 0.5 T_m (T_m is the melting temperature in Kelvin). A common example of DIGM is seen if e.g. a polycrystalline thin film is heat treated in a vapor of an another element and the vapor atoms diffuse into the GB faster than the out diffusion of the atoms of the film. Fig. 1.1a illustrates schematically the basic phenomenon in a binary system [2].

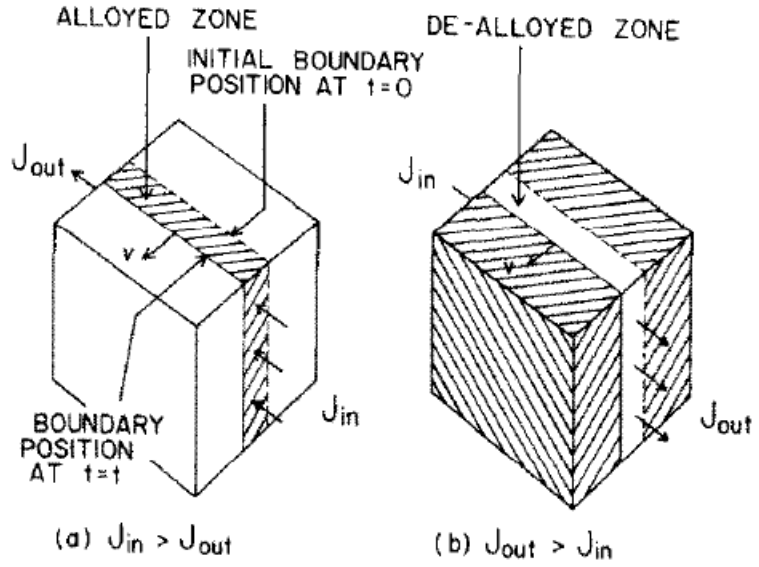

Fig.1.1 DIGM schematically [1]: a) solute atoms diffuse into the GB of a pure thin film or b) solute atoms diffuse out of the GB of an originally alloyed film. The GB motion leads to the formation of an alloyed or de-alloyed zone in its wake (see also the text).

The perpendicular GB motion is usually not uniform along the boundary and different segments can move even opposite directions forming bulges on both sides (Fig. 1.2. [3]). In addition the volume swept by the moving boundary has ~~a~~ significantly

different composition; in case a) of Fig. 1.1 alloying of the originally pure film happens (enrichment by the solute), while in case b) the swept area is depleted with the solute element (de-alloying): see also the corresponding chapters of recent handbooks [4][5]. In thicker polycrystalline samples (in contrast to the schematic picture shown in Fig. 1.1) GBs migrate only in the regions close to the initial surface (the exposed thickness obviously depends on the penetration depth of the GB diffusion) and the deeper regions remain unchanged (Fig. 1.3). It turned out that similar phenomena can be observed not only in metallic, but in a number of oxide systems (see e.g. the reviews [6][7][8]) and in semiconductors [9] too. In addition to DIGM an interesting phenomenon, the so called Diffusion Induced Recrystallization, DIR, was also observed already in the very early time of DIGM [1][10][11][12]: nucleation of entirely new grains at the GBs, with a characteristic, increased and homogeneous solute content. These observations, already just after the recognition of the above effects (see also Section 2 below), evoked ideas for practical applications, such as surface alloying/dealloying or even production of homogeneous reaction products in nanocrystalline thin film couples [13][14][15][16][17][18] [19][20][21]. In this review we restrict ourselves to DIGM in metallic systems.

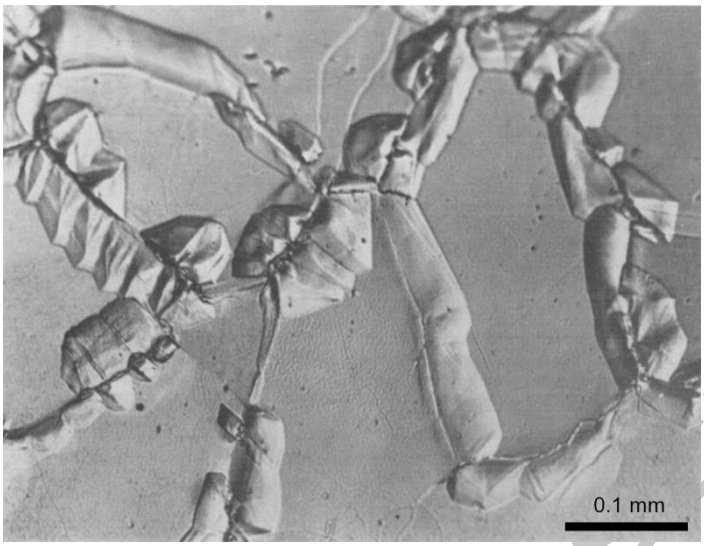

Fig. 1.2 Optical micrograph illustrating the surface relief that accompanies the zincificacion of an iron foil, heated in Zn vapour for 4 h at 600 C^{o} [3]. Interference contrast, x700.

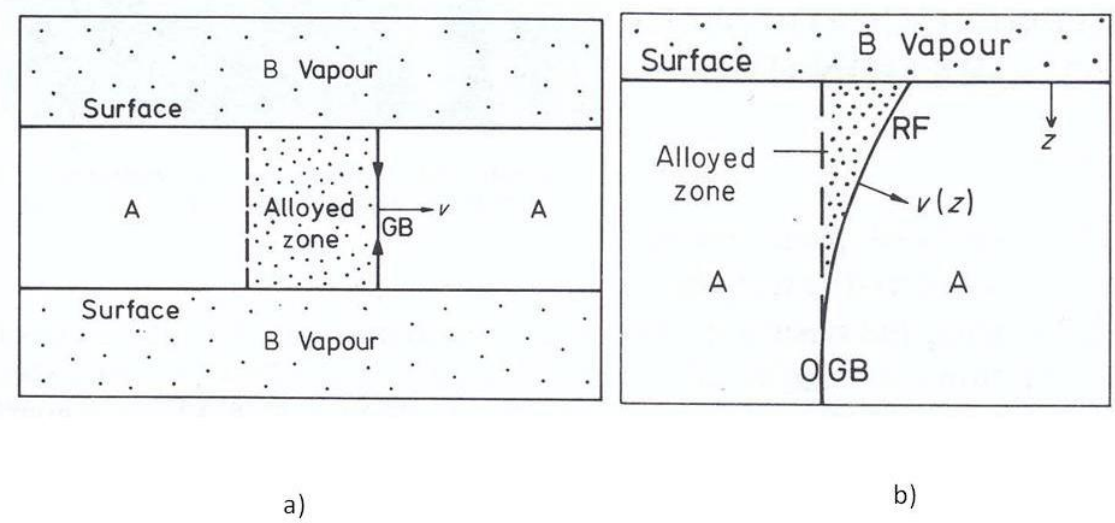

Fig. 1.3 Schematic diagram illustrating DIGM in thin (a) and thick specimens, respectively [22].

As we will see in the next chapters, especially after the well devised experiment by Hillert and Purdy [3] in 1978, a huge number of publications appeared and widened our knowledge on different varieties of possible effects all evoked by the interdiffusion

along the GBs. The central question, which has been put about DIGM was the following: why does it occur at all (see e.g. [6] [23])? As we will see below the main effect is the relaxation of diffusion induced stresses. First, one has to make a clear distinction between the cases when the bulk diffusion is completely frozen out (this is the main subject of this review) and when some bulk penetration of the diffusing atoms into the bulk just ahead of the moving boundary can happen. In the latter case the original idea of Hillert [24] provides the basic of the widely used coherency strain model ([6][16]); the bulk penetration of the solute first creates an alloyed, coherent zone near the GB. Since, either the sizes of the solute and matrix atoms are different or the bulk diffusion coefficient of the solute differs from that of the matrix (related also to the bulk Kirkendall effect, see also Chapter 3) there is an accumulation of bulk diffusion induced ~~stress free~~ strain (the diffused in zone is constrained to the large unalloyed part). It is quite widely accepted that this coherency stain energy is the dominant contribution to the driving force for DIGM at relatively high temperatures where some bulk penetration happens [6][25]. The relaxation of the above diffusion induced stresses can happen in different ways: i) the boundary shifts (DIGM), ii) if the stress (related to the induced stain) is high enough, then the coherency can be lost and even new grains (with different compositions than the original matrix) can nucleate [26], i.e. diffusion induced recrystallization, DIR, takes place. There are numerous papers in the literature, which treat different details of the above relaxations or discuss additional driving forces, other than originating from the coherency strain (see also the Chapters 2 and 5), and of course the role of the GB structure [6][16][17][25]. If the bulk diffusion is completely frozen out, the stress caused by the GB diffusion induced strain (in the GB layer) can relax only by the shift of the boundary and thus at low temperatures mainly this is what has been observed [27]. In this case the situation is very similar to the bulk

interdiffusion [28][29]: if the resultant volume flow $\Omega_A J_A - V_A J_A$ is not zero in a binary diffusion couple (i.e. if the $\Omega_i D_i$ products are different see e.g. Eq. (60) in [28]), a diffusion induced strain is created, which can be relaxed by the classical Kirkendall shift (Ω_i and J_i are the atomic volumes and atomic fluxes: $J_i = -D_i \mathrm{grad}\rho_i$, respectively and D_i and ρ_i denote the intrinsic diffusion coefficient as well as the density). The main difference is that while this shift is parallel with the direction of the atomic fluxes, in case of GB interdiffusion the shift is perpendicular to the GB along which the interdiffusion takes place (see Chapter 3). Once more, if the grain size of the sample is smaller than the double of the migration distance complete homogenization can also be reached (cold homogenization) [21].

The organization of this review is as follows. After summarizing the most important historical milestones of the grain boundary interdiffusion (Chapter 2), we provide general, phenomenological description of DIGM at low temperatures (Chapter 3). In Chapter 4 the possible atomic mechanism of this low temperature DIGM will be described, while in Chapters 5 and 6 we will shortly summarize the features of high temperature DIGM and DIR. Chapter 7 describes the temperature dependence of DIGM, i.e. the transition between the low and high temperature regimes. In Chapter 8 it will be treated what happens when instead of a solid solution, for which most of the present theories apply, intermetallic compounds form at low temperatures. We will name this as grain boundary diffusion induced solid state reaction, GBDIREAC. Chapter 9 provides a review of experimental data. Again the primary emphasis will be given to GB interdiffusion at low temperatures. In Chapter 10 the possible applications will be reviewed. The main points addressed are: cold homogenizations of thin films (i.e. when the GB migration distance is larger than the half of the grain size) and

whether during cold homogenization with GBDIREAC the system can reach the equilibrium (two- or multiphase) state dictated by the equilibrium phase diagram or not. Different possible applications (lead free soldering at low temperatures, nanoscale metallization, thin films for perpendicular magnetic data recording, nanoscale sintering) will be also considered. Chapter 11 contains the unsolved questions.

2. Historical perspective

First of all, it is worth mentioning that, before the DIGM was recognized, it was a common view that e.g. surface alloying in polycrystalline materials can happen by a combination of bulk and GB diffusion in the so called A-regime of GB diffusion [30] (see Fig. 2.1, after Fig. 7 in [31]). In this case, besides the diffusion along standing GBs, there is a considerable penetration into the adjoining grains and if the bulk diffusion penetration distance is larger than the half of grain size then an alloyed zone can be formed in the surface layer. Only this model failed to explain the orders of magnitude higher bulk diffusion coefficients obtained, than those extrapolated from volume diffusion data in single crystals at high temperatures. Thus it turned out that such an alloying or de-alloying of polycrystalline materials could have occurred only by combination of GB interdiffusion and GB migration, i.e. by DIGM.

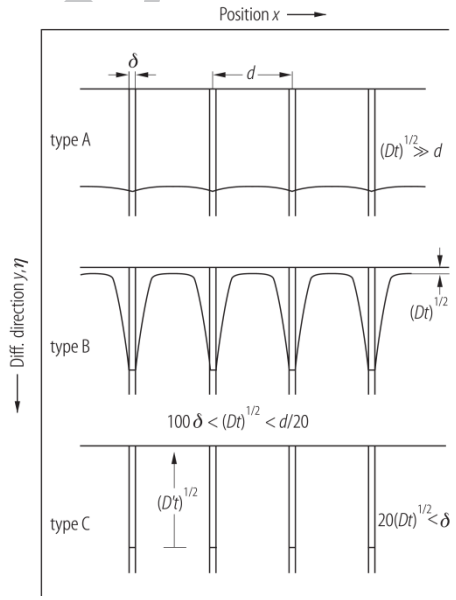

Fig. 2.1 Three types of GB diffusion regimes after Harrison [30]: d and δ are the grain size and the GB width, respectively, and $(D't)^{1/2}$ is the bulk penetration distance (D' is the volume diffusion coefficient and t is the annealing time) [31].

Most probably the first observation of such GB migration was published by Rhines and Montgomery in 1938 [32] during the Zn diffusion into a Cu bicrystal,. The next pioneering papers, from practically independent observations of the groups, are by den Broeder in 1972 [1], Tu in 1977 [33], Hillert and Purdy in 1978 [3] and Cahn et al. in 1979 [34]. In addition DIGM was identified in solid-liquid mixtures by Yoon and Huppmann in 1979 [35]. As it was already mentioned in the introduction, in the paper by Hillert and Purdy [3] the essential experimental features of DIGM were established and the authors also pointed out the close relation of this phenomenon to discontinuous precipitation. Following the above mentioned observations a large interest in DIGM has been developed and many communications were published on new experimental results and on the possible driving forces.

Regarding the possible driving forces, the suggestion by Hillert [24] on the coherency strain energy in the solute diffusion zone ahead of the moving GB evoked the largest interest. This idea, in fact, was based on the initial proposal of Sulonen for discontinuous precipitation [36]. Hillert [24] found that the driving force per unit area of GB in an elastically isotropic material is given by (in notations used in [37])

$$\Delta G_m = \frac{E\eta^2(c'_- - c'_+)^2}{(1-\nu)}, \qquad (2.1)$$

where E is the Young modulus, ν is the Poisson ratio, η is the misfit parameter (relative change in lattice spacing per unit change in solute mole fraction) and c'_+, c'_- are the solute mole fractions in the bulk well in front of and well behind the GB (see also [37]). Although the elastic driving force arises from elastic stresses it is not an elastic force in the usual sense [37]. It was already mentioned by Hillert [24], that the actual coherency strain energy itself is not too high, but the driving force, which has also a chemical nature via the bulk intermixing, can be considerable (see also Chapter 5.2 too). In 2004

Penrose [37] has provided a complete and elaborate description (in term of the elastic energy-momentum tensor in general anisotropic solid: see also Chapter 5.2) and has shown that the relation (2.1) is still valid when c'_+ and c'_- are not small (as was originally assumed by Hillert) and has given a generalized formula for $Y=E/(1-\nu)$, valid for anisotropic solids. Furthermore, he made predictions on the direction of motion of the GBs, in accordance with the qualitative description of Sutton and Balluffi [23]; the solute atoms initially diffused into the GB begin to penetrate into the two adjoining crystals and if the boundary layer is asymmetric the GB will be driven to move toward the crystal with the higher strain energy in order to consume it. An another contribution to this type of shift can be the stress relaxation by plastic flow on one side of the GB [25]: the formed dislocations take up the lattice parameter change between the enriched and original regions. Indeed, such dislocation arrays were observed [3][38] (Fig. 2.2). There is a key parameter [25] [37] in the coherency strain energy model: D'/v, where D' is the bulk diffusion coefficient and v is the GB velocity. It is required that the length scale for composition variation and elastic deformation must be larger than the thickness, δ, of the boundary:

$$D' / v \gg \delta. \tag{2.2}$$

It is important to emphasize that at low temperatures this condition does not fulfills (i.e. there is practically no bulk diffusion penetration), but some of the experimental results indicated that DIGM still occurred [6][39]. The most probable resolution of this contradiction, although there are other propositions in the literature for it (either noting that the continuum models are not able to include some diffusion along the outer layers of both grains, carrying enough solute [25], or the continuum models naturally should not be accurate along bulk diffusion distances comparable with the lattice spacing [39][40]), is the idea proposed by Cahn et al. in 1979 [34] and, in a more elaborated

form by Balluffi and Cahn in 1981 [2]; there exists a shift of the GB without bulk penetration.

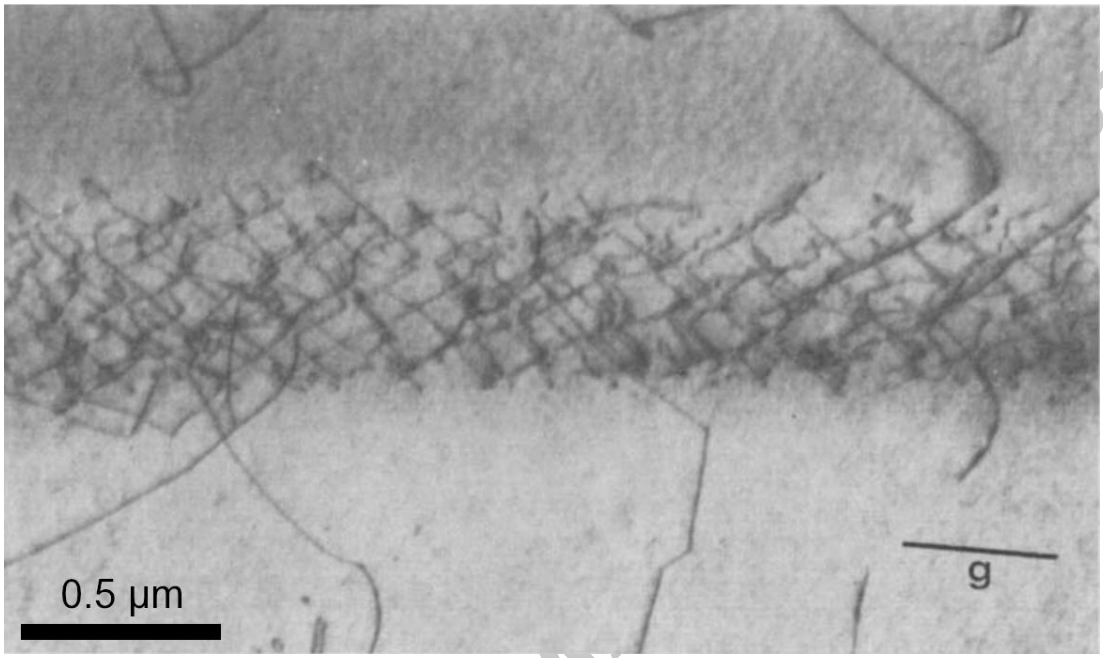

Fig. 2.2 Dislocation array left behind the moving boundary (after Hillert and Purdy [3], x3500)

In [2] the authors not only gave a plausible explanation on the driving force, but also offered an atomistic mechanism for the GB migration if the bulk diffusion is frozen out. The principal idea is the difference of the GB diffusivities of the elements in binary systems. This is really similar to the bulk interdiffusion by vacancy mechanism: the inequality of the diffusion coefficients (and therefore the opposite atomic fluxes) leads to Kirkendall shift (*parallel* with the diffusion direction). Although it was not emphasized in [2], in general the Kirkendall shift (in the form of GB shift) can be seen as a way of relaxation of diffusion induced strains, grown by the GB interdiffusion itself. In fact the Darken description of the bulk interdiffusion is based on the presumption that the stress relaxation by lattice shift is complete and fast enough [29]. So a similar macroscopic treatment of GB interdiffusion is possible if one takes into

account that in the GB case the diffusion induced strain can be relaxed by the shift of the boundary (*perpendicular* to the GB plane: see Chapter 3 below). Balluffi and Cahn [2] (and also Smith and King [41], which was published at the same time) rather concentrated on the atomic mechanism of the GB shift: the GB dislocation, present in the GBs, can be sinks of extra atoms arriving in, due to the inequality of the atomic fluxes of the solute and matrix atoms. This causes a climb of these GB dislocations along the GB and the GB steps, belonging to these GB dislocations, will be shifted, resulting in displacement of the GB perpendicular to the boundary plane.

So interestingly, both high and low temperature limits of DIGM are related to elastic stresses accumulated by the diffusion mixing itself (i.e. created either by the unequal diffusion fluxes or by the difference of the atomic volumes or by both [29]), and to their relaxations. The ways of stress relaxations, besides the main effects (i.e. the shift of the boundary and alloying), can be much diversified. Indeed there are many experimental indications that in both cases the relaxation of these stresses can also cause additional spectacular effects: formation of dislocations (see Fig. 2.2), micro-twinning (see Fig. 2.3) [27], stacking faults by vacancy deposition during DIGM [42], nanopore formation along GB triple junctions [43], expansion of volume elements perpendicular to the boundary plane (edge formation) [44], surface relief formation and shape change [45], faceting of the migrating GBs [46] (see Fig. 2.4), etc. It is also worth mentioning, confirming some indications in the literature [17], that the role of the inequality of the bulk atomic currents can have also a contribution to the DIGM at high temperatures, where the role of bulk diffusion is important.

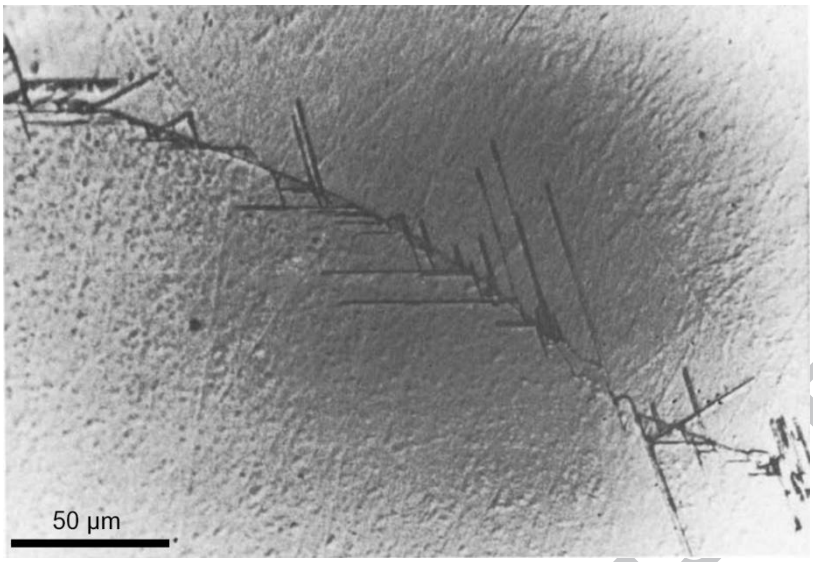

Fig. 2.3 Micro-twinning at grain boundaries of $Cu_{95}Zn_5$/Cu after 120h at 300^{o}C (x400) [27].

It is interesting that a deeper understanding and explanation of DIR came into existence only in 2010 [26]. Before this, in many reviews on the topic (see e.g. [6] [25]), open questions related first of all to the driving force and nucleation were emphasized, although the role of the coherency strain in the region ahead of the GB was accepted as one of the important factors [6]. The breakthrough was achieved by the paper of Schmitz et al. [26]. It was shown in [26] that if the (bulk) diffusion induced stress exceeded 70% of the critical maximum shear strength of the matrix then a break of coherency happened and on the basis of this thermoelastic model (taking into account the size mismatch of the solute and matrix atoms) predictions on whether DIR can be expected or not and also on the characteristic solute content levels were given (see also Chapter 6).

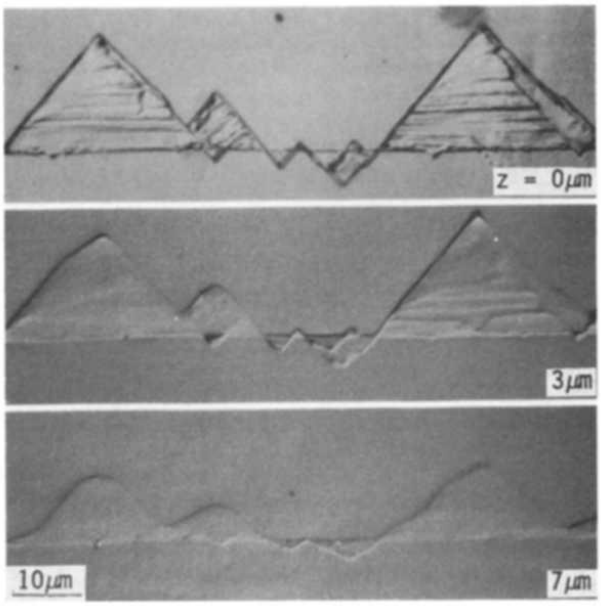

Fig. 2.4 DIGM of asymmetric Σ19a{133} tilt boundary exhibiting facets (Zn diffusion into Cu bicrystal [46]). *z* is a coordinate measured from the free surface.

Ultimately, it has to be noted that investigations of the so called cold homogenization by DIGM [21] (i.e. when the GB migration distance is larger than the half of the grain size in nanocrystalline bilayers or multilayers and the bulk diffusion is frozen out) became the most actively studied area in the last two decades [20][47][48]. The key issues here are the following: i) what about the GB velocity (is it constant or has time dependence leading to termination of the GB shift), ii) what are the compositions in the DIGM zone on both sides of the bilayered nanocrystalline films and how they depend on the temperature, iii) in case of reactive diffusion (GBDIREAC) the terminal state of the initially pure A/B nanocrystalline film is in accordance with the equilibrium phase diagram or not? These questions will be treated in Chapters 3, 8, 9 and 10.

3. Phenomenological description of interdiffusion along grain boundaries in binary systems, if the bulk diffusion is completely frozen out

There is a long standing debate in the literature about the description of the grain boundary (GB) interdiffusion itself [2][44][45][49][50]. This can be contrasted with the two clear extremes of bulk interdiffusion. For bulk diffusion the Darken 's limit with the Kirkendall-shift (as a way of easy and complete relaxation of diffusion induced stresses, equalizing the initially different intrinsic fluxes of the two components) as well as the Nernst-Planck limit (where the gradients of diffusion stresses equalize the initial fluxes) [29] are the two limits with interdiffusion coefficients $D_D^{'} = c_A^{'} D_B^{'} + c_B^{'} D_A^{'}$ and $D_{NP}^{'} = D_A^{'} D_B^{'} / (c_A D_A^{'} + c_B^{'} D_B^{'})$, respectively [29] [28] [51] ($c_A^{'}$ and $c_B^{'}$ are the atomic fractions in the bulk).

During GB interdiffusion in a binary, approximately ideal, system the unequality of the two intrinsic GB diffusion coefficients and the atomic sizes lead to an imbalance in the GB "volume" transport (i.e. $\Omega_A J_A \neq \Omega_A J_A$) and a non-uniform stress free strain [28] developes which can create deposition/removal of atoms ~~in the boundary plane~~ even if the bulk diffusion is completely frozen out [2]; this is what we will assume below. This stress free, or diffusion induced, strain is equvivalent to a diffusion stress and can also lead to the shift of the boundary perpendicular to the GB plane, leading to DIGM (we use the note "stress free strain" in the sense as it was introduced by Stephenson [28]). We emphasize again that at low temperatures where the bulk diffusion is frozen out, the driving force for such migration cannot originate from the well-known coherency strain produced by bulk penetration ahead of the moving boundary, but definitely the above mentioned difference of the GB fluxes plays the determining role. At the same time not only the shift of the boundary can happen, but – as a manifestion of another ways of

stress relaxation – surface relief and GB wedges of extra atoms can form [18][44], GB Kirkendall porosity formation can appear [43] and the stress accumulation can also slow down the boundary motion [45].

In the literature typically the following two limits are discussed:

a) The GB velocity and the composition left behind the sweeping boundary is estimated neglecting the stress accumulation [2] [50].

b) Assuming that the boundary does not move and after a transient period the stress gradients will cease the difference between the fluxes. Hence the diffusion induced deformations and the concentration distributions can be estimated [44][45][49].

For instance in their classical work Balluffi and Cahn [2] developed a model (analogous to bulk interdiffusion of Darken-type) giving an atomistic interpretation of the boundary shift: the difference of the diffusion fluxes cause a self-sustaining climb of GB dislocations and motion of the corresponding GB steps (see also Fig. 3.2 below). This can be compared with the climb of bulk dislocations by annihilation of vacancies leading to bulk Kirkendall-shift. On the other hand, assuming immobile GBs, the stress/deformation fields and the composition distributions were calculated in [44] and [45].

It is important to note that in both above limits some problems arise related to the meaning of the GB interdiffusion coefficient. Shewmon [45] mentioned that "presumably Darken equation should be valid", and indeed such type of relation was suggested in [50], while in [44] the authors argued that although their model was analogous to the bulk Nernst-Planck regime, their calculated composition profiles did not confirm that the slowest component gave the main contribution to the GB interdiffusion coefficient.

The following parts of this section contain a unified, general phenomenological description of the problem assuming that removal or deposition of atoms (i.e. relaxation of diffusion induced stresses) can happen at GB steps, leading to GB shift and thus to DIGM.

3.1. Basic equations and relations in solid solution forming binary systems

3.1.1. Free standing thin B film in A vapor (the GB diffusion of A is faster than B)

Let us consider first the behaviour of a single grain boundary of δ width in free standing pure B film of h thickness during diffusion of A atoms from vapor sources on both sides (Fig. 3.1).

3.1.1.1. Flux equations and conservation of mass

The GB fluxes of the two species, J_A and J_B, along the direction y (in units of atoms per unit time and unit length: the line along which this unit length is taken is perpendicular to the plane shown in Fig.3.1), are given by the following expressions at the beginning:

$$J_A = -\frac{D_A \delta}{\Omega}\frac{\partial c_A}{\partial y}, \qquad J_B = -\frac{D_B \delta}{\Omega}\frac{\partial c_B}{\partial y}, \tag{3.1}$$

where $\Omega_A \approx \Omega_B = \Omega$ is the atomic volume (i.e. we neglect the size difference of the atoms), c_A and c_B are the atomic fractions of A and B atoms in the boundary. D_A and D_B are the intrinsic diffusion coefficients [4][5], (for the sake of simplicity we assume that the GB thermodynamic factor is unity i.e. we consider an approximately ideal system).

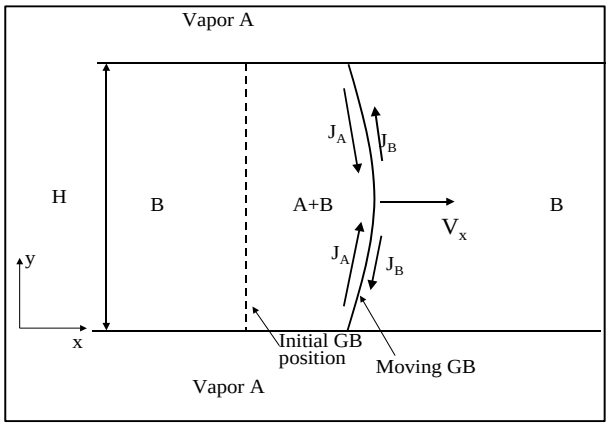

Fig. 3.1 Scheme of the GB interdiffusion process: material A diffuses into the GB of pure B from the gas phase.

Permit us now look into what happens when the diffusion is switched on. Since $D_A > D_B$, and $J_A > J_B$, accumulation/deposition of atoms takes place (more A atoms arrive in than B atoms step out from the GB) and a stress field develops normal to the boundary [44][45][49]. Accordingly equations of (3.1) should be corrected with the terms proportional to the stress gradient (see also [44])

$$J_A = -\frac{D_A \delta}{\Omega}\frac{\partial c_A}{\partial y} - \frac{D_A c_A \delta}{\mathrm{k}T}\frac{\partial \sigma}{\partial y}, \qquad J_B = -\frac{D_B \delta}{\Omega}\frac{\partial c_B}{\partial y} - \frac{D_B c_B \delta}{\mathrm{k}T}\frac{\partial \sigma}{\partial y}. \tag{3.2}$$

Here kT has its usual meaning. σ is the normal traction on the boundary at y and the form of the second terms in (3.2) originate from the additional term in the chemical potential $\Delta\mu = \sigma\Omega$ [52] (see also e.g. [53] and [54]) and if the syetem is not ideal the thermodynamic factor should appear in the denominator of the second term [4][55]. Furthermore, assuming that the stresses can relax, at least partly, by the motion of the boundary along the direction x with v_x velocity, the condition of mass conservation for both components can be written in the form;

$$\frac{\partial c_A}{\partial t} = -\frac{\Omega}{\delta}\frac{\partial J_A}{\partial y} - \frac{v_x}{\delta} q_A c_A, \qquad \frac{\partial c_B}{\partial t} = -\frac{\Omega}{\delta}\frac{\partial J_B}{\partial y} - \frac{v_x}{\delta} q_B c_B. \tag{3.3}$$

The second term in these expressions takes into account the relaxation of stresses by the boundary shift and the interchange of atoms between the bulk and the GB during its motion. The atomic fractions in the boundary and in the bulk (c_A and c'_A respectively) are obviously interrelated: this is taken into account by the q_i *(i=A,B)* factors (see below). It is also worth noting that in the following – in accordance with the original idea of Baluffi and Cahn [2] (see in details below) or also in accordance with the treatment of [44] – we assume that the sum of atomic fractions in the GB is constant (i.e. $\frac{\partial(c_A+c_B)}{\partial t}=0$) and the ability of the GB to incorporate additional (incoming atoms) is simply taken into account by the volume change.

If only the segregation would be important, then $q_A = c'_A/c_A = 1/s$ where s is the segregation factor. Consideration of the segregation effects is not a trivial task (see e.g. [56] [57]), due to the fact that it is difficult to establish the segregation equilibrium during the stop and go motion of the boundary [58] and the effective segregation coefficient can be even orders of magnitude less than the equilibrium one [57][58]. This is why we – as a first approximation – neglect the classical segregation effects here. On the other hand, one also has to take into account that in any atomic picture, with simultaneous deposition (or removal) of atoms during the GB shift, the transferred part from one bank of the GB (to its other bank) contains not only the *A* atoms diffused in and deposited into the boundary. This means that in the area left behind the moving boundary the bulk composition, c'_A, will be different from the GB composition, c_A. Thus, for a complete description one needs the knowledge of $q_A(c'_A,c_A)$ (see below).

It is worth mentioning that equations (3.3) differ from (A1) and (A2) of [50] where q_i=1 was taken and there was a factor of 2 in the second terms, because it was assumed that the extra atoms are deposited at *both* banks of the GB, with composition

equal to the GB value. Furthermore, our equations are also different from the equations given in [44] (see Eq. (4a) there), where it was assumed that the GB is immobile, and the rate of formation of a wedge of extra atoms appears in the second terms instead of v_x, and the diffusion induced stress gradients were not neglected. In fact we assume here that the GB shift in (3.3) is a consequence of the stress relaxation (in analogy with the bulk Kirkendall-shift in the Darken regime) and – in accordance with experimental observations – it happens in one direction, but the sign of this can be either positive or negative and randomly distributed along the GB plane (depending on the distribution of GB steps: see also below).

Now we can consider the following limits after a certain transient period:

a) The GB fluxes are equalized by corrections due to the stress gradients (see the second terms in (3.2)) - assuming that the GB does not move, i.e. v_x=0: Nernst-Planck-type limit.

b) The relaxation of stresses is realized via the shift of the boundary and (if this relaxation is fast and efficient enough) one can neglect the second terms in (3.2). This is the Darken-type limit.

3.1.1.2. Nernst-Planck limit

In this limit – in analogy with bulk interdiffusion – the stress fields should make the differences of the atomic fluxes disappear, i.e. there will be no net volume transport, and we can assume that $v_x=0$. Then from the condition $\frac{\partial c_A}{\partial t} + \frac{\partial c_B}{\partial t} = 0$, one arrives at

$$\frac{\partial\left(J_A + J_B\right)}{\partial y} = 0 \quad . \tag{3.4}$$

The integral of (3.4), assuming that the gradients are zero far from the part of the GB where the GB intermixing takes place, gives the condition $J_A = - J_B$, and we obtain

$$\frac{\partial \sigma}{\partial y} = -\frac{kT}{\Omega} \cdot \frac{(D_A - D_B)}{D_A c_A + D_B c_B} \cdot \frac{\partial c_A}{\partial y}, \tag{3.5}$$

and

$$J_A = -\frac{D^{NP}\delta}{\Omega}\frac{\partial c_A}{\partial y} \quad , \quad J_B = -\frac{D^{NP}\delta}{\Omega}\frac{\partial c_B}{\partial y} \tag{3.6}$$

with

$$D^{NP} = \frac{D_A D_B}{c_A D_A + c_B D_B}. \tag{3.7}$$

Here D^{NP} has the form of a Nernst-Planck like interdiffusion coefficient. According to (3.6) indeed J_A = - J_B since c_A+c_B=*1*, and thus $\frac{\partial c_A}{\partial y} = -\frac{\partial c_B}{\partial y}$.

We have to add that it is not expected that the Nernst-Planck limit is observed in the above "pure" form. First, at the beginning of GB interdiffusion processes, there are no diffusion induced stresses and the atomic fluxes are usually different, thus in this first stage the Nernst-Planck limit will not be established and the system can approach this limit only after a certain time period. Second, usually the GBs are very efficient sources and sinks of atoms/vacancies and thus the incoming extra atoms (or extra vacancies) can easily build into the GB and in the atomic plains surrounding the GB. The stresses can at least partly relax e.g. by the overall expansion of the film, yet if the GB does not move. This process is in fact the wegde formation [54][44] at around the GBs and can be taken into account by an additional term on the right hand side of (3.3) even if v_x=*0*. This was treated in details in [44] for a standing boundary and this wedge formation process was also called as a kind of GB Kirkendall effect. The authors of [44] also assumed that $c_A + c_B = 1$ and assumed that the extra incoming atoms were symmetrically deposited on both sides of the standing GB into the bulk. This wedge formation should be distinguished from the case when the stress gradient is completely

relaxed and the deposition of atoms leads to the shift of the GB, as it will be discussed in the next section. Since the authors of [44] did allow the wedge formation (what we neglected above during the derivation of Eqs. (3.50)-(3.7)) it is not surprising that they could not reproduce the relation (3.7), because the wedge formation in fact implies some stress relaxation. As it was mentioned above in real cases the Nernst-Planck limit can be reached after some time if the wedge formation (or the shift of the GB) will be stopped by certain external constraints (e.g. for bilayers of thin films on a rigid substrate: see also Chapter 9.2.1) and the stress gradients developed will be high enough. The detailed treatment of such cases would need handling a complicated coupled elastictity and GB diffusion problem (see e.g. [54], where the diffusion deformation of a pure thin film was described under the stretching effect of the substrate).

3.1.1.3. Darken limit, grain boundary motion as a manifestation of Kirkendall shift

In the case b) we can disregard the terms containing the stress gradients in (3.2). In fact the GB shift is accompanied by expansion (or shrinkage) of the material. As it is illustrated in Fig. 3.2 the shift of the GB along the x direction is the result of the motion of GB steps of ξ height up or down depending on which side of the boundary these are situated, and on whether deposition or removal of atoms during the process takes place. Indeed it was mentioned already in 1985 [59] that GB steps can serve as probable locations for the initialization of the GB shift. Let us note that this step model can be considered as a macroscopic one, although, as we will see below from the comparison with an atomic model (in Chapter 4), the value of β in Fig. 3.2 can be in the order of the normal component of the Burgers vector of a certain GB dislocation belonging to this step.

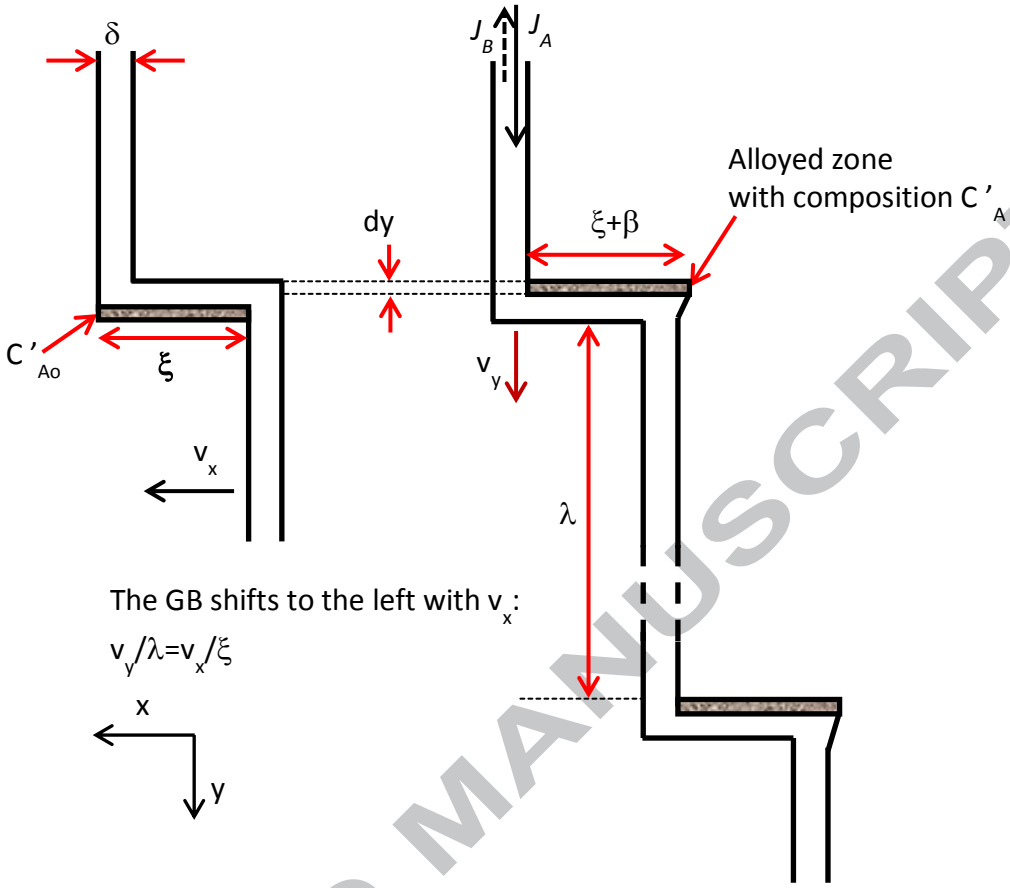

Fig. 3.2 Schematic picture of the GB step mechanism of GB shift (see also the text). The flux of A atoms, J_A, is oriented down. If the GB step of ξ height and λ long in the material *B* shifts down by *dy* (see also the text), the $\beta dy/\lambda\delta=\beta dx/\xi\delta$ relative volume change is transferred to the bulk (the ξ wide layer is transferred to the $\xi+\beta$ wide one, and the considered GB area is $\lambda\delta$). λ is the average distance between the steps. In the left figure the dashed area of the pure *B* matrix is ξdy and it expands by βdy.

Let us take a volume element of λ long in the boundary: $V_o=\delta\lambda z_n$ (where z_n is the unit length perpendicular to the *x*-*y* plane shown in Fig. 3.2). λ can be taken as the average characteristic distance between the steps in the GB. Thus – assuming that all the extra volume deposited in the GB is transferred to the bulk – the time derivative of

the relative change of the above volume element should be equal to the sum of the first terms on the right hand side in Eqs. (3.3):

$$\frac{d(\frac{\Delta V}{V_o})}{dt} = -\frac{\Omega}{\delta}\frac{\partial(J_A+J_B)}{\partial y} = (D_A - D_B)\frac{\partial^2 c_A}{\partial y^2}, \tag{3.8a}$$

if the diffusion coefficients are constant. Since $c_A+c_B=1$, from the sum of Eqs. (3.3) we get

$$(D_A - D_B)\frac{\partial^2 c_A}{\partial y^2} = \frac{v_x}{\delta} q \quad , \tag{3.8b}$$

with $q_A c_A+q_B c_B=q$. Furthermore, the volume change of the bulk during a shift of the volume element of V_o by dy is $\Delta V=\beta dyz_n$ for expansion, i.e. when the step moves down as it is shown in Fig. 3.2 (β denotes the expansion in the x-direction caused by deposition of extra atoms due to inequality of GB fluxes.) Thus,

$$\frac{d(\Delta V / V_o)}{dt} = \frac{v_y \beta}{\delta\lambda} \quad . \tag{3.8c}$$

Since the velocity of the step along y is related to the velocity of the shift of the step along x, the v_y/λ ratio in (3.8c) can be given as $v_y/\lambda=v_x/\xi$ (see Fig. 3.2: during the shift of the step by a distance λ down, the GB shits by a distance ξ). Thus we have

$$\frac{d(\Delta V / V_o)}{dt} = \frac{\beta}{\xi}\frac{v_x}{\delta} \tag{3.8d}$$

The comparison of Eqs. (3.8) gives that $q=\beta/\xi$. Thus we have

$$v_x = (D_A - D_B)\frac{\delta}{q}\frac{\partial^2 c_A}{\partial y^2} \quad . \tag{3.9}$$

Note that the $q=\beta/\xi$ factor, which is in fact the relative expansion of the bulk along the x direction (Fig. 3.2), was called in [2] as a dilution factor (see also Chapter 4).

In order to get an expression for the GB interdiffusion coefficient one has to put v_x, as expressed from (3.9), into the first one of (3.3), and obtains

$$\frac{\partial c_A}{\partial t} = D^D \frac{\partial^2 c_A}{\partial y^2} \,. \tag{3.10}$$

with

$$D^D = D_A\left(1-\frac{q_A}{q}c_A\right)+D_B\frac{q_A}{q}c_A = D_A+\frac{q_A}{q}c_A(D_B-D_A). \tag{3.11}$$

Expression (3.11) has a similar form as the bulk interdiffusion coefficient in the Darken limit, but the GB diffusion coefficients are weighted by the corrected values of the GB atomic fractions. Note that relation (3.11) coincides with the expression (A10) of [50] if q_A/q=1 as it was implicitly assumed there.

It's also worth noting that from a comparison of Eq. (3.9) with the velocity of the classical bulk Kirkendall shift ($v_K = (D'_A - D'_B)\,{\partial c'_A}/{\partial x}$), we obtain that the main difference is that the GB shift velocity is propotional to the second derivative of the GB concentration, while v_K is proportional to the *first* derivative of the bulk concentration.

3.1.1.4. Composition left behind the moving boundary

As a next step, we demand the knowledge of q_A, which can be determined in steady state following a similar procedure as used in [2]. Since during the deposition of excess atoms the ξ thick layer of the step in the original grain with c'_{Ao} bulk atomic fraction will be converted to the $\xi+b_n$ thick layer of the alloyed zone with composition c'_A (Fig. 3.2), the conservation of *A* atoms leads to the condition

$$-\frac{\Omega}{\delta}\frac{\partial J_A}{\partial y} = \frac{v_y}{\lambda\delta}\left[(\xi+\beta)c'_A-\xi c'_{A0}\right] = \frac{v_x}{\xi\delta}\left[(\xi+\beta)c'_A-\xi c'_{A0}\right] \tag{3.12}$$

where again the $\lambda/v_y = \xi/v_x$ relation was used. Then, in steady state for the A atoms, i.e. accepting that $\frac{\partial c_A}{\partial t} = 0$ (see also Eq. (3.3))

$$q_{Ast}c_{Ast}=[(\xi+\beta)c'_{ASt} - \xi c'_{Ao}]/\xi=[(1+q)c'_{ASt} - c'_{Ao}]. \quad (3.13)$$

It can be seen that for $c'_{Ao}=0$ the relation between the GB and bulk concentrations is: $q_{Ast}c_{Ast}=(1+q)c'_{ASt}$, and thus $q_{Ast}c_{Ast}/q=(1+1/q)c'_{ASt}$.

For the estimation of the composition left behind the sweeping boundary in steady state, from the first equation of (3.3), with the use of (3.9), we obtain

$$\frac{q_{ASt}c_{ASt}}{q} = \frac{D_A}{D_A - D_B}. \quad (3.14)$$

Thus – using (3.13) -

$$c'_{ASt} = \alpha\frac{D_A}{D_A-D_B} + \frac{c'_{Ao}}{1+q}, \qquad \alpha = \frac{\beta}{\xi+\beta} = \frac{q}{1+q}, \quad (3.15)$$

which is equivalent to relations (6) and (7) of [2] (see also Chapter 4). It can be seen that the $\frac{D_A}{D_A-D_B}$ ratio is higher than unity ($D_A>>D_B$) and the role of the multiplying factor, α, is important in determining the composition. Of course in our phenomenological approach, since β/ξ can be different for different individual step heights, it should have some average value, but probably it has the same order of magnitude as estimated in [2] from the microscopic model (see also Chapter 4).

It can be seen that the two interdiffusion coefficients obtained (Eqs. (3.7) and (3.11)) – as it is expected - give the same conclusion as one can get from the bulk analogous of them: if $D_A>D_B$, then $D^D \cong D_A$ and $D^{NP} \cong D_B$, respectively, i.e. the GB intermixing in the Darken limit is controlled by the diffusivity of the fast component, whereas in the Nernst-Planck limit - by the diffusivity of the slower one.

3.1.1.5. Requirement of a steady state

There is one peculiar behaviour of the required steady state for A atom. As it can be seen from (3.11) and (3.14) in steady sate $D^D=0$, whereas D_A, D_B, c_A, and c_B, differ from zero. This corresponds to such a special case when there is no further intermixing in the GBs while the shift of the boundary is still preserved. In fact D^D characterizes the intermixing inside the GB and $D^D=0$ means that c_A does not change in time. This means that the divergence of the original $J_A=-D_A\delta(\partial c_A/\partial y)/\Omega$ flux is compensated by the second term in (3.3). Of course before reaching the steady state the atomic fraction in the DIGM zone, c'_A is less than c'_{ASt} i.e. $q_Ac_A/q < q_{ASt}c_{ASt}/q=D_A/(D_A-D_B)$, and thus $D^D > 0$.

One can try to estimate the time necessary to reach the steady state starting from the assumption that $\partial^2 c_A/\partial y^2 = const. = K$ in Eq. (3.10). Note that it also means that the velocity of the GB shift is constant. Furthermore, we assume that the condition $\frac{\partial^2 c_A}{\partial y^2} = K$ is reached during much shorter (negligible) time, t_K, than the time necessary to reach the steady state, t_{St}. Then, from (3.10), with the use of (3.11) and (3.14), we have

$$\frac{\partial c_A}{\partial t} = D_A\left(1-\frac{q_Ac_A}{q_{ASt}c_{Ast}}\right)K, \tag{3.16}$$

from which

$$\int_{c_{AK}}^{c_A}\frac{dc_A}{1-q_Ac_A/q_{ASt}c_{Ast}} = D_AKt, \tag{3.17}$$

with $c_A=c_{AK}$ at $t_K\cong 0$. Take $c'_{Ao}=0$, and assume that $q_{AK}=(1+q)c'_A/c_A\cong const.$ i.e. $c'_A/c_A=const$, and $q_{AK}\cong q_{Ast}$ for t>0. And so, after integration,

$$\frac{1-c_A/c_{Ast}}{1-c_{AK}/c_{Ast}} = \exp\left(-\frac{D_AKt}{c_{Ast}}\right) = \exp(-\tau). \tag{3.18}$$

It can be seen that it gives back the steady state result after a certain time, when τ is large enough so that e.g. $\exp(-\tau) \cong 5 \times 10^{-5}$, *i.e.* $\tau \cong 10$.

Since τ can be rewritten as

$$\tau = \frac{KD_A}{c_{ASt}} t = \left(\frac{q_{ASt}}{q} \right) K \left(D_A - D_B \right) t = \frac{v_x q_{ASt} t}{\delta} = \frac{\Lambda q_{ASt}}{\delta}$$

(see also Eq. (3.9)), where $\Lambda = v_x t$ is the sweeping distance of the GB. Taking $\delta \cong 0.5$ nm and making an estimate $c'_A/c_A \cong 0.2$, we get that q_{ASt}/δ is about 0.5 nm^{-1} and from the condition τ = 10, Λ=20 nm is obtained. This sweeping distance is necessary to fully transform a nanostuctured film of an average grain size of 40 nm. Thus, this order of magnitude estimation shows that the saturation by cold homogenization, in films with grain sizes less than about 40 nm, can be reached even before the steady state is established. This indicates that one has to be cautious if the above estimations for the steady state bulk compositions are compared with experimental data. Furthermore, we can get estimations for the t_K, as well as t_{st} times. t_K should be in the order of magnitude of the time necessary for GB diffusion distance equal to the film thickness. Thus, taking a typical value for the GB diffusion coefficient at $T/T_m \cong 0.3$ (see Fig. 2 in [31]), $D_{GB} \cong 10^{-8} m^2/s$, $t_K \cong$20s. On the other had in thin film experiments the typical time to reach the saturation is in the order of 1 h [60], i.e. we can take $t_{st} \cong$1h. Thus the above assumption $t_K \cong 0$ as compared to t_{st} is not a bad approximation.

3.1.2. Free standing A film in B vapour

The above discussion can be easily carried out for *A* in *B* vapour. Note that a similar relation for the steady state bulk composition in this case was not derived in [2]. Using similar considerations, carried out in Chapter 3.1.1 in the Darken limit, the relation

$$D^D = D_A\left(\frac{q'_B c_B}{q'}\right) + D_B\left(1-\frac{q'_B c_B}{q'}\right) = D_B + (D_A - D_B)c_B\frac{q'_B}{q'}. \tag{3.19}$$

can be obtained. Now, we have to determine the q'_{Bst},and $q'=q'_A c_A+q'_B c_B$ values different from q and q_{Ast} above.

For the calculation of q' we have to take into account that now there is a shrinkage while the step moves up in Fig. 3.2, since more atoms leave the GB than arrive at that location. In addition, in this case the corresponding relative change is proportional to $-\beta/(\xi+\beta)$ i.e.

$$q'=- q/(1+q). \tag{3.20}$$

Furthermore, instead of (3.12) we can write

$$D_B\frac{\partial^2 c_B}{\partial y^2} = \frac{v_x}{(\xi+\beta)\delta}\left[(\xi c'_B - (\xi+\beta)c'_{B0}\right], \tag{3.21}$$

i.e.

$$q'_{BSt}c_{BSt}=[(\xi c'_{BSt} - (\xi+\beta)c'_{Bo}]/(\xi+\beta) =[c'_{BSt}/(1+q) - c'_{Bo}]. \tag{3.22}$$

Furthermore, in steady state

$$\frac{q'_{BSt}\,c_{BSt}}{q'} = -\frac{D_B}{D_A - D_B}, \tag{3.23}$$

and using (3.22)

$$c'_{BSt} = q\frac{D_B}{D_A - D_B} + (1+q)c'_{Bo}. \tag{3.24}$$

Before turning to the atomic mechanism of low temperature DIGM it is worth summarizing the most important predictions following from the outcomes of this whole chapter. It is not expected that the expressions for the GB interdiffusion coefficients (relations (3.7) and (3.11)) can be directly applied since measurements of the time evolution of concentrations inside the boundary slab only would be very difficult. On the other hand predictions on the GB velocity and especially on the atomic fractions in

the DIGM zone have much stronger relevance, since these can be directly compared with experimental observations (see also Chapters 5 and 9.2). Let us sum up the most important predictions of the step model. First of all this description, in contrast to the atomic model by Balluffi and Cahn [2], is not restricted to vacancy mechanism and can be valid e.g. for interstitial diffusion too, in accordance with experimental observations of DIGM during interstitial diffusion [61] [62]. Furthermore, the atomic fraction in the alloyed zone can be less than 0.5 even in a completely miscible binary system: it is determined by two factors i) the type of the boundary (it affects the value of β) and ii) the kinetic parameters $\frac{D_A}{D_A-D_B}$ in Eq. (3.15) and $\frac{D_B}{D_A-D_B}$ in Eq. (3.24). Considering a thin film diffusion couple, formed between pure *A* and *B*, the relations (3.15) and (3.24) for $D_A > D_B$, applying the well-known thumb rule that at a fixed temperature $D_A > D_B$ if the melting point of *B* is higher than that of *A* (see e.g. [31]), predict that t*he solute content in the DIGM zone in the film with higher meting point (i.e. on the B side) should be larger than in the film with lower* T_m *(i.e. on the A side).* Furthermore, since the value of *q* in (3.15) and (3.24) lies in the order of 0.1 (see also the chapter below), rather low atomic fractions are predicted if the D_A/D_B ratio is larger than 2 (this is in fact a prerequisite to get high enough difference in the GB atomic fluxes to produce GB shift): $c'_A = 0.18$ and $c'_B = 0.05$ for $D_A/D_B=2$ (with $q=0.1$) as well as $c'_A = 0.10$ and $c'_B < 0.01$ for $D_A/D_B=20$, respectively. So, in general, the atomic fractions in the DIGM zones are relatively small if only this mechanism works.

3.2. About the driving force for low temperature DIGM

Till now we only qualitatively discussed the possible contributions to the driving force of DIGM at low temperatures. While the form of the driving force for high temperature DIGM was quite extensively treated in the literature already from the very

early time of the DIGM (see Chapter 2 and the following section), it is worth to devote some comments on the form of the driving force for low temperature DIGM. According to the well known expression (Nernst-Einstein equation) for the GB velocity

$$v=MF \tag{3.25}$$

where M is the mobility and F is the driving force, and M is related to the apparent atomic diffusion coefficient, D_a (see e.g. [63]), by the relation $M=D_a/kT$ (if the thermodynamic factor is unity as we assumed). Note that e.g. in Eq. (2.1) ΔG_m is not given in units of force, but it is given in units of pressure (energy/volume) and if F is replaced by ΔG_m then a factor of Ω/δ should be included into the mobility: see e.g. the expression for v for high temperature DIGM in [64] and [16].

Now, if we want to investigate the more general case (i.e. do not use the assumption that $\Omega_A=\Omega_B=\Omega$ in the expressions (3.1)), according to the Vegard law, Ω should be replaced by $\Omega=c_A\Omega_A+c_A\Omega_A$. Furthermore, in this case Eqs. (3.8a) and (3.9) will have the form

$$\frac{d(\frac{\Delta V}{V_o})}{dt} = -\frac{1}{\delta}\frac{\partial(\Omega_A J_A+\Omega_B J_B)}{\partial y} \tag{3.26}$$

and

$$v_x = -\frac{1}{q}\frac{\partial(\Omega_A J_A+\Omega_B J_B)}{\partial y}. \tag{3.27}$$

It can be seen from the comparison of (3.25) and (3.27) that the driving force is

$$F = -\frac{kT}{qD_a}\frac{\partial(\Omega_A J_A+\Omega_B J_B)}{\partial y}. \tag{3.28}$$

On the basis of (3.28) we can estimate separately the driving forces belonging to the difference of the intrinsic diffusion coefficients and to the difference of the atomic sizes only (F_D and F_Ω, respectively). Thus (assuming that D_B=D_A for F_Ω)

$$\frac{F_D}{F_\Omega} = \frac{D_A - D_B}{D_A} \Big/ \frac{\Omega_A - \Omega_B}{\Omega}. \tag{3.29}$$

As seen, with D_A>>D_B (as usually happens) the first ratio is close to unity, whereas the second one is in the order of a few percent. Thus, the driving force caused by the difference of the GB diffusion coefficients noticeably exceeds the driving force arising from the size mismatch.

4. Atomic (vacancy) mechanism: climb of grain boundary dislocations

4.1. Balluffi—Cahn-model

As it was mentioned already in the preceding chapters, in 1981 - discarding certain concepts for the driving force and mechanism of DIGM - Balluffi and Cahn [2] proposed that the differences in the GB diffusion coefficients cause a self-sustaining climb of GB dislocations, GBD, and motion of their associated steps (i.e. motion of disconnections as defined later by Hirth and Pond [65]). It turned out that this concept is really useful for the interpretation of DIGM at low temperatures, and perhaps can also be important (as a possible atomic mechanism of GB shift) at high temperatures too, where the coherency strain model is the most widely accepted interpretation (see also Chapter 5) for the driving force. In addition the Balluffi-Cahn model naturally contains the GB Kirkendall-effect (see also the macroscopic description in the previous Chapters). In this model it is assumed that the GB diffusion occurs by a vacancy mechanism, and the climbing GBDs are sources and sinks of GB vacancies, similarly as bulk dislocations can absorb and emit bulk vacancies during bulk interdiffusion. In this latter case the Kirkendall shift (parallel with the direction of the atomic fluxes) is the result of the climb of bulk dislocations (perpendicular to the Kirkendall shift), while in GB interdiffusion the climb of GBDs results in motion of the GB steps (related to these GBDs) *parallel* with the GB plane and thus the GB moves *perpendicular* to the directions of the GB fluxes. Fig. 4.1 illustrates this for a simple edge GBD and its associated step in a symmetric tilt boundary. The Burgers vector, *b*, is the vector of the DSC lattice produced by the adjoining two (I and II) crystals. The GBD is sessile in the boundary plane and when it climbs crystal II will translate (relative to crystal I) by a displacement given *b* and the GB will migrate according to the motion of the GB step. If the solute, *A*, diffuses faster than the matrix atoms, *B*, there will be a net inward flux

of atoms *A*. In this case the GBD acts as a sink for *A* atoms (i.e. it emits a GB vacancy) and the GBD climbs downward. At the same time the boundary shifts to the left in Fig. 4.1. Although it was not emphasized in [2] it was implicitly assumed that, during the continuous climb motion of the GBD, the accommodation of the incoming atoms is easy and no stress accumulation takes place. The incoming atoms thus continuously shuffle at the advancing step, decreasing the solute concentration in the GB core and thus the shift becomes self-sustaining.

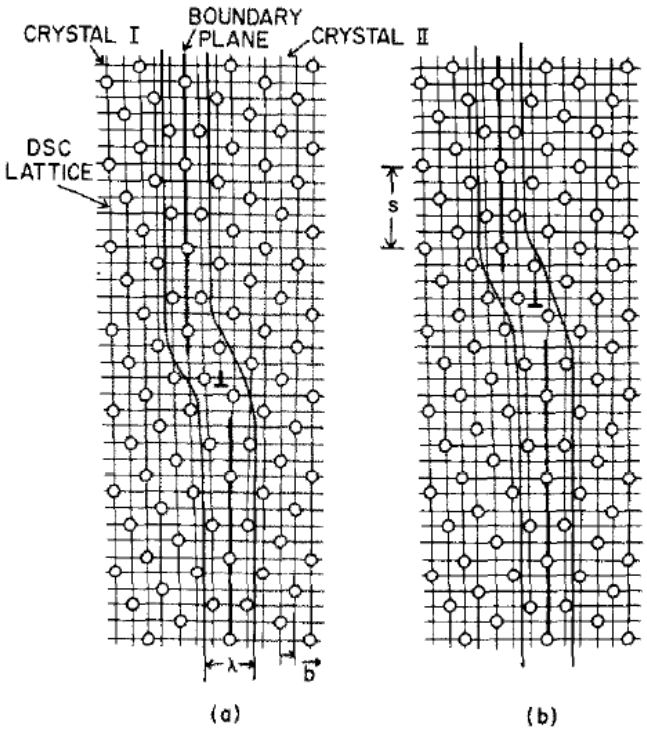

Fig. 4.1 Climb of GBD in symmetric tilt boundary in simple cubic structure. The tilt angle is 36.9^{o}; $b(\equiv b_n)$ is the Burgers vector; $\lambda(\equiv\delta)$ is the grain boundary core width. (a) Initial structure. (b) GBD after climb by the annihilation of a vacancy [2].

The analytical expressions for this mechanism can be formulated as follows. We can use the (3.2) flux equations by neglecting the second terms and thus the net flux of

A atoms (now, as in [2], expressed in unit volume/distance time, i.e. Ω from the denominator is missing) is

$$J_A + J_B = (D_B - D_{A)}\delta\frac{\partial c_A}{\partial y}. \tag{4.1}$$

This is constant along the GB, except at GBDs, where can be a discontinuous change in the concentration gradient $\Delta(\partial c_A/\partial y)$ and net deposition of atoms is possible:

$$-(J_A + J_B) = (D_B - D_{A)}\delta\Delta\left(\frac{\partial c_A}{\partial y}\right), \tag{4.2}$$

which results in a GBD climb velocity along *y*, $v_d(=v_y)$,

$$v_d b_n = (D_B - D_{A)}\delta\Delta\left(\frac{\partial c_A}{\partial y}\right). \tag{4.3}$$

Here b_n is the Burgers vector of the GBD perpendicular to the GB plane.

Comparing (4.3) with (3.9) it can be recognized that these two equations are equivalent if we take that into account $v_y/\lambda = v_x/\xi$ (see Fig. 3.2) and $\Delta(\partial c_A/\partial y)/\lambda \cong \partial^2 c_A/\partial y^2$, where λ is the characteristic distance between the GB steps, i.e. between the GB dislocations. Indeed, the two equations are equivalent if $\beta=b_n$. This is the atomic interpretation of the expansion of the *dy* thick layer, of the step of ξ height, along the x direction, β, (Fig. 3.2); it corresponds to the normal component of the GBD, belonging to this ~~is~~ step.

It is worth noting that the values of the b_n/ξ dilution factor were estimated to be in the order of 0.1 in [2] and thus the order of magnitudes of the experimental data were reproduced.

Beside deriving an expression for the GBD velocity, Balluffi and Cahn [2], assuming a balance of the solute *A* atoms, and using similar considerations as deriving

relations (3.12) and (3.13) (see Eqs. (3) and (5) in [2]) arrived to a relation equivalent to (3.15) with $\beta=b_n$.

Closing this subchapter it is worth emphasizing that the validity of the predictions of this model is strongly dependent on the details of the GB structure [16] [66]. Although this model allows of rationalization of the variability of DIGM from boundary to boundary and e.g. certain dislocations existing on certain GB may give rise to zero step heights and such GBs should be immobile. Furthermore, as it was listed by the original Hillert's paper [24], this has several shortcomings (see also [16]): i) it is applicable only for vacancy mechanism, ii) according to this model the concentration of solute behind the moving boundary should be constant and independent of the dislocation (step) density in the boundary plane, iii) problem arises when the Burges vector of the GBD is not exactly perpendicular to the boundary plane and thus the motion of a defect should cause grain boundary sliding too. The phenomenological step model has some advantage in this regard since it does not take any concrete details: if once a step exists and mobile then the GB Kirkendall effect will be noticed.

4.2. Liquid metal embrittlement

The significance and the probable more general role of the dislocation climb mechanism can be well illustrated by its successful application to the understanding of the so called liquid metal embrittlement, LME, phenomenon. It can be observed when a liquid metal is in contact with polycrystalline sample and very deep liquid grooves are formed at the intersections of the GBs and the liquid/solid interface. In many metallic systems [66] the fast penetration of the liquid film finally leads to brittle intergranular fracture under a modest stress. This is the effect of LME, which is very important in different technical applications of material processing and in nuclear reactor technology

in which liquid metals are used as coolants and as spallation targets [66][67]. Interestingly the history of different trials of the explanation of the driving forces and mechanisms of this phenomenon is very similar to that of the DIGM [66][67][68][69][70]: each of the previous approaches was capable of explaining one or many aspects of LME, but e.g. none of them could successfully explain the effect of stress on liquid film penetration [66].

In the recent paper of Nam and Srolovitz [66] a series of molecular dynamics simulation was reported, on the liquid Ga/Al bicrystal model system, and the authors identified the GBD climb as the main operating mechanism. The new picture of LME can be shortly summarized as follows [66]: "First, Ga diffuses down the grain boundary in Al below the liquid groove root and causes stresses large enough to nucleate a dislocation in the grain boundary. The first dislocation climbs down by stress- enhanced Ga hoping across the dislocation core, leaving a tail of Ga behind. This Ga hopping leads to a constant dislocation climb rate that is applied stress-independent. Once the dislocation moves far enough from the groove root, another dislocation is nucleated. It too climbs down the grain boundary at the same rate, resulting in a uniform spacing of climbing dislocations. With Ga at the grain boundary, applied strains enhance the grain-boundary opening and in turn more Ga is inserted from the liquid groove into the grain boundary to relieve the residual stress (i.e. Ga layer thickening process). The Ga penetration rate mirrors the dislocation climb rate and so is time independent. In order for LME to occur, the solute must diffuse quickly in the grain boundary, a stress must be applied to nucleate dislocations and keep the grain boundary open, and the solute must be capable of making grain-boundary decohesion at sufficient concentrations." Thus the authors were also able to derive an expression for the steady state disclocation velocity. For the details we refer to the original paper.

5. Possible contribution of bulk penetration (Hillert's chemical as well as coherency strain driven force models)

5.1. Early models

In their original work Hillert and Purdy [3] called the phenomenon as Chemically Induced Grain Boundary Migration, CIGM, and argued that the driving force is the chemical Gibbs energy of mixing of two different elements. Recognizing the similarity with the discontinuous precipitation, for the estimation of the slute content of the alloyed zone in a thin film specimen of *h* width (exposed to the solute vapor from both sides, producing c'_o solute content at the free surfaces of the thin film), they started from the Cahn's solution [71], which can be obtained from the mass balance in the steady state. In this case, if the planar GB (perpendicular to the outer surfaces) migrate with constant *v* velocity from one grain, having a solute sontent *c'(y)*, at a certain *y* depth measured from the centre of the thin film perpendicular to the free surface, into an another one with atomic fraction c'_1, and the diffusion takes place only in the GB one can write for the mass balance:

$$\delta D \frac{d^2 c(y)}{dy^2} + v\left(c'_1 - c'(y)\right) = 0, \tag{5.1}$$

where *c(y)* is the GB concentration and is directly related to the bulk concentration through the segregation factor, *s*:

$$c(y) = sc'(y). \tag{5.2}$$

The solution of this equation is

$$\frac{c\prime(y) - c\prime_1}{c\prime_o - c\prime_1} = \frac{\cosh\left({}^{y\sqrt{\alpha}}/_{h}\right)}{\cosh\left({}^{\sqrt{\alpha}}/_{h}\right)} \quad . \tag{5.3}$$

The parameter α has the form:

$$\alpha = \frac{vh^2}{s\,\delta D}. \tag{5.4}$$

Furthermore, in this chemical driving force model the GB velocity is given by the well-known relation

$$v = M\,\Delta G_m, \tag{5.5}$$

where M is the GB mobility and ΔG_m is the chemical driving force, i.e. the Gibbs free energy of mixing per atom.

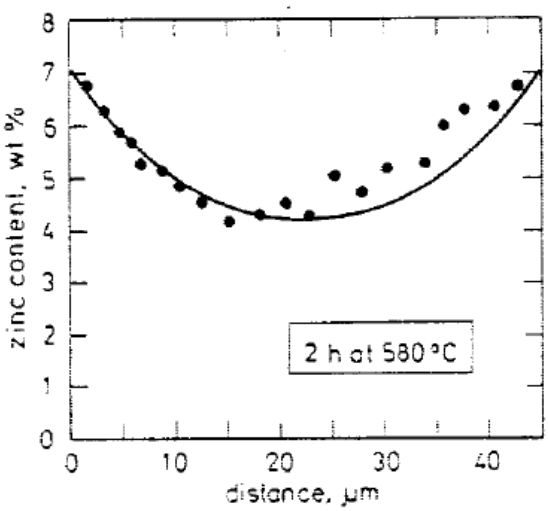

Fig. 5.1 Experimental concentration profile of zinc from one side of the thin Fe specimen to the other in the zincified region [3].

Thus Hillert and Purdy fitted Eq. (5.3) to the composition profiles (see Fig. 5.1 as an example) and estimated the values of the GB diffusion coefficients, D, and the velocities. They arrived to the end that the GB diffusivities were several orders of magnitude larger than the values reported for stationary boundaries. However, later on in [46], using (5.1) and that the composition versus the distance measured from the surface had exponential dependence in thick sample (i.e. when $h\rightarrow\infty$, see also Fig. 1.3) it was shown for Zn diffusion into symmetric and asymmetric GBs of Cu that the GB diffusivities were in a good agreement with those obtained by radiotracer techniques for stationary boundaries. In addition, it was also observed that the calculated grain

boundary diffusivities exhibited a strong dependence on the misorientation angle, similarly as it was observed from tracer GB diffusion data in different bicrystals [22]. In later communications from the same group it was emphasized [22] [57] that getting such a good agreement with the GB triple product, $s\delta D$, obtained from DIGM experiments and from radiotracer measurements can be quite a difficult task, because i) the GBs usually have a stop-and-go type motion (i.e. v is not constant), ii) the segregation factor should be replaced by a so called dynamic segregation factor, which can be orders of magnitude smaller than the equilibrium one and iii) the strong composition dependence of the GB diffusion coefficients. Furthermore, it is worth noting that the Cahn's model can be considered as an alternative of the description presented in Chapter 3.1, since it is assumed in both that the bulk diffusion is frozen out. The main difference is that in the Cahn's model the velocity is proportional to the driving force, whatever it can be, while in the other v is proportional to the difference of the GB diffusivities and to the second derivative of the atomic fraction along the GB (see (3.9)), i.e. it offers an explanation on the mechanism (steps, or GB dislocations) by which DIGM is linked to the driving force too. In this respect we agree with the conclusions presented in the review of A. H. King [16]: "…it is appropriate to draw a distinction between two different types of driving force: the first kind is indirect and constitutes a generalized reduction of free energy which may occur if DIGM takes place, and such driving forces require some form of mechanism in order for the requisite grain boundary motion to occur. The second type of driving force is more direct and arises as a directed impetus on the grain boundary so that the migration itself is driven, rather than merely facilitating other processes which reduce the free energy of the system." Furthermore, in the Cahn's model the solute content in the alloyed zone is the ratio of the GB atomic fraction and the segregation factor and depends on the depth

measured from the free surface, while e.g. in Eq. (3.15) it depends on the $^{D_A}/_{D_B}$ ratio (at certain depth from the surface), and contains a proportionality factor characterizing the type of the boundary.

The above relations were derived for negligible bulk diffusion and assuming that the driving force is the mixing free energy. There were publications, already in the early times of DIGM, where it was established that both of the above conditions were very restricting [2] [72]. The idea of the chemical driving force was quite extendedly criticized by Balluffi and Cahn [2]. The most important criticism contrary to the chemical driving force was that DIGM occurred under a whole range of conditions, including both alloying and de-alloying in systems with a positive or either a negative heats of mixing. In addition, Tashiro and Purdy [72] have shown that DIGM can occur at temperatures for which the diffusion of solute out of the GB is significant. Thus in one of his next papers Hillert [24], used the analogy with the discontinuous precipitation, which is a combination of the precipitation of a new phase and the growth of one parent grain into another. For the case, when the new phase is liquid, separating the two grains (liquid film migration, LFM), he has provided a model of direct driving force for DIGM, which depends on the strain energy produced by the solute diffusion into the bulk just ahead of the boundary. As it was already mentioned in Chapter 2 this driving force per unit area of GB in an elastically isotropic material is given by equation (2.1) [37]. Hillert also emphasized the role of the $^{D'}/_{v}$ parameter (i.e the thickness of the solute enriched layer: see also relations (2.2)), which gives a guideline: if $^{D'}/_{v}$ exceeds a critical value the frontal diffusion layer cannot be coherent and no migration can occur. On the other hand, if it is smaller than the interatomic spacing no elastic driving force will develop and only chemical (mixing) driving force should operate. In

fact, as it was shown already earlier, during liquid film migration solute atoms diffuse into the crystal lattice when liquid comes into contact with a planar surface of a crystal and first a coherent layer with a strain $\eta(c'_+ - c')$ will develop and the elastic energy of this can be expressed as

$$\frac{E\eta^2(c'_+ - c')^2}{(1-\nu)}. \tag{5.6}$$

Here c' is the mole fraction in the alloyed zone, which is coherent with the grain of c'_+ initial mole fraction. Hillert [24], considering the constrained equilibrium between the liquid phase and the two grains (see also Fig. 5.2), pointed out that during the formation of a coherent as well as an incoherent nucleus with equilibrium concentrations, c_c and c_-, respectively, the following relation should hold

$$\frac{c'_c - c'_-}{c'_+ - c'_-} = \frac{2c'_- E\eta^2}{RT(1-\nu)}. \tag{5.7}$$

Here R and T have their common meaning (appeared from the ideal solution expressions of mixing). In deriving (5.7) Hillert, expressed the driving force for the transfer of material from the coherent layer to a stress-free grain as the difference of the corresponding Gibbs free energies, and assumed that c'_c and c'_- can be neglected as compared to unity (dilute limit) and $c' - c'_c << c'_+$, arrived at relation (2.1). Note that the experimental verification of relation (5.7) is difficult not only because of the finite probe size of the experimental techniques used for the determination of the local solute contents, but because, besides the determination of the mole fraction well in front (c'_+) and well behind (c'_-) the GB, the knowledge of the solute content in the coherent zone would also be necessary. This is why in most of the cases when the validity of the coherency strain model was investigated rather the check of the validity of the driving force was considered. Note that the GB velocity is given by putting (2.1.) into the expression (5.5).

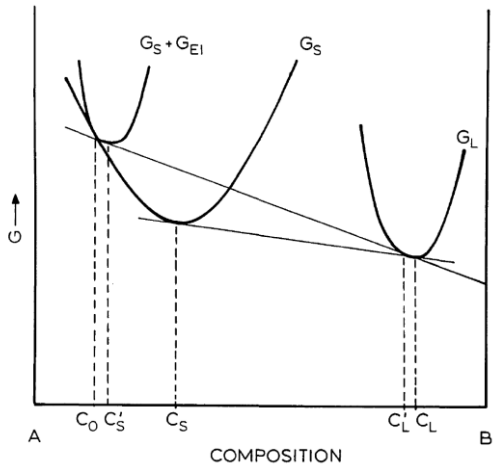

Fig. 5.2 Free energy curves for solid and liquid phases in a two component (A and B system) [16]: curves G_L and G_s apply to the liquid and the unstressed solid phases, respectively. The usual tangent construction gives the compositions of the solid and liquid in contact with each other at equilibrium ($C_s \equiv c'_+$, and C_L, respectively). For the solid with the initial composition ($C_o \equiv c'_-$) the free energy is increased by an amount of $G_{el}(\equiv \frac{E\eta^2(c'_+ - c'_-)^2}{(1-\nu)})$ due to the formation of an elastically stressed layer by bulk diffusion into it. New equilibrium compositions at $C'_s (\equiv c'_c)$ and C'_L are established. (The correspondence between notations of the compositon used in [16] and in this work is indicated in the parentheses.)

5.2. Refinements of the Hillert's coherency strain model

Just after the publication of the first papers [2][24][3][34] a huge research activity was noticeable, both regarding the theory as well as experiments of DIGM and LFM. As the result of these numerous investigations (see especially the research results from Yoon's group [6] [73]) now it seems clearly established that indeed the main driving force (for temperatures at which the thickness of the solute enriched layer due to the bulk penetration is not negligible) is due to the elastic coherency stress. In fact, replacing in (5.5) the chemical driving force with expression (2.1) one arrives at the

result that the migration rate should have a parabolic dependence on the coherency strain. In [73], using liquid phase sintered Mo(85w%)-Ni(15w%) alloys, three different solute atoms were used to vary the coherency strain. Thus the coherency strain, δ_o, was calculated as a combination of two terms (e.g. in the case of Co addition, it is the sum of the $\eta_{Ni}(c'_{Ni}-c'_{Nio})$ and $\eta_{co}(c'_{Co}-c'_{Coo})$, where the parent grain had the initial compositions c'_{Nio} and c'_{Coo} respectively, and δ_o was changed by exposing the liquid phase sintered Mo-Ni with Co-added liquid and thus a diffusion Co in and diffusion of Ni out took place) and can be tuned to be either positive (by adding Sn) or negative (by adding Co). It was also observed that the rate of the boundary shift was constant, i.e. the migration distance was proportional to the annealing time. The results are shown in Fig. 5.3. The observed zero migration rate (migration distance) at zero value of the coherency stain, δ_o, shows indeed that the coherency strain provides the determining contribution to the driving force.

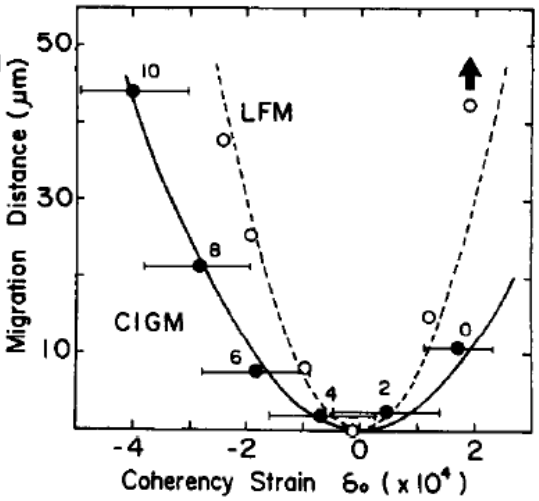

Fig. 5.3 Observed variation of the migration distance for DIGM (labelled CIGM) and LFM for Mo-Ni (Co,Sn) alloys held at 1460^o C for 2 hours (embedded into a Mo-Ni-Co-Sn liquids as a function of coherency strain δ_o. The solid and dotted lines are the

parabolic fits to the experimental data. (The numbers above the full circles indicate the decimal fraction of Co [73]).

There are numerous publications in which, still remaining in the framework of the coherency strain model, trials to avoid the assumptions involved in the original Hillert 's model were published. For example, in a more detailed analysis, it was shown in [64] that the effect of the boundary curvature can be important and that the orientation dependence of the apparent elastic modulus (in the shrinking grain), *Y*, replacing $E/(1-\nu)$ in Eq. (2.1) valid in isotropic solids, can predict the faceting of the migration interface (as shown in Fig. 2.4). The effect of the GB curvature can also lead to interesting effects: the GB can stop and turn back. Baik and Yoon [74] has shown that the grain boundary curvature increased during the GB migration in Mo-Ni alloy in contact with liquid Cu, causing a migration reversal and consequently an oscillatory motion. It was illustrated that the reversal of the grain boundary migration resulting in an oscillatory motion was a natural consequence of the coherency strain hypothesis for the driving force if the inhibiting effect of the grain boundary curvature was taken into account. The repetition of the original work of Sulonen [36], on discontinuous precipitation in Al-21,8at%Zn alloy by Chung et al.[39], is also worth mentioning. Here the change of the boundary velocities was determined as a function of the applied stress and the motion of two types of boundaries (parallel and transverse to the stress) was investigated. The results are shown in Fig. 5.4. The different slopes were interpreted as an additive driving force (of different sign) to the Hillert's coherency stain term ($G_{el}=\frac{Y\eta^2(c'_+-c')^2}{(1-\nu)}$) in Eq.(5.5) due to the application of tensile stress.

In 2004 Penrose [37] provided a general description of the coherency strain model, which thus was not included in previous reviews on the DIGM. He has shown

that the relation (2.1) is still valid when c'_+ and c'_- are not small (as was originally assumed by Hillert) and, following also the results of Cahn [75], Khachaturyan [76] and Hilliard [77], he has given a generalized formula for $Y=E/(1-\nu)$ for anisotropic solids. Furthermore, he made predictions on the direction of motion of the GB: the solute atoms initially diffused into the GB begin to penetrate into the two adjoining crystals and if the boundary layer is asymmetric the GB will be driven to move toward the crystal with the higher strain energy in order to consume it. He stated that "The usual kind of elastic force acts on all the atoms in a given region in the same way, tending to change the local macroscopic configuration of the material, but the force considered here acts differently, tending the change the *microscopic* configuration of the atoms in such a way the they fit the lattice of the growing grain rather than the shrinking one, but not changing the macroscopic configuration. It is analogous to the forces acting on dislocations and other imperfections, discussed by Eshelby in his paper on the elastic 'energy/momentum' tensor." It was pointed out in [37] that although the elastic driving force arises from elastic stresses, it is not an elastic force in the usual sense, since although the stress tensor is discontinuous across the boundary its normal component is continuous and the material macroscopically is in elastic equilibrium. This kind of elastic force acts tending to change the microscopic configuration of atoms in such a way that they fit the lattice of the growing grain rather than the shrinking one (but changing the macroscopic configuration)." In other words the GB can be considered as an interface between two different "phases": the "phase" (the grain) behind the moving GB has lower elastic energy and grows at the expense of the other having a higher elastic energy. It was also pointed out by Penrose that his treatment is exempt from such questionable assumptions like "the boundary is a very thin liquid layer, both faces of which are in equilibrium with the neighbouring crystal " and instead of assuming phase

equilibrium the diffusion potential (depending also on the local elastic stress as it was treated by Larche and Cahn [78]) had to be continuous. Thus, in spite of many similarities, this theory of DIGM is different from the LFM models: the presence of the two interfaces on the two sides of the liquid film is essential in LFM and the role of the diffusion is also different (for LFM the controlling factor is the rate at which atoms can cross the liquid film).

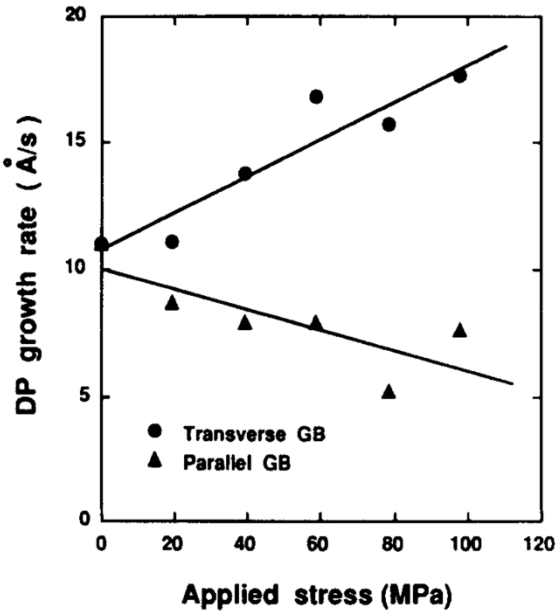

Fig. 5.4 Average growth rate of the discontinuous precipitation as a function of the applied stress for boundaries parallel as well as transverse to the stress in Al.-21.8at%Zn alloy at 75^{o}C for 1 hour [39].

In addition to the elastic strain caused by the size mismatch of the two types of atoms, stress free strain can also be developed due to the differences of the bulk diffusion coefficients like in classical bulk diffusion couples where most of the stresses of such origin can relax by the classical Kirkendall shift and some porosity can also be observed [29]. This can also contribute to the driving force for DIGM [17][79] and, as the consequence of the unequal atomic bulk fluxes in case of vacancy mechanism, can

lead to vacancy supersaturation and deposition. These may be left behind the moving boundary and indeed stacking-fault tetrahedra, formed by the agglomeration of vacancies, have been observed in copper alloyed with zinc by DIGM [42].

It was shown by Rabkin et al. [8] [80] [63] that the gradient energy correction [75] [77] to the free energy of an inhomogeneous alloy, stored in the region of steep chemical gradient, can lead to an additional driving force (since the driving force is proportional to the difference of the chemical potentials, in which the gradient energy corrections are included). If the lattice parameter misfit is small or negligible (i.e. the coherency strain terms are negligible) then this can drive the GB motion and it was illustrated that even a relatively small discontinuity in the solute distribution across the grain boundary area provides enough driving force for grain boundary migration.

Further contribution to the driving force due to the coherent strain energy can arise if one takes into account the diffusional flux of vacancies across the GB [81], from which the activation energy of DIGM can be predicted, having the meaning the activation energy for an atom to jump from the matrix into the boundary. Experimental results for DIGM in the Cu(Zn) system were in reasonably good agreement with this prediction. Other models were based on the solute atom induced effects in the GB: i) variation of the GB energy [81] or ii) structural transformation [12].

Despite the different attempts, most of which were listed above, considerable experimental evidence in favour of the coherency strain model has been accumulated and thus it is widely accepted as the main driving force of DIGM at high temperatures where the bulk diffusion is not negligible.

6. Grain boundary diffusion induced recrystallization (DIR)

As it was already shortly mentioned in Chapter 2, in many experiments on DIGM, in addition to GB migration and alloying, nucleation and growth of entirely new grains, with homogeneous solute contents inside, were formed (DIR). These solute contents are characteristic of the diffusion couple; the larger the lattice mismatch the larger the solute level [26]. This DIR phenomenon remained a major mystery during almost four decades, although the role of the coherency strain in the region ahead of the GB was accepted as one of the important factors [6]. In 2010 the group of G. Schmitz published a paper in which it was pointed out that, if the size mismatch is high enough, the coherency strains (caused again by the bulk penetration ahead of the boundary, as treated in details in [37] for DIGM), can lead to the break of the coherency by spontaneous relaxation via nucleation of new grains. The works of this group illustrated that the number of different solute content levels (in the new grains) increased with the lattice mismatch between the diffusing components [82][83][84][85]. It was pointed out in [26] that, from the requirement of the local equilibrium at the boundary between the newly formed (stress free) and stressed grain, it was possible to calculate (from the measured compositions inside the stress free grains) the stress and the maximum solute concentration in the stressed zone. Thus the measured compositions of the newly formed grains can be used as the measure of the stress, σ_{exp}, in the diffusion zone and it was plotted as the function of the ideal shear strength, σ_{ideal}. It can be seen in Fig. 6.1 that a linear relation with the slope of 0.7 was obtained. On the basis of this it was concluded that a break in coherency by nucleation of new grains happens if the diffusion induced stresses exceed 70% of the maximum shear strength. Thus predictions, whether DIR can happen or not, can be given by taking the lattice

mismatch, the initial composition difference between A and B in an A/B bilayer and the elastic stiffness. In addition the composition in the DIR zone can also be predicted Observe that, as it was recognized in [26] and can also be picked up in Fig. 6.1, the calculated stress values (σ_{exp}) were surprisingly high (in the order of a few GPa), much larger than the bulk yield strength of the investigated metals. The authors of [26] argued that if the stressed zone (the bulk diffusion penetration distance) is small enough, as it was experimentally demonstrated in quite thin films, then plastic flow relaxations via dislocations is difficult, and instead of the yield strength the maximum shear strength appears. For the details we refer to the original article.

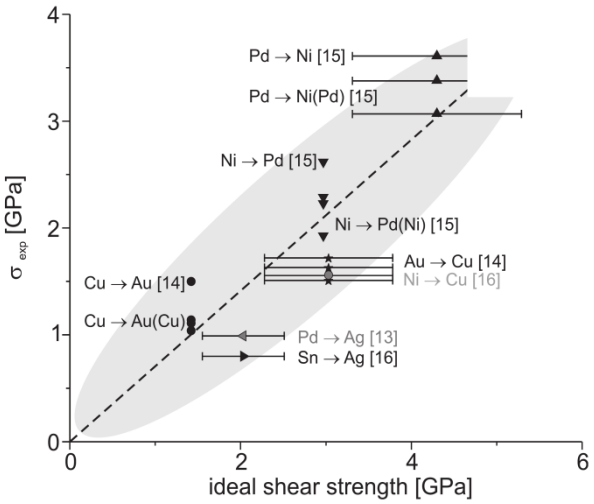

Fig. 6.1. Stresses in the diffusion zone in front of migrating GBs during DIR versus the theoretical ideal shear strength (the slope of the dashed line is 0.7 and error bars show the scatter of theoretical data) [26].

7. Temperature dependence of DIGM

According to the coherency strain model and the step model of DIGM a certain transition between the high and low temperature mechanisms of DIGM is expected. Indeed, with decreasing temperature the bulk diffusion distance (and the D'/v parameter) decreases and at the same time the difference of the fluxes of A and B atoms (in an AB thin film couple) increases because the GB diffusion coefficients have Arrhenius type temperature dependence and D_A-D_B increases. So indeed a gradual transition is expected between the high and low temperature regimes, i.e. between the processes described by the coherency strain as well as by the step model. It is important to emphasize that the step (GBD dislocation climb) mechanism of DIGM is not inconsistent with the coherency strain model [16]: the GB steps can provide the local symmetry breaking which is necessary for the coherency strain model in initially symmetric boundaries, i.e. they can serve as probable locations for the initialization of the GB shift (see also Fig. 5 in the paper by Li and Raith [59]). Thus in certain cases the step model and the coherency strain mechanism may act synergistically [16]. As a general picture we can summarize the DIGM process as follows. Diffusion induced stress free strains create a stress field. At higher temperatures this – besides the strain developed inside the GB itself, due to the inequality of atomic fluxes – leads to the development of coherency strain ahead of the GB (both the size mismatch and the difference of the bulk atomic fluxes can contribute to this), and the determining effect, DIGM, can be observed. But the same diffusion induced stresses (under certain conditions as discussed in the preceding Chapter) can also lead to DIR. At lower temperatures (the bulk diffusion is frozen out) the stress free strain develops inside the GB only and relaxes mainly by the motion of GB steps and shift of GBs. Thus the main

effect is the shift of the GBs in both limits. At the same time different other ways of stress relaxations can take place (related to another shape and volume changes) as it was listed in Chapter 2. Since these can be considered as concurrent ways of relaxations as compared to the GB shift, their contribution can lead to different GB velocity (or its time dependence: see also Chapter 9.2.) and even to different alloying levels in the same system if e.g. the conditions for the mechanical constraints are different. Thus the large scatter in the experimental data is not surprising, but even could be expected. It is also worth mentioning that formation of new grains, i.e. DIR, as a concurrent way of relaxation, was usually observed typically in the high temperature regime only [27]. Furthermore, it is important underlying that the GB motion is not a continuous shift, but has a stop-and-go character [27][58]: this is an interesting fingerprint of the stress accumulations and subsequent relaxations during the process (Fig. 7.1).

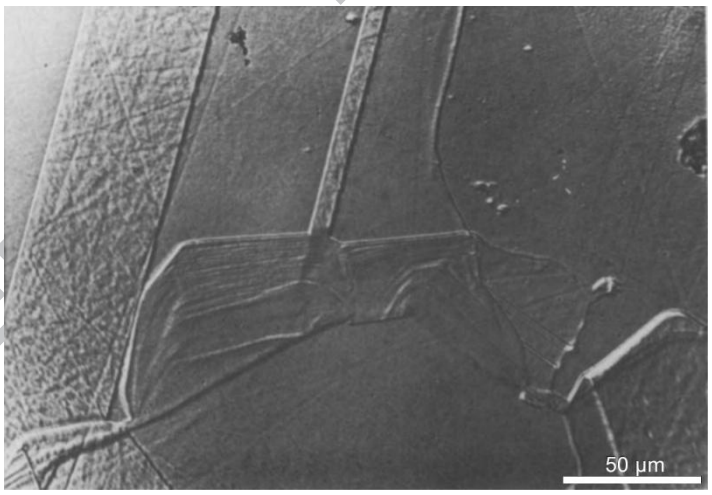

Fig. 7.1 Ghost lines in migrated regions of $Cu_{90}Zn_{10}$/Cu diffused for 40 h at 350 °C, reflecting previous GB positions and indicative of jerky GB motion. (Magnification, 400 x) [27].

In the light of the above general picture it is interesting to consider experimental results on the temperature dependence of DIGM. In this respect first of all the papers by

Grovenor [58] and den Broeder [27] can be referred. Both authors came to the conclusion that two well defined temperature regimes could be distinguished; that in which DIGM occurs alone (at relatively low temperatures) and that in which DIR and DIGM occur simultaneously (higher temperatures). This is in accordance with the above picture.

8. Formation of intermetallic compounds during grain boundary motion (GBDIREAC)

It was pointed out already in the very early time of DIGM and DIR that compound phases can also be formed. Tu [33] has demonstrated that during the solid state reaction between Pb and Ag-20at%Pd the Pb_2Pd compound was formed between 160 and 200^{o}C. Although later on, in almost all cases, the alloy systems studied have been restricted to solid solutions, this work gave a clear indication that not only solid solutions, but intermetallic compounds can also be formed and the question was also raised that whether DIGM-like phenomenon can be involved in the low temperature ordering of certain compounds or not (see also [33]). Kajihara and his co-workers (see [86] and citations therein) have shown that both intermetallic phases were formed, present in the equilibrium phase diagram of Ag/Sn system, during DIR. So it is rather plausible that DIGM/DIR can lead to grain boundary diffusion induced solid state reactions (GBDIREAC). On the other hand, the theoretical description of these reactions is in infancy, since there is a lack of clear involvement of the additional chemical driving force of compound formation in the models of DIGM/DIR. Especially the experimental evidence, accumulated more recently (see Chapter 9.2.2 below), that during solid state reactions at low temperatures (bulk diffusion is frozen out) the thin film diffusion couples always terminate to the phase equilibrium dictated by their phase diagram. In contrast, in systems forming solid solutions the compositions in the alloyed zone are determined by kinetic constraints (see Eqs. (3.15) and (3.24)) and the terminal state is not the solid solution with compositions given e.g. by the initial thickness ratio of the film formed from a pair having complete solubility.

9. Review of experimental data

9.1. Experimental methods

First general technique for the characterization of DIGM kinetics was the metallographic investigation, in which morphological features of the DIGM/DIR were nicely presented. In addition, by this method the determination of the migration distance and thus the shift rate could be easily determined, even in the function of the depth from the initial surface, by gradually removing slides perpendicular to the GBs (see Fig. 2.4). For the determination of compositions in the DIGM/DIR zone electron microprobe techniques were generally employed, combined with either SEM or TEM (see e.g. Fig. 5.1: on which an electron microprobe analysis, carried out in a SEM [3], is shown). In [38] the DIGM zone was investigated by SEM, TEM and STEM, equipped with energy dispersive X-ray spectrometer in Au/Cu and Ag/Au thin film diffusion couples. Fig. 9.1.1 illustrates another example. Here STEM micrograph of an alloyed zone in the wake of a migrating [111] tilt boundary in the gold layer of a Cu/Au/Cu thin film specimen after 137 h anneal at 150^{o}C [38] is shown. This also nicely demonstrates the problems, accompanied by this type of analysis: the composition profile obtained is a certain average over depth and the averaging extends to approximately 1μm, or in thin film specimens the averaging is over the foil thickness [38]. Thus, in the profile in Fig. 9.1.1 there is an instrumental convolution of the data (and perhaps it is the reason of the tailing off the profile at the final boundary position, where it is expected that the true profile is a step function).

In addition to the above methods, depth profiling, with chemical analysis of the composition in the removed layer, can also be used to study the time dependence and temperature dependence of DIGM averaged over many random boundaries in the same specimen. Thus, already in 1982, Auger Electron Spectroscopy technique was employed

to provide information supplementary to the results of the more detailed TEM and STEM studies [38]. With this technique the profile is obtained by continuously sputtering the material away with an ion beam while simultaneously analyzing the composition of the surface layer by Auger Electron Spectroscopy. Information about the extent of the alloyed zones could then be obtained from the average concentrations measured in the profiling.

For the time being structural investigations are normally taken out by transmission electron microscopy (TEM), selected area electron diffraction (SAED), and X-ray diffraction (XRD).

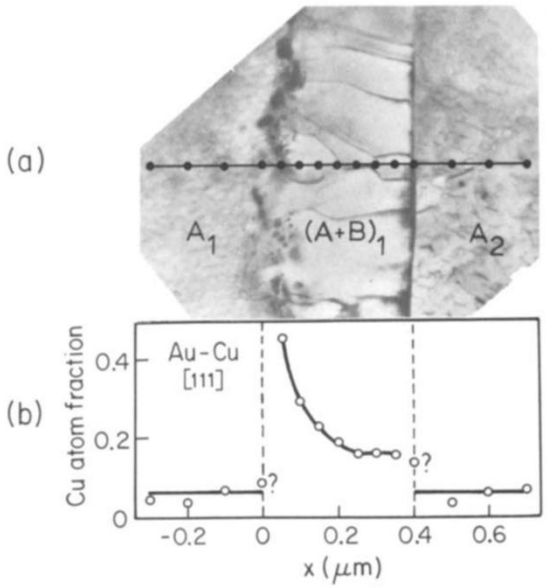

Fig. 9.1.1 (a) STEM micrograph of an alloyed zone in the wake of a migrating tilt boundary in the gold layer of a Cu/Au/Cu thin film specimen after 137 h anneal at 150°C. Specimen viewed along normal to surface of thin film. Points along horizontal line mark the locations of individual X-ray microanalyses. (b) Results of STEM X-ray microanalyses across the alloyed zone in (a). The two question marks indicate the regions where large concentration gradients were expected. The apparent values of the

copper concentrations resulting from the X-ray analyses in these regions are unreliable (see also the text) [38].

In the bi-layer systems, with a noticeable difference between the lattice parameters, misfit dislocation (MD) networks can be formed at the interface, as well as moiré fringes with the period, which depends on the lattice spacing difference. They can be easily observed by TEM. During interdiffusion, when the spacing of the conjugated lattices becomes similar, the periods of MDs and moiré fringes increase, and finally disappear completely. This fact allows the reliable identification of the areas with different stages of interdiffusion [87]. The crystallite size and lattice strain in the grains can be determined using the X-ray peak broadening techniques. X-ray diffraction peaks are broadened both due to the small grain size and lattice strain in the material. The individual contributions of these effects to the total broadening can be separated using standard techniques and these may be found in Refs. [88] [89] [90][91]. Most commonly the crystallite size is approximated by measuring the Bragg full width at half maximum (FWHM) and using the Scherrer formula [92]:

$$d = \frac{0.9\,\lambda}{B\cos\theta}, \tag{9.1}$$

where d is the crystallite size, λ is the wavelength of the X-radiation used, B is the FWHM, and θ is the Bragg angle. This method can give correct approximate values only if proper corrections for instrumental and strain broadening have been made.

Since the lattice parameters of the binary alloys vary with composition, high-angle X-ray reflectometer in Bragg–Brentano (θ-2θ) geometry can be used to determine preferred compositions and its variation with the film depth.

As an example we refer to [93] as a very careful investigation in which detailed analysis of stresses developed in Cu/Ni thin film system was carried out. Here the microstructural development and the stress evolution during diffusion annealing have been investigated employing ex-situ and in-situ X-ray diffraction, transmission electron microscopy and Auger-electron spectroscopy (in combination with sputter-depth profiling).

For the detection of kinetics of DIGM during cold homogenization in thin bi-layered metal films one can use electrical resistance measurements as well, which are very sensitive to any variation of the film composition. Formation of alloys during GB interdiffusion can lead to well-noticeable change of the resistance [94] [95].

Besides the Auger depth profiling there is another possibility to follow the compositional changes in thin nanocrystalline films as it is illustrated in Fig. 9.1.2. Recently the composition profiles were determined by Secondary Neutral Mass Spectrometry, SNMS, during depth profiling (see e.g. [48][60][94][96] [97] [98] [99] [100]). In the SNMS device, the primary ions are extracted from the rf-Ar plasma by means of negatively biased sample. The plasma density corresponds to extractable Ar+ current densities of 1 –5 mA/cm^2. The ion current has high lateral homogeneity. The low primary ion energies (in the order of 100 eV) and the homogeneous plasma profile result in an outstanding depth resolution (<2 nm) [98] [101]. In this case, the detection limit of the SNMS is about 100 ppm [101][102]. The concentration-depth profiles can be measured by transformation of the raw SNMS data (intensity vs time) to concentration-depth profiles, measuring the depth of the crater by means of a profilometer after different annealing times.

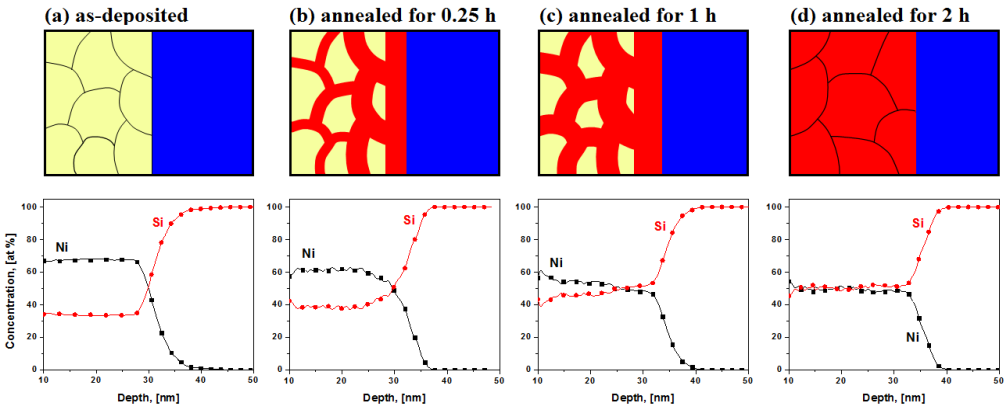

Fig. 9.1.2 Schematic view the time evolution of the growth of *NiSi* reaction product by GBDIREAC mechanism (upper row) if the nanocrystalline Ni_2Si film is deposited on a (single crystalline) substrate and the GB diffusion of substrate atoms result in the formation of the reaction product. The bottom row shows the time evolution of the composition profiles with increasing time in the case of formation of NiSi phase (red) from the Ni_2Si nanocrystalline film (yellow) deposited on a single crystalline Si substrate (blue) and annealed at 180^{o}C (see also [94]). In this case the terminal value corresponds to the composition in the DIGM (GBDIREAC) zone. The compositions were determined by SNMS depth profiling method (see the text).

9.2. DIGM at low temperatures (bulk diffusion is frozen out)

9.2.1. Systems forming solid solutions

As it was mentioned in the previous Chapter, the SNMS depth profiling technique is a very useful tool for investigation of the time evolution of the average compositions on both sides of a nanocrystalline A/B thin film system. It is expected in this case that the system first will develop to reach the atomic fractions predicted by equations (3.15) and (3.24), i.e. first the system will reach a state determined by these kinetic constraints. But in completely miscible binary systems, since after the above

first step there will be still a composition gradient present ($c'_{ASt} > c'_{BSt}$, if $c'_{Ao} = c'_{Bo} = 0$ at the beginning), a next stage of DIGM is expected with initial compositions corresponding to solute contents given by Eqs. (3.15) and (3.24) for $c'_{Ao} = c'_{Bo} = 0$. Thus, in principle a cascade of composition development is expected until the system will terminate at a homogeneous alloy with composition given by the ratio of the initial film thickness. This kind of complete cold homogenization, if indeed can be realized, can also offer good test for the investigation of low temperature miscibility gaps in different binary systems.

Thus the results of low temperature DIGM investigations (cold homogenization) in different binary systems will be summarized and we will try to answer the following questions: i) does the first step indeed result in solute contents predicted by Eqs. (3.15) and (3.24), i.e. is the concentration is higher in the component with higher melting point?, ii) does the temperature dependence of the above concentrations follow the dependence predicted from the temperature dependence of the D_A/D_B ratio, iii) does the cascade of composition evolution indeed observed?

It is not inevitably expected that the relations obtained in free standing films for the expected compositions in the DIGM zone are valid for bi-layered (A/B) films because steady state concentration distribution doesn't exist during interdiffusion between *A* and *B*. However, as it is seen in Fig. 9.2.1.1, in the Ag/Au system the concentration distributions after the first annealing (1.5 h), due to accumulation of Au on the surface of Ag film (y = 0) and accumulation of Ag at the Au-Si interface (y = 30 nm) concentration distributions in bi-layered system becomes similar to those in free standing films (see the schematic picture shown in Fig. 3.1 too). This indicates that the diffusion along GBs was fast enough to saturate the diffusant on the other side of the films creating a surface/interface source before the real DIGM process started. Thus one

can use Eqs. (3.15) and (3.24) for the estimation of atomic fractions during interdiffusion in bi-layered films.

As it was already mentioned at the end of the Chapter 3.1.2, in general, the expected solute contents in the DIGM zones are rather low if only the mechanism, described by relations (3.15) and (3.24), operates, and these can be considerable only if the D_A/D_B ratio is not considerably different from unity, which is the case for the Ag/Au system (see also below).

Although there are many publications on DIGM in different binary systems, there are only few papers dealing with processes taking place on both sides of the *A/B* thin films (see e.g. [38] and [27]) and, until very recently, most of the articles published results at intermediate or higher temperatures, where the contribution from bulk diffusion cannot be ruled out in DIGM and DIR can also appear [26][58][27]. In the more recent investigation, cited above, on nanocrystalline Au/Ag thin film system at 150^o C [43], from the determination of the depth profiles in both Ag and Au layers by SNMS, it has been demonstrated that the average solute contents in the midpoint of the Au and Ag layers gradually increased (Fig. 9.2.1.1a) and finally arrived at certain saturation values (Fig. 9.2.1.1b), different in Au and Ag. Since the condition $\Lambda > d/2$ is fulfilled, it was assumed that the saturation values of the average solute contents corresponded to the values given by the compositions left behind the moving boundaries. Thus, in this case the interdiffusion led to homogenization in both the Ag and Au layers up to the levels corresponding to expressions (3.15) and (3.24) (see also below). The process was indeed slightly asymmetrical, i.e. the saturation atomic fraction in the faster component (with lower melting point) was always less than in the slower one, as it can also be predicted from the above relations ~~too~~. Furthermore, from the temperature dependence of the above saturation values (Fig. 9.2.1.2) Q_{Au} - Q_{Ag} = 0.17

eV was obtained using relations (3.15) and (3.24) (and making a correction taking into account the amount of the diffusant inside the GBs) in good agreement with tracer GB diffusion data [60] (Fig.9.2.1.3). At the same time the D_{Ag}/D_{Au} ratio changed between 5 and 2.

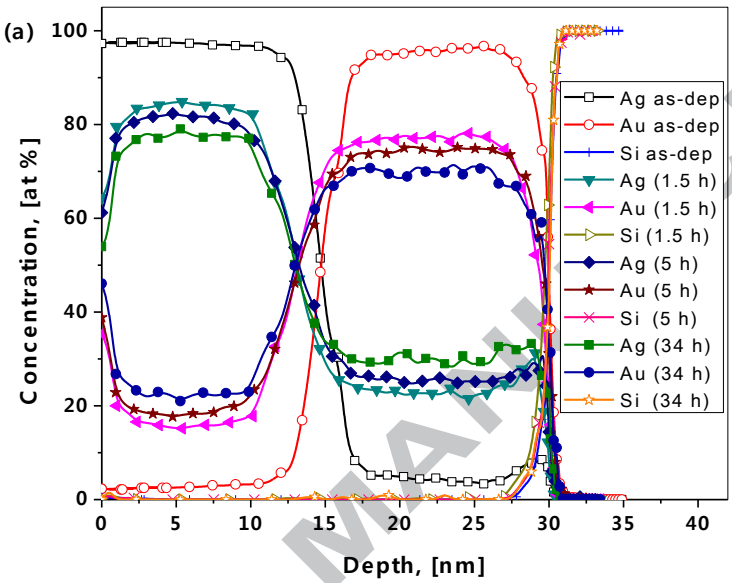

b

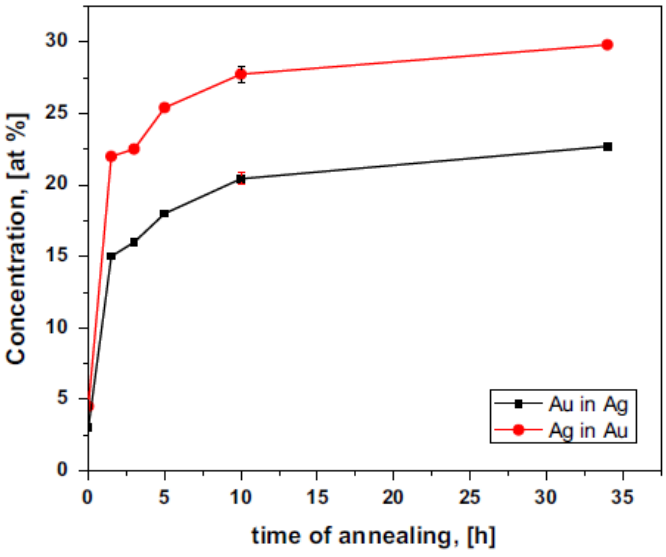

Fig. 9.2.1.1 Concentration-depth profiles in Ag (15 nm)/Au(15nm) bilayer; (a) as-deposited and annealed for different times at 150 ^{o}C, (b) average atomic fraction in centre of the Au and Ag films [43].

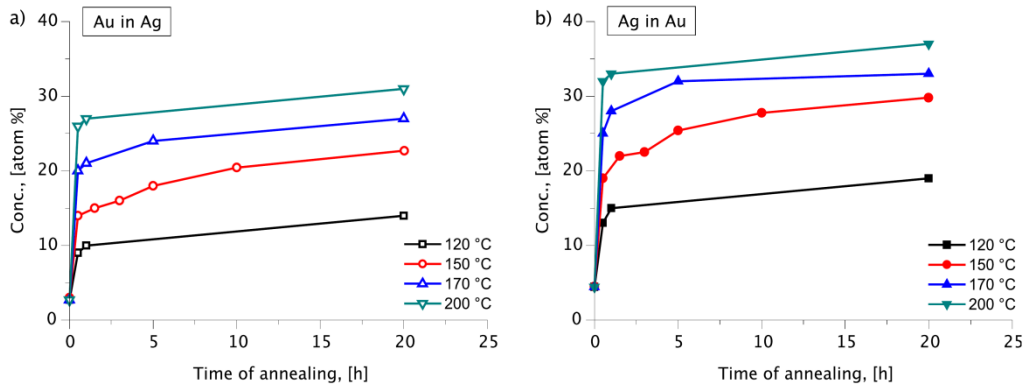

Fig. 9.2.1.2 Average concentration of Au and Ag inside the Ag (a) and Au (b) layers, respectively, versus the annealing time at different temperatures [60].

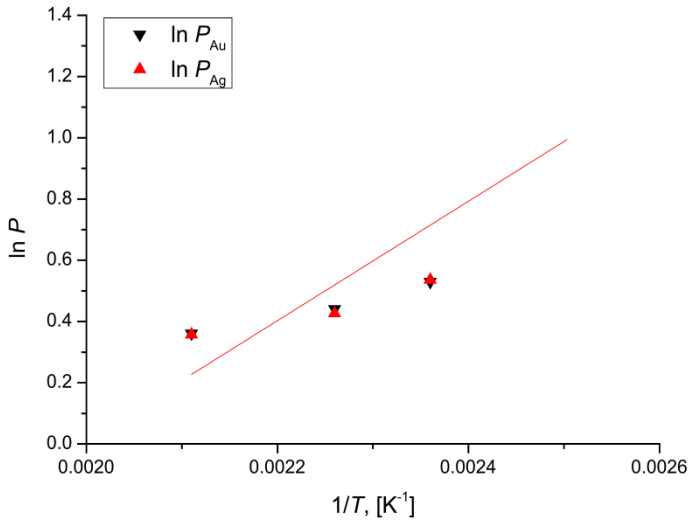

Fig. 9.2.1.3. ln P ($P = D_{Ag}/D_{Au}$) versus $1/T$ in the Ag/Au system. P_{Au} and P_{Ag} are the D_{Ag}/D_{Au} ratios calculated from the saturation values measured in *Au* and *Ag*, respectively [60]. The straight line is the common fit to both data.

From the above results one can conclude that the steady state approximation gives quantitative explanation for the experimental observations in Ag/Au system assuming that the observed leveling off corresponds to the first step of the supposed cascade of homogenization. Furthermore, in the Ag(15nm)/Pd(15nm)/substrate system

similarly a qualitative agreement with predictions obtained from the above relations was found, i.e. the atomic fraction was larger on the Pd-side [60]. In addition, the values of the cocentrations on both sides were smaller than in the Ag/Au system in accordance with the fact that the D_{Ag}/D_{Pd} ratio is about 10 times larger than D_{Ag}/D_{Au} [103].

On the other hand an interesting and surprising result was observed in [60]: if the film sequence was inverted (i.e. instead of Ag/Au/substrate or Ag/Pd/substrate the Au/Ag/substrate as well as Pd/Ag/substrate sequence was applied) the saturation values of the compositions on the slower side (in Au or in Pd) and in the faster (Ag) side were also inverted (see Figs. 9.2.1.4 and 9.2.1.5, respectively). This is in contrast to the above model. Similarly, Fig. 9.2.1.6 shows the SNMS concentration profiles obtained in the Ni(20nm)/Cu(20nm)/substrate system where, since the D_{Cu}/D_{Ni} ratio is similarly larger than unity (like the D_{Ag}/D_{Pd} ratio in the Ag/Pd system), it would be expected that the atomic fraction inside the Ni should be larger than in the Cu. It can be seen that the experimental result is just opposite. This is also in line with the results shown in Fig. 1 of [93], where depth profiles obtained in the Ni(50nm)/Cu(50nm)/substrate system at 175 and 225 ^{o}C showed higher Ni concentration inside Cu than the Cu concentration in the Ni film.

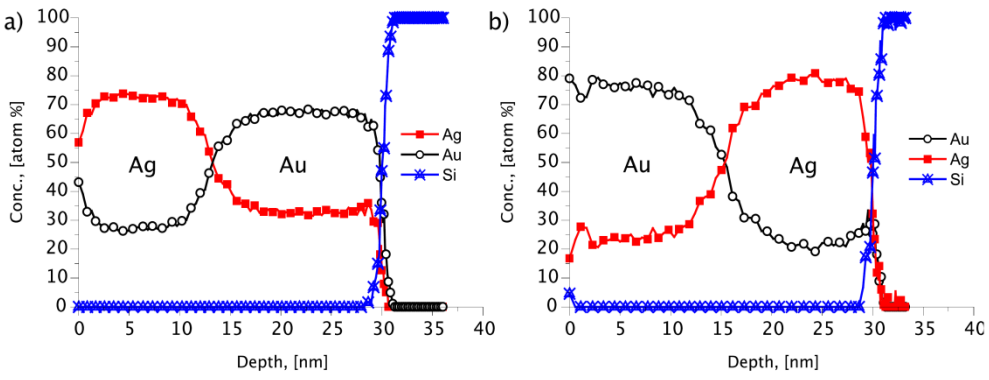

Fig. 9.2.1.4 Depth profiles of Ag(15nm)/Au(15nm)/substrate (a) and Au(15nm)/Ag(15 nm)/substrate (b) film systems after 20 h at 175 °C [60].

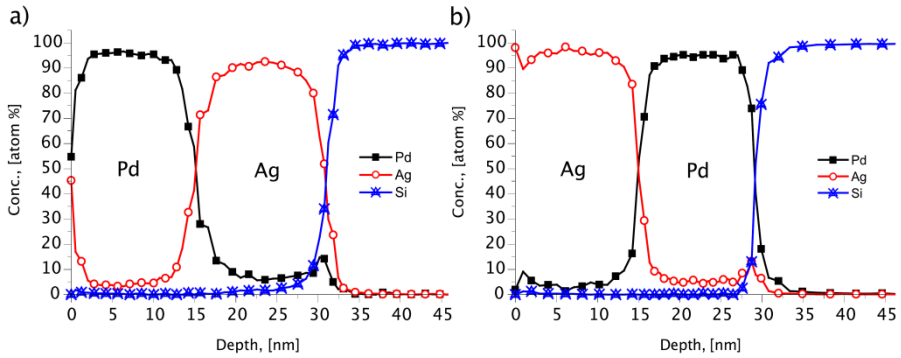

Fig. 9.2.1.5 Comparison of depth profiles obtained after 8 h of heat treatment at 150 °C. (a) Ag(15 nm)/Pd(15 nm)/substrate, (b) Pd(15 nm)/Ag(15 nm)/substrate systems. It can be seen that the reversal of the film sequence leads to the reversal of the inequality of the concentrations in the centre of Pd and Ag layers [60].

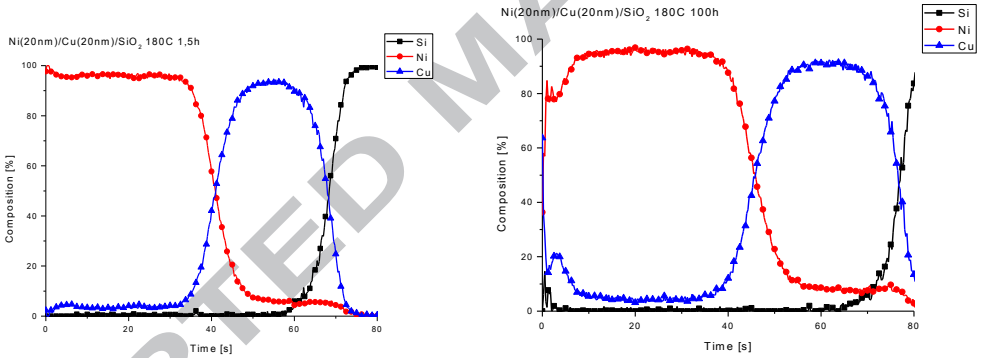

Fig. 9.2.1.6 SNMS composition sputtering time profiles in the Ni(20nm)/Cu(20nm)/substrate system after 1 h (a) and 100 h (b) heat treatments at 180°C. It can be seen that, besides the segregation of Cu at the Ni surface, the saturation value in Cu is larger than in Ni (b).

Thus we can conclude that the above model gives an acceptable description for the atomic fractions in the DIGM zones, if the faster component is outside of the bi-layered film. At the same time it fails to predict the inequality between the concentrations inside the slower and faster components if the slower component is

outside in the thin film couple. One of the possible explanations for this can be the additional stresses related to the incomplete relaxation of stresses created by the unequal GB fluxes: the overall stress development in the two different film systems, due to elastic coupling between them, and between the films and the substrate [60], can change the conclusions obtained by fully neglecting the stress effects.

Indeed, during homogenization of nanocrystalline *A/B* players the expansion of *B* (the slower component) and contraction of *A* is hindered, i.e. a stress field surely develops. Our observations in the Ag/Au system indicate that nevertheless the homogenization can still take place at least up to a certain saturation level. At this moment it is not a fully explored area that whether such stress developments lead to a time dependent transition from Darken's to Nernst-Planck's limit and thus lead to a gradual slowing down of the DIGM velocity and the alloying practically stops at a certain concentration level below those corresponding to the atomic fractions determined by Eqs. (3.15) and (3.24) or such a slowing down is due to other effects. Nevertheless, it was shown in Ag(330nm)/Au(750nm)/substrate thin film system (with an average grain size of about 330 nm in Au) on a rock salt substrate [38] that the average migration distance of the boundaries in Au, Λ, versus the square root of the annealing time, at 250^{o}C showed saturation character i.e. the migration rate decreased with increasing *t* and saturated at about Λ_{max}=55 nm shift (Fig. 9.2.1.7). Interestingly, this curve was just a slight bit different from the same curve obtained on free standing films: in the latter (low constrained) case the slope and the saturation distance was only a little bit larger (by about 10%). This small change is probably related to the fact that from the point of view of the stresses the constraint due to the influence of the substrate is less important than the stresses of different sign rising on the Ag and Au sides of the diffusion couple and present in both high and low constrained cases above. Thus, the

saturation levels obtained in initially pure samples do not correspond to the ones expected for complete intermixing and further mixing takes place only if fresh samples are produced. Thus we can conclude that if the faster component is outside then the stress gradient developed is such that the additional flux created by this would like to compensate the initial difference of the GB fluxes [see Eq. (2)] and, if it can not fully relax, it will diminish the DIGM velocity and will also change the composition in the DIGM zone.

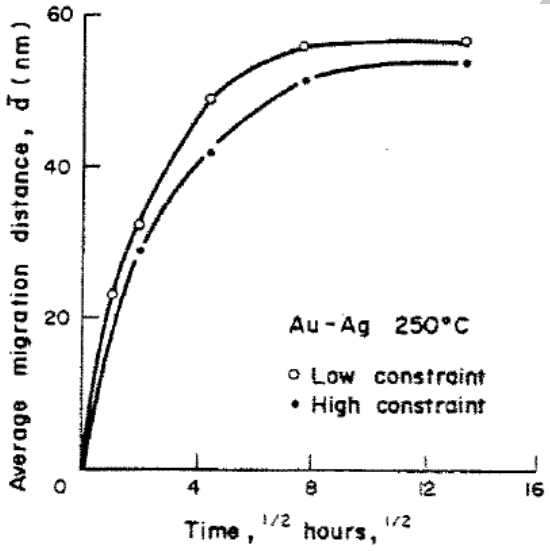

Fig. 9.2.1.7 Average migration distance of boundaries in the gold layer in Ag/Au/substrate specimen as a function of the square root of the annealing time at 250^{o}C [38].

In order to understand better the reason of the slowing down in Ag/Au/substrate system new samples, with approximately the same initial compositions as the observed saturated values at 170 °C, were prepared [60]. The concentration–depth profile of this Ag(27% Au)/Au(31% Ag)/substrate as-deposited sample is shown in Figure 9.2.8a. The sample was annealed at 170 °C for different times and the concentration–depth profiles are shown in Figure 9.2.1.8b. It is clear that there is still intermixing on both sides

reaching higher saturation levels (see Figure 9.2.1.8.c). Thus, the saturation levels obtained in initially pure samples do not correspond to the ones expected for complete intermixing and further mixing takes place only if fresh samples, free of diffusion induced stresses, are produced. In [60], beside the stress effects, constraints due to a finite-size effect were also cited as a possible reason of slowing down. For thin films, the second derivative of the atomic fraction along the GBs should gradually decrease (because of the reflections from the film boundaries) and thus the interface velocity can also gradually decay, since it is proportional to the second derivative of the composition (see also Eq. (3.9.)). Nevertheless, it is interesting that estimations for the saturation values, using expressions (3.15) and (3.24) with initial compositions corresponding to the freshly prepared Au(Ag) and Ag(Au) films in the experiments shown in Fig.9.2.8, gave a very reasonable agreement with the experimental results. Thus the new saturation values indicated that probably the gradual decline of the second derivative is important [60].

We can summarise the above results as

i) in binary films the first step of homogenization results in a composition as predicted by Eqs. (3.15) and (3.24) only if the slower component was deposited onto the substrate. In this case the temperature dependence of the compositions in the alloyed zones followed the expected temperature dependence of the D_A/D_B ratios. In the reversed sequence the concentration in the low melting point component was higher, which contradicts to the predicted inequality of the atomic fractions.

ii) it is observed that the shift of the GBs during DIGM gradually slowed down and stopped at a certain cocentration level

iii) in addition to effects of ii) only the first step of the homogenization cascade was observed, but by preparing a new thin film couple with initial compositions obtained at the end of the first cascade, the next step i.e. further homogenization was observed.

The above deviations from the predictions obtained from the simple steady state approximation, by assuming a full relaxation of diffusion induced stresses, were interpreted with possible accumulation of remaining stress field and finite size effects.

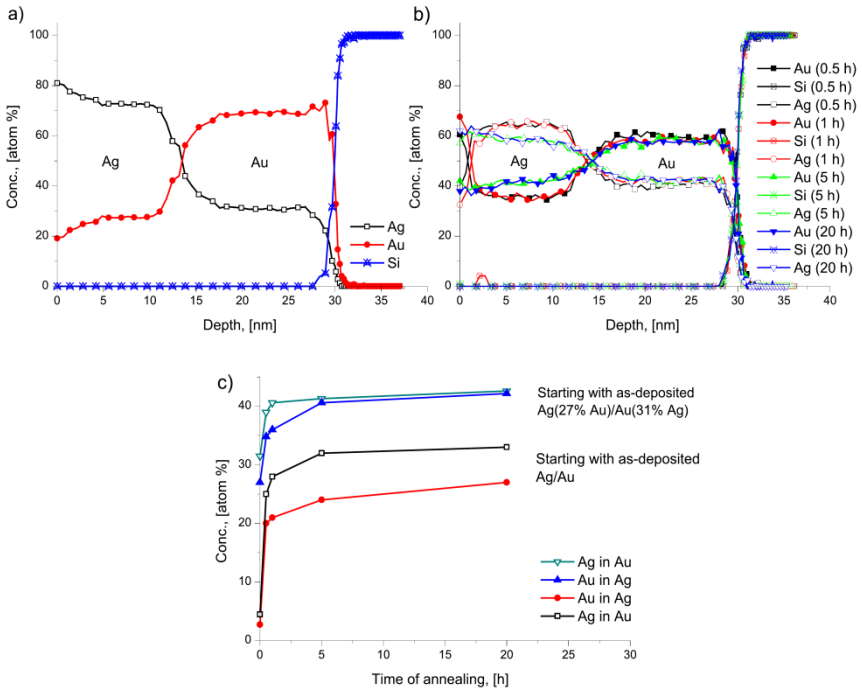

Fig. 9.2.1.8 Concentration –depth profile of Ag(27%Au)/Au(31%Ag))substrate system, (a) as-deposited, (b) annealed at 170 °C for different annealing times and the average concentration of Au and Ag inside the Ag and Au layers versus annealing time at 170 °C in initially pure Ag/Au as well as Ag(27% Au)/Au(31% Ag) bilayers (c) [60].

Let us close this section with two more general remarks;

1) There are opinions in the literature (see e.g. [25] and [104]) that the inequality of the GB atomic fluxes can be sufficient to support the nucleation of new

grains. Such type of DIR certainly would require a different interpretation than that of offered in [26], and there is a lack of clear experimental evidences whether DIR can indeed be observed in the low temperature regimes, where the bulk diffusion can be completely neglected.

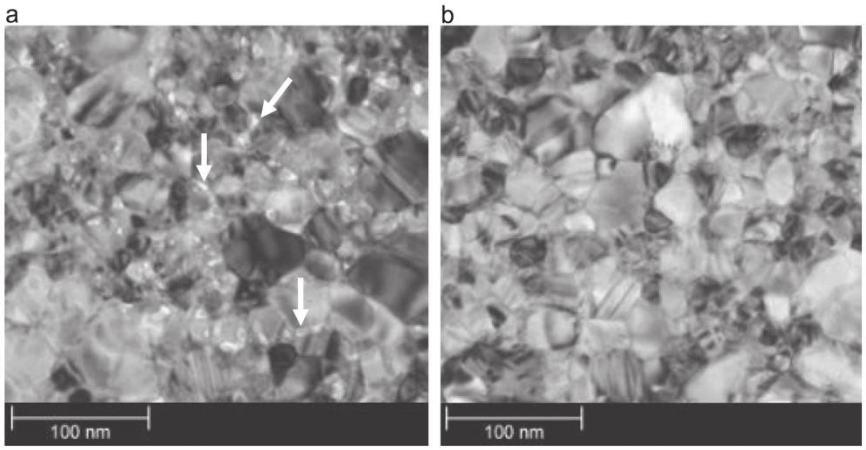

Fig.9.2.1.9 Top view TEM ofAg(15nm)/Au(15nm) bilayer annealed at 150^{o}C for 5h under (a) low (1bar) and (b) high (100bar) pressure [43].

2) It is usually assumed that high angle GBs are very effective sources and sinks of vacancies, thus vacancy super-saturation is not as easy as in the bulk interdiffusion couples. Thus, formation of GB porosity can be less probable as well. Nevertheless, there are observations of GB porosity formation in the literature [105] [106] [107] on a macroscopic (μm) scale and at relatively higher temperatures, and in a the very recent paper nanopore formation along Ag GBs and triple junctions in Ag/Au thin films at 150^{o} C was also published [43]. In this communication a clear experimental evidence was provided on porosity formation along grain boundaries in the Ag film during intermixing in nanocrystalline Ag(15nm)/Au(15nm)/substrate thin film at low temperature (at 150^{o}C), where the bulk diffusion processes were completely frozen out. The porosity formation, in full analogy with the classical

Geguzin's experiment [108] in which a similar small hydrostatic pressure was used to suppress the porosity formation in bulk Cu/Ni diffusion couple, was inhibited by application of 100bar pressure (Fig.9.2.1.9).

9.2.2. Formation of intermetallic compounds by grain boundary diffusion induced solid state reactions (GBDIREAC) at low temperatures

As it was already mentioned in Chapter 8, it was demonstrated already in the very early time of DIGM and DIR that intermetallic compounds can also be formed during DIGM and DIR [33] [86]. Interestingly enough in the past decades investigations in this direction, especially if one compares the huge activity in studying DIGM and DIR in systems forming solid solutions, were relatively rare. It is so even if the research activity on solid state reactions in thin film systems, in which transport along GBs played an important role, was quite high (see e.g. [19] and the reviews [22][20][109][110][111]). In recent years an increased interest raised and new results on cold homogenization by low temperature GBDIREAC were published (see e.g. the reviews [20][112]). This kind of cold homogenization has also a practical interest in cases when production of intermetallic compounds at moderate temperatures is desired. Hence the organization of this (and the next) chapters is as follows. In this chapter, we review those experimental results, in which answers to the following question are found; does the initially binary thin film evolves to the final state corresponding to the equilibrium phase diagram or not? Remember: in case of formation of solid solutions these systems usually arrived at saturation concentrations determined by the kinetic constraints (the ratio of the GB diffusion coefficient) and not to a fully homogeneous state. In the next chapters (Chs. 10.1 and 10.2) important applications will be summarized, including lead free soldering (Ch. 10.1.1), metallization of semiconductor

electronic units (Ch.10.1.2), magnetic data recording (Ch.10.1.3) as well as nanoscale sintering in powder mixtures (Ch.10.2).

Turning back to the problem of the final state of cold homogenization in thin films, in [100] investigations of the cold homogenization of Au/Cu thin films by using depth profiling with a secondary neutral mass spectrometer, SNMS, and structure investigations by XRD and TEM at low temperatures were carried out. It was shown that while the bulk diffusion was frozen, a complete homogenization took place, leading to formation of intermetallic phases. Different compounds formed depending on the initial thickness ratio. The process started with grain boundary interdiffusion, followed by a formation of reaction layers at the grain boundaries that led to the motion of the newly formed interfaces perpendicular to the grain boundary planes. Finally, the homogenization finished when all the pure components have been consumed. The process was asymmetric: it was faster in the Au layer. Fig. 9.2.2.1 illustrates the atomic fractions, corresponding to different film thickness ratios investigated, in the equilibrium phase diagram.

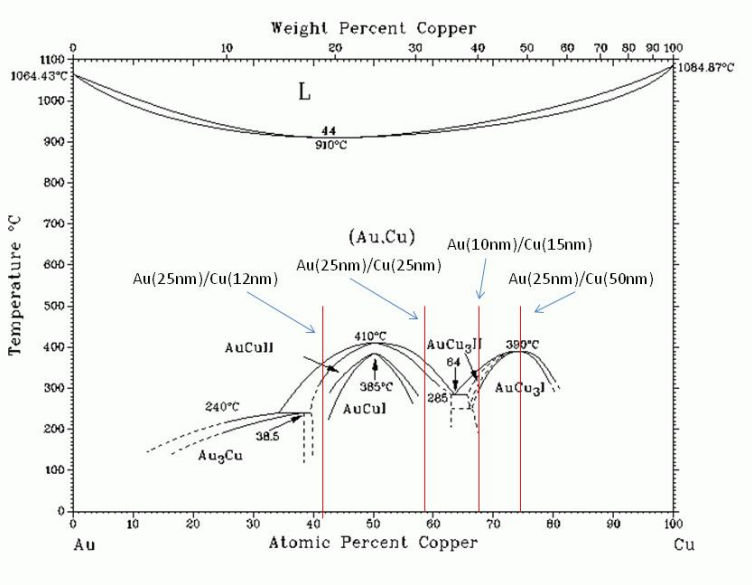

Fig.9.2.2.1 The Au-Cu phase diagram with cocentrations, corresponding to the film thickness ratios investigated in [100].

In Au(25nm)/Cu(50nm) samples the final state is the $AuCu_3$ phase, which is partially ordered (Fig. 9.2.2.2 and 9.2.2.3). Decrease of the film thicknesses, as was expected, resulted in the acceleration of the process, but the final state was the same. Figure 9.2.2.4 illustrates schematically the process.

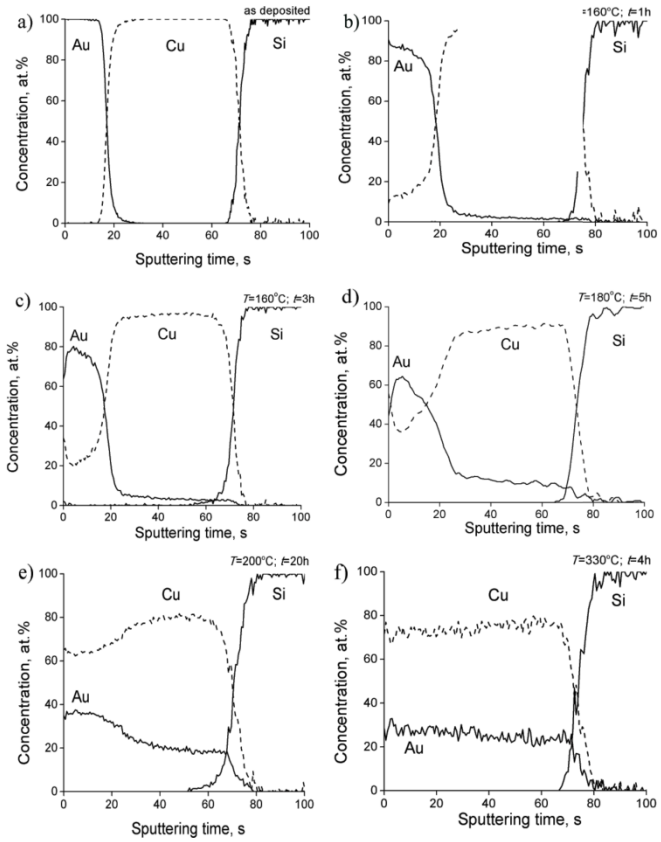

Fig. 9.2.2.2 Concentration profiles of Au(25nm)/Cu(50nm) system a) as deposited sample and annealed b) at 160 °C for 1 h and c) 3 h, (d) 180 °C for 5 h, (e) 200 °C for 10 h, (f) 330 °C for 4 h. It can be seen that the final state is a homogeneous sample corresponding the $AuCu_3$ phase [100].

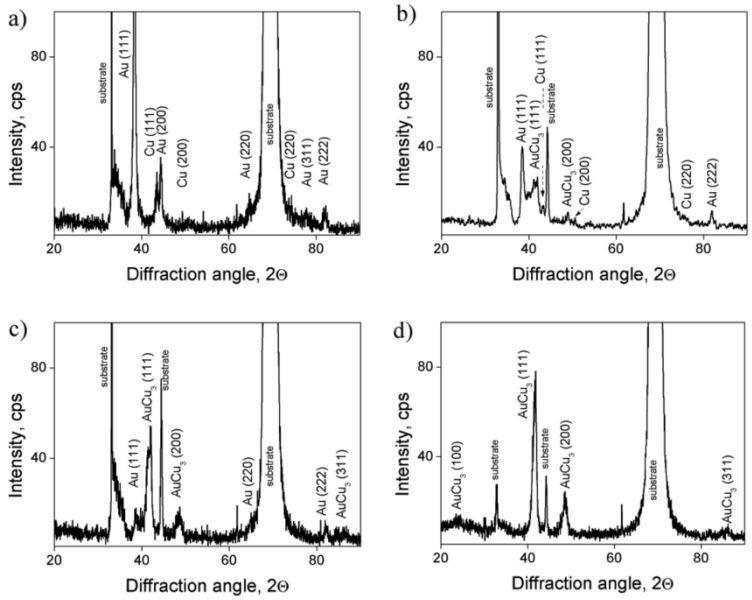

Fig. 9.2.2.3 XRD θ–2θ patterns of Au(25nm)/Cu(50nm) samples a) as deposited, b) annealed at 180 °C for 5 h, c) for 10 h and d) at 200 °C for 44 h. The weak reflection at 23.7°, belonging to super lattice structure in d), indicates that the $AuCu_3$ phase is partially ordered [100].

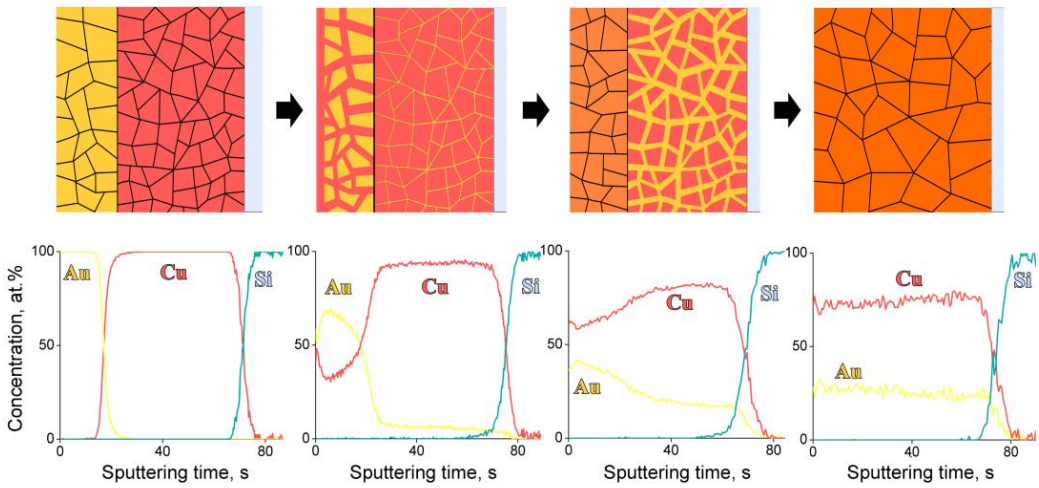

Fig. 9.2.2.4. The upper row shows the schematic picture of GBDIREAC in Au(25nm)/Cu(50nm) system: the cold homogenization takes part first in the Au layer and the final homogeneous $AuCu_3$ state is reached by GBDIREAC in the Cu film.

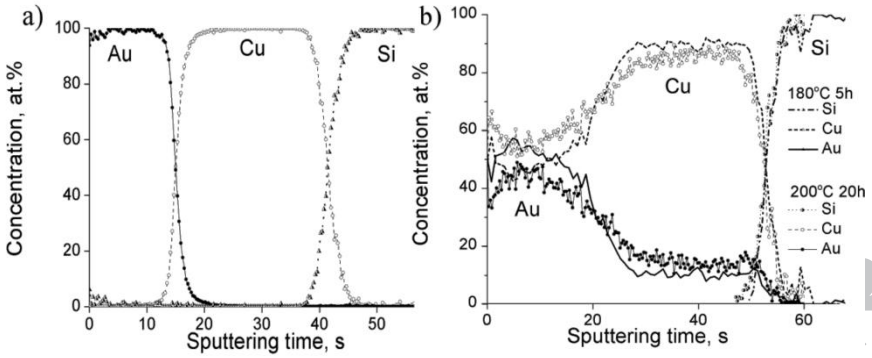

Fig.9.2.2.5 Concentration profiles in Au(25nm)/Cu(25nm) system a) as deposited sample and b) annealed samples [100].

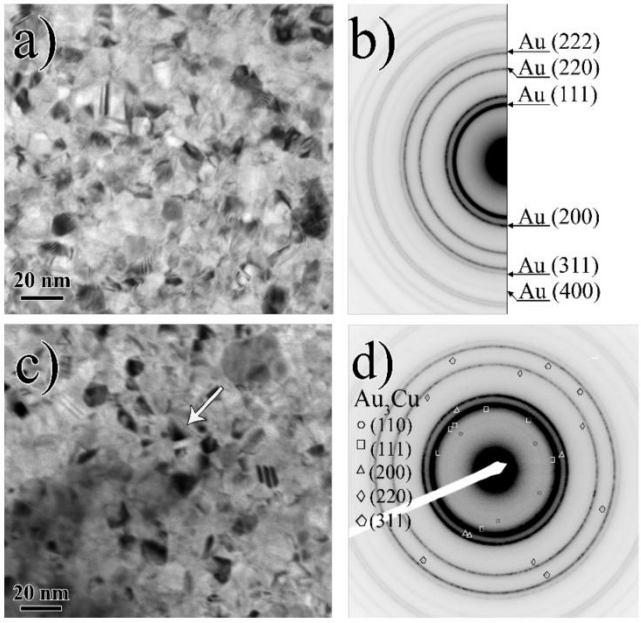

Fig. 9.2.2.6 Bright field (top view) TEM images of Au(10nm)/Cu(15nm) bilayer a) as deposited and c) after 1 h of heat treatment at 160 °C. The arrow indicates the area of formation of a new phase. Selected area electron diffraction patterns: b) as deposited and d) after 1 h of heat treatment at 160 °C [100].

It was also illustrated in [100] that changing the thickness ratio the time evolution also followed a pathway which was directed towards a final state in

accordance with the equilibrium phase diagram. It can be seen in Fig. 9.2.2.5 that in the Au(25nm)/Cu(12nm) sample the process is not fully finished even at 200°C after 20 h: , first (at 180°C after 5 h) a plateau developed in the place of Au with 50-50%at (i.e. the AuCu phase has been formed) which was followed here by a gradual shift of the concentration to get a Cu rich phase (with a mixture of Cu_3Au and CuAu phases) at 200° after 20h. On the other hand, since on the Cu side close to the Si substrate the Au concentration is still about 15% (even at 200°C), which practically corresponds to average composition expected in the very first stage when the Au is still in the Cu GBs and the formation of the GBDIREAC zone would only start later (taking $d=10nm$ for the grain size and $\delta=0.5nm$ for the GB thickness: c_{Au} $(\cong 3\delta/d) \cong 15\%$). The above results were likewise confirmed by TEM investigations. Fig. 9.2.2.6 illustrates this in Au(10nm)/Cu(15nm) thin film. It can also be seen that there was no detectable change in the 10 nm grain size after the heat treatment. The electron diffraction patterns show clear reflections from Au (Fig. 9.2.2.6b) and after annealing additional peaks appeared corresponding to the ordered Au_3Cu phase (these reflections pertained to phase formed near to the Au GBs, as indicated by the arrow in Fig. 9.2.2.6c) .

If the interface velocity is constant, the average cocentration in the centre of the films should linearly increase with time (by gradually consuming the initial material of the grains) and the slope of this function is proportional to the interface velocity, v (i.e. to $6v/d$) [94][112]. By using this simple assumption the interface velocity in both the Cu and Au layers were estimated from the linear increase of the average concentration (Fig. 9.2.2.7) and its value was about two orders of magnitude larger in Au (it was about 10^{-11} m/s) than in Cu.

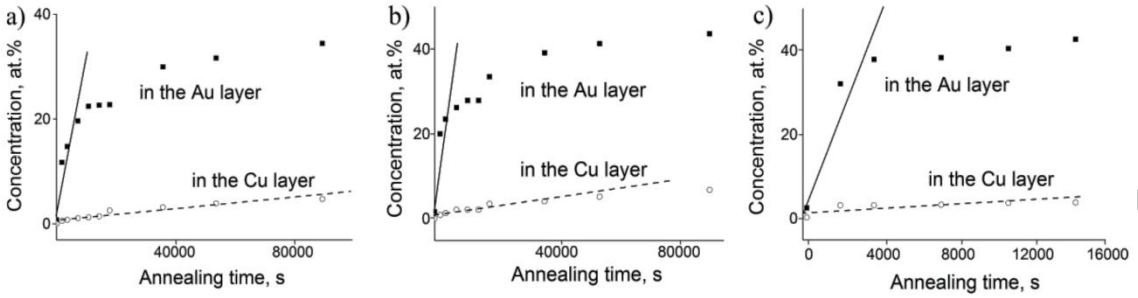

Fig. 9.2.2.7 Dependence of the average concentration of elements on the annealing time at 150 °C in a) Au(25nm)/Cu(50nm), b) Au(25nm)/Cu(25nm) and c) Au(25nm)/Cu(12nm) systems [100].

Similar investigations were carried out in the Pd/Cu systems [48] [99] using the same techniques as in [100] and the heat treatments were carried out long enough to reach saturation. It was found [48] that the final states were in agreement with the equilibrium phase diagram, i.e. mixtures of those phase were obtained which are present in the phase diagram. There were four more observations of [48] and [100], which preserve attention.

The first is that super-lattice reflections of the intermetallics were also present, indicating that the phases formed were at least partially ordered.

Secondly, the grain sizes of the new phases were not considerably different from the initial values of the parent films. This can be an indication that contributions from DIR (when the grains of new phases can be different) and from recrystallisation caused alloying (when grain growth would be observed) are not significant.

Third, the observations that there were practically no continuous thin reaction layers present in the vicinity of the original interface and that in the first stage of such cold homogenization the interface velocity was approximately constant, mean that during such reactions the amount of the new phase should grow linearly with time, indicating a linear growth kinetics. But this linear kinetics is different from the usually

used explanations of linear kinetics in thin film systems (where it is assumed that a planar layer grows linearly with time) and explained by the reaction control at the planar interface. In the case of GBDIREAC the linear growth rate is simply a result of the linear interface shift.

Lastly, it is interesting that the zone left behind the moving interface always has a solute content, corresponding to one of the phases present in the equilibrium phase diagram and not to an atomic fraction determined by any kinetic constraint (like the D_A/D_B ratio as in the case of systems forming solid solutions). Nevertheless, there is one similarity between the behaviour of the systems forming solid solutions or compounds: DIGM/GBDIREAC is always faster on the side of the slower diffusing element. This can be a strong argument in favour that the unequality of the GB diffusion fluxes produces the primary driving force: first the DIGM/GBDIREAC starts from the GBs of the slower element, because they will be faster saturated by the faster element. Of course, this "rule" can be breached if the two thin films in contact have very different grain sizes: e.g. if the grain size in faster component is considerably larger than in the slow one.

10. Applications

10.1. Thin films

10.1.1. Lead free soldering at low temperatures

Low-temperature soldering is one of the central problems in the interconnection technology for electronic products, mainly due to nanoscale size of the joints. Reliability of any individual joint can control the overall lifespan of an electronic product, and thus the solder joints are known as the weak links in electronic products. Soldering involves chemical reactions between the solder and the two surfaces to be joined together and thus understanding the mechanism and the kinetics of chemical reactions between the solders and bonding elements is very important for interconnection technology. In addition, lead-free solders have been increasing in use due to regulatory requirements, plus the health and environmental benefits of avoiding lead-based electronic components. They are most exclusively used today in consumer electronics. Thus, every efforts was used for the development of lead free soldering technologies [113][114][115][116][117] in the last two decades.

The direct contacts with the solders are the so-called under bump metallurgy (UBM) regions. Copper is the most popular choice for the surface layer of the UBM, mainly due to its good wetting property with solders [114][118]. Among all the binary systems, the Cu–Sn is the most important one in many respects. Ag and Au are used as so-called finishers, whereas Ni is used as a diffusion barrier. During assembly or normal service of the device, the Cu layer can be consumed completely, exposing the Ni layer to the solder. Various lead-free solders can contain In, Zn, Bi, and other easily melted metals, and thus besides Cu-Sn, reactions of bonding metals with the mentioned easily melted metals, such as Au-Sn, Ni-Sn, Ag-Sn, Cu-In, Cu-Zn, Ag-In, etc., are likewise of a great interest for soldering. It is well known that a thin, continuous and uniform

intermetallic layer is an essential requirement for good bonding, and thus the details of the solder/conductor metal interactions are important for the understanding of the reliability of the solder interconnections and for optimization of the soldering.

As the solder joints and adjacent regions can be heated noticeably above room temperature (RT), the kinetics of interphase reactions in the above mentioned systems was repeatedly studied in a wide temperature range [114][115][116].

Formation of intermetallic phases, IMPs, near RT when the bulk diffusion processes were practically frozen, was observed in many above mentioned metal couples. Indeed kinetics of diffusion phase formation in nano-grained thin films, which is active at relatively low temperatures, is of a great interest both for fundamental materials science and numerous technical applications. It was also shown that grain boundary diffusion is a dominant transport mechanism during formation of new phases in dispersed polycrystalline objects [119][120][121]. However, one of the main problems unsolved till now is the interplay between GB diffusion and the kinetics of solid state reaction necessary for the formation of the new phase. Nevertheless it was established that low temperature propagation of IMPs occurs mainly towards the element with the higher melting temperature, as a rule, due to penetration of solder atoms through IMP by GB diffusion [115][122]. During interdiffusion in a thin bi-layer couple, both components rapidly penetrate through the layers and then the average concentration of IMP grows with time [123]. If the solder diffuses in a thick layer of the bonding element (Cu, Au, Ag or Ni), the IMP propagates following parabolic or linear kinetic law, depending on whether the diffusion or reaction limits the kinetics [124] [125].

It is worth noting that some results obtained in different studies concerning the growth direction of the propagating intermetallic phases, their compositions and

possible mechanisms contradict one another [115]. For instance, in the case of Cu–Sn couple, in the first studies [126] it was concluded that the Cu_6Sn_5 (η-phase) grows due to faster Cu diffusion towards Sn and it propagates towards Sn, whereas in other studies [127][128][129] it was shown that Sn diffuses faster and the propagation occurs towards Cu. One can meet similar contradictions in studies of other systems, which are also of interest for soldering [115]. Let us illustrate this by the examples of two systems: CuSn and CuAg, in which not only the compositions of the forming intermetallic phases and their thickening kinetics were determined, but the low-temperature (close to RT) mechanisms of intermetallic growth by GBDIREAC during interdiffusion in thin nano-crystalline films were also investigated recently. Indeed, in recent years, due to new requirements caused by nano-sized technologies, interphase reactions were repeatedly studied at RT as well, because of the effective high diffusivity in thin nano-grained films [130].

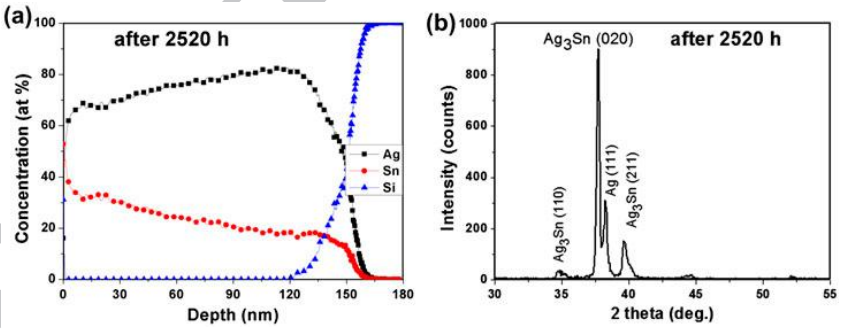

Fig. 10.1.1.1. (a) Concentration-depth profiles of Sn(50 nm)/Ag(100 nm)/SiN sample, and (b) XRD pattern after 2520 h, at room temperature. It can be assured that all Sn has been used up and only a modest amount of Ag remained [123].

In [123] the interdiffusion in Ag/Sn nanocrystalline thin film system (the grain sizes of the initial Ag and Sn films were 27 and 33 nm. respectively) was investigated at room temperature by means of SNMS and XRD techniques. While the final state was

the Ag_3Sn phase (with some remaining Ag or Sn, depending on the initial thickness ratio, Fig. 10.1.1.1), the reaction started already during the deposition process (see Fig.10.1.1.2a).

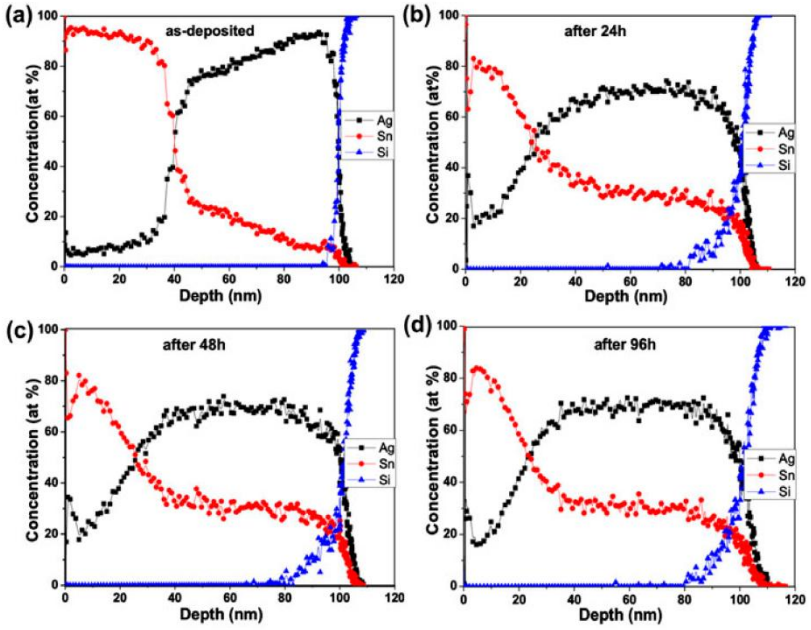

Fig.10.1.1.2 Concentration-depth profiles of Sn(50 nm)/Ag(50 nm)/SiN sample at room temperature: (a) as-deposited, (b) after 24 h, (c) after 48 h, and (d) after 96 h [123].

One day after the preparation, an expressed intermixing is visible: increased Sn as well as Ag concentrations were observed on the Ag- as well as Sn-sides, respectively. With increasing ageing time, the Sn diffuses into the Ag layer more than Ag into the Sn. The Sn concentration in the plateau region in Ag increases with the ageing time and saturates at about 30%, which is near to the equilibrium composition of the Ag_3Sn phase in the phase diagram. Therefore, the homogenization of this phase is reached very easily and some excess Sn remained. It is interesting that in the depth profiles in Figure

10.1.1.2 a small step near to the interface (at about 22 –28% of Sn: see e.g. Fig. 10.1.1.2(a) –(c)) can be observed, and the thickness of which gradually increases with increasing the ageing time. This was interpreted by a GB diffusion controlled planar layer growth (see Fig. 10.1.1.3 which schematically shows, after [131], the similar case of planar growth of Ni_2Si by GB diffusion between Ni and Si). It was found that the growth of the planar reaction layer was parabolic with time, while the other process, taking part in the region far from the initial interface, was attributed to cold homogenization by GDBIREAC. Thus the following interpretation (in accordance also with the observations of [132]), shown schematically in Fig.10.1.1.4, was offered. From the planar growth rate the GB diffusion coefficient was calculated ($1.1x10^{-16}cm^2/s$), as well as the interface velocity was estimated (0.22 nm/h) from the initial slope of the concnetration versus time plots from the GBDIREAC region (similarly as it is shown in Fig. 9.2.2.7).

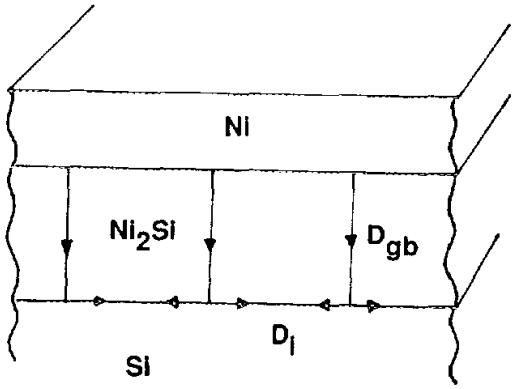

Fig. 10.1.1.3. Schematic model of planer growth of reaction layer by GB diffusion mechanism [131].

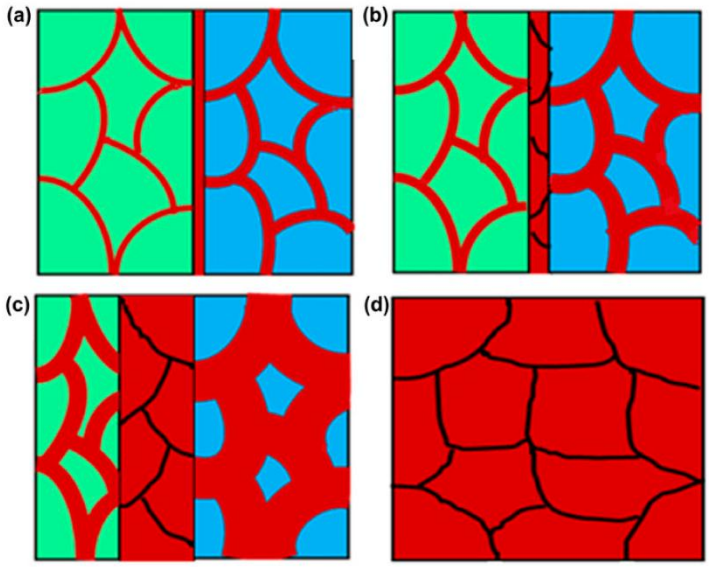

Fig. 10.1.1.4 Sketch of diffusion intermixing of Sn (light green) and Ag (light blue) films forming Ag_3Sn (red) for as-deposited and aged samples at room temperature (black lines illustrate the GBs in Ag_3Sn). The aging time increases from (a) to (d) [123].

On the other hand, very recently the same Ag/Sn thin film system was investigated, but in a different geometry and length scale [125]. In contrast to [123], where finite size effects are always present due to the finite film thickness, here the Sn and Ag films were deposited onto a glass substrate with a small overlap. Thus in this case the lateral propagation of the intermetallic phase could be investigated and no finite size effects set up [133]. One can a bit worry about the contribution of surface diffusion, but it was shown in [125] that these can be avoided by using a thin carbon film as a coverage. It was observed (Fig. 10.1.1.5) that the Ag_3Sn film grows as a continuous layer, bordered with sharp, planar interfaces. The kinetics of the lateral phase spreading obeyed parabolic growth. The important result was that the rate of this was inversely proportional to the grain size of Ag, *d*. For the interpretation of this, the authors used the modified model of [121], assuming that the formation of the intermetallic phase can be controlled either by GB diffusion or reaction rate at the Ag_3Sn interface and taking also

into account the slight deviation of the composition of the Ag_3Sn from the equilibrium values. Finally, they arrived at the following expressions for the time dependence of the thickness of the new phase, λ:

$$\lambda \approx 2\,\frac{C_1-C_2}{C_1}\frac{\Omega}{\omega}\beta t, \qquad (10.1.1.1)$$

for reaction control and

$$\lambda^2 \approx 4D\delta\frac{C_1-C_2}{C_1 d}\frac{\Omega}{\omega}t \qquad (10.1.1.2)$$

for GB diffusion control. Here $C_1 - C_2$ is the existence range of Ag_3Sn in the phase diagram, ω is the average atomic volume in the compound, Ω is the atomic volume per Ag atom in the Ag_3Sn phase ($\Omega=\omega_{Sn}+3\omega_{Ag}$), and β is the reaction rate coefficient. It can be seen that Eq. (10.1.1.2) indeed gives that the growth rate is inversely proportional to the grain size, *d*. Using Eq. (10.1.1.2) the values of the GB product $D\delta$ were calculated and it was found that it had Arrhenius type temperature dependence ($D=8.1x10^{-14}exp[(-55.4$ kJ/mol$)/RT]$. It is an interesting question how these results can be related to those of [123]? First, one has to realize that the length scales are different (nm versus μm), and if the GBDIREAC is active on the side of the Ag the approximately planar front between the Ag_3Sn and Ag can be the result of the knitting of the GBDIREAC zones and the whole growth process is indeed can be controlled by the GB diffusion along the Ag_3Sn interfaces.

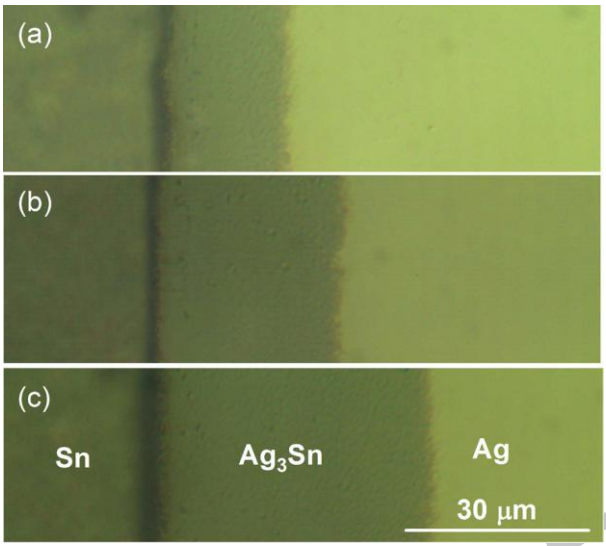

Fig. 10.1.1.5 Optical micrograph on successive stages of Ag3Sn phase propagation during lateral interdiffusion between Ag and Sn films. T = 200^o C, (a) – t = 5 min, (b) – 15 min, (c) – 30 min. Averaged grain size in Ag film l = 106 nm [125].

Investigations, similar to those published in [123], were carried out in the Cu/Sn thins film system [122] at room temperature. From a very similar analysis as shown in the case of the Ag/Sn system, from the planar growth rate the GB diffusion coefficient was calculated ($2.3x10^{-15}cm^2/s$), as well as the interface velocity was estimated (0.5 nm/h) from the initial slope of the concentration versus time plots from the GBDIREAC region. It was emphasized in [122] that the low temperature cold homogenization offers a way for solid phase soldering at low temperatures (even at room temperature), i.e. to produce homogeneous Cu_6Sn_5 intermediate layer of several tens of nanometers during reasonable times (in the order of hours or less).

Thus we can conclude this chapter by emphasizing that using nanocrystalline layers a complete homogenization can be reached during soldering at low temperatures, yet if the understanding of the details of the GB diffusion controlled processes, i.e. the interplay between the planar growth or growth by interface motion perpendicular to the

original interface, still call for further investigations (see e.g. [124]). In very thin bilayered films the GBDIREAC process results in thickening of the IMP layers and thus in the increase of the average concentration within the contacted films. If, however, the film of the bonding metal is thick, the IMP will propagate towards it, because the diffusivity of the solder exceeds markedly the diffusivity of the bonding material.

10.1.2. Metallization (formation of silicides)

Metal silicides play an important role as contact materials in the ultra-large-scale integrated circuits (ULS IC) and complementary metal–oxide–semiconductor (CMOS) technologies [134][135][136][137]. The problem of controllable formation of ultrathin metal silicide films in the sub-10 nm regime represents a chief challenge [138][139][140], since e.g. the scaling of CMOS devices require reproducibly obtained silicide films in the 3–6nm regime. Nickel mono-silicide has many advantages over the other silicides due to its lower resistivity, lower formation temperature, lower consumption of Si during the silicidation process and no resistivity increase in a narrow line [134][135][136][137]. The contacts based on NiSi are usually obtained by solid state reaction between Ni and Si using the self-aligned silicidation process [141]. The preparation of contacts is currently performed in two annealing steps. First, Ni_2Si or Ni-rich phases are formed during a heat treatment by rapid thermal annealing at 280°C (RTA1), and then the not reacted metal is removed by selective etching. As a second step the NiSi phase is obtained after a second high temperature rapid heat treatment at 390°C (RTA2). In addition, during annealing at high temperatures the $NiSi_2$ phase can also be formed, which is a major disadvantage for its integration in devices because of its relatively high resistivity. In these high temperature technologies the phase nucleation and formation is based on a mixed contribution of bulk and grain boundary

diffusion processes during the rapid thermal annealing processes. In [94] a production scheme based exclusively on grain boundary diffusion and low temperature heat treatment, i.e. on cold homogenization was presented. We trace it as a general case work on the application of cold homogenization for production of nanosized thin films of controlled composition and thickness.

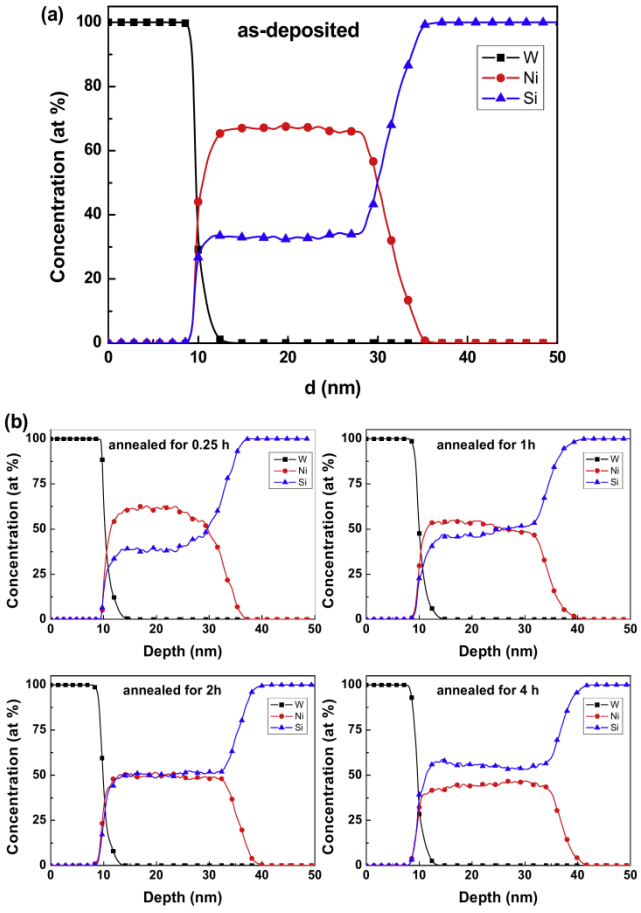

Fig. 10.1.2.1 Concentration-depth profiles of W(10 nm)/Ni_2Si(20 nm)/Si; (a) as-deposited, (b) annealed at 180 ◦C. (The neutral W layer was used as a cap layer to prevent the oxidation) [94].

In [94] this process was reported as a way to obtain thin (5 –20 nm thick) NiSi layers on Si(100) substrate from magnetron deposited Ni_2Si thin films at low temperatures (180–200^{o}C). The time evolution of the transformation was followed by means of

Secondary Neutral Mass Spectrometry, transmission electron microscopy and resistance measurements. It was established that there exist a certain temperature-time and thickness-time windows inside of which the formation of NiSi takes place. Fig. 10.1.2.1 illustrates the time evolution of the cocentration profile at 180°C. It is clear that the as-deposited Ni_2Si film is homogeneous. By increasing the time of annealing, the film is still Ni rich until 1 h, while homogenous NiSi is formed after 2–3 h. It is obvious that there is no formation of planar reacted layer at the initial interface, which would be expected for a "normal (i.e. bulk diffusion assisted) growth".

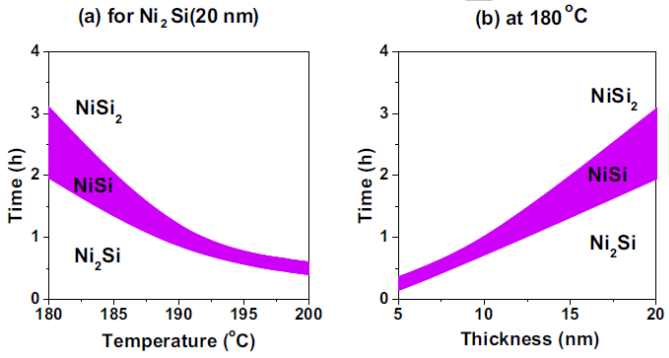

Fig. 10.1.2.2 (a) Temperature-time and (b) thickness-time windows for the formation of NiSi [94].

From the investigation of the temperature and thickness dependence, it was possible to construct the temperature-time and thickness-time windows inside of which the formation of NiSi took place (Fig. 10.1.2.2). It was concluded that the formation of the NiSi phase – instead of nucleating at the original Ni_2Si/Si interface and growing as a compact planar layer with parallel phase boundaries – showed a growth process typical for GBDIREAC. It is worth mentioning that a closer look of concentration profiles between 0.5 and 2 h in Fig. 10.1.2.1 reveals that, simultaneously with the overall

increase of the atomic fraction in the layer, there is a small step in the Si concentration near to the Si substrate, which gradually diminishes with increasing time. This can be the effect of DIR: nearby the original interface the stress accumulation can be strong enough to initiate the formation of small new grains with NiSi composition, similarly as e.g. it was observed in the Au/Cu system [85]. Indeed the cross sectional TEM picture of the as deposited sample (Fig. 10.1.2.3) shows that during, even a very careful preparation, the sample suffered warming up (which can be equivalent e.g. to annealing for about 0.25 –1 h at 180°C), and while the grain size in the 75% of the original Ni_2Si layer is about 5 nm in the vicinity of the Si layer the grain size is much less, as it is expected for new grains formed by DIR. For the schematic view of the time evolution of the process see Fig. 9.1.2 in Chapter 9.1. From the initial linear increase of the atomic fraction in the midpoint of the layer, similarly as it was done on the other systems showing GBDIREAC (see also Fig. 9.2.2.7), the velocity of the interface shift was estimated to be $1x10^{-4}$nm/s.

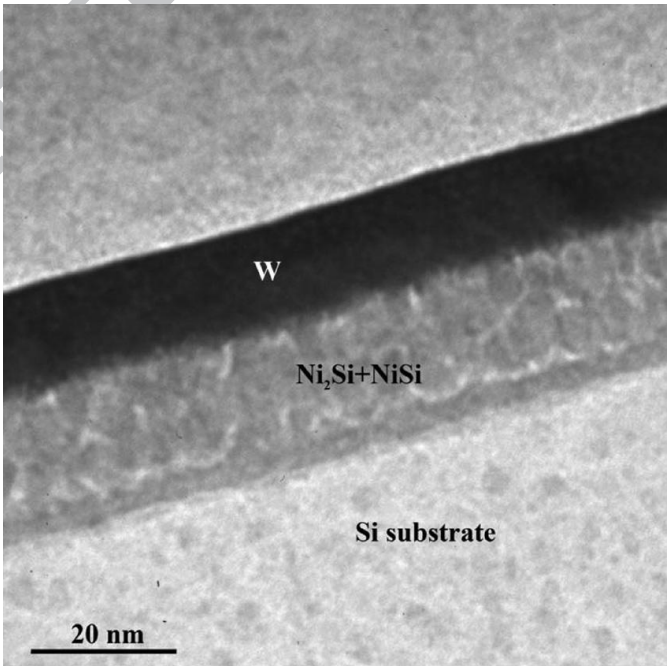

Fig. 10.1.2.3 TEM picture of the as deposited W(10 nm)/Ni2Si(20 nm)/Si sample [94].

In addition to the above results, important comments on the frequently used description of the growth process of silicides was made in [94]. Usually this growth is divided into two regimes: formation or nucleation and growth regimes [109] [142] [143] The activation energy, Q_g, of growth constants, K_g, for the parabolic growth of the Ni_2Si, was equal to the activation energy of the GB diffusion of the Ni (the faster component) indicating that the GB diffusion should have an important contribution [109] [131], even at higher temperatures than those used in [94]. In the formation regimes the nucleation and lateral growth of the nuclei takes place. The picture is much more puzzling here and sometimes even linear growth was observed: this is why sometimes it is called reaction rate control regime. Thus the analysis of experimental data is frequently carried out by the so-called linear-parabolic growth law giving a unified description of the linear and parabolic regimes. Although there were indications in the literature [109][142][144] that the nuclei can be formed and grow not only at the original interface, but also e.g. at triple junctions of GBs, in general not too much attention was given to understand the linear dependence [109]. It is important to mention that using experimental techniques in which only the amount of the product phase is detected as the function of the time (e.g. X-ray diffraction, electrical resistivity, etc.) one cannot know about where the new phase was formed and how it was grown. So the authors of [94] offered a plausible explanation for the linear growth kinetics at low temperatures: if the front velocity is constant, the amount of the product phase should grow linearly with time and the activation energy obtained from this part should be close to the activation energy of GB diffusion. This can also explain why the activation energy, Q_f, obtained from the temperature dependence of linear growth constant, K_f, (in the $x=K_ft$ relation) is a little bit less than Q_g [144] [145]. (According to the reaction rate control it would be expected that $Q_f>Q_g$ [109][142][144][145]). Indeed

the normalized values of the resistance, proportional to the amount of the new phase, showed linear time evolution in this system and yielded similar value for the interface velocity in agreement with the one estimated from the linear time dependence of the concentration in the centre of the reacting layer [94]. In our opinion similar comments apply for other results obtained from investigations of solid state reactions in nanocrystalline systems.

10.1.3. Thin films for magnetic data recording

Nanostructured thin films and heterostructures are at the forefront of fundamental as well as applied research. These systems are used in almost all areas of both everyday life and also in high-tech applications. The family of magnetic materials is a well-known and diverse group for such thin films and heterostructures; magnetic storage applications, sensors, spintronic applications, multiferroics are just a few examples for that. In particular, there is a high demand for magnetic $L1_0$-FePt thin films with high magnetic anisotropy in perpendicular magnetic data recording [146][147] [148][149][150]. In several cases the desired structures are created by post-annealing after deposition by various techniques (e.g. magnetron sputtering, evaporation, PVD/CVD techniques, atomic layer deposition etc.). In most cases, these changes in the structure involve diffusion based processes, thus by exploiting processes like grain boundary diffusion, or GB diffusion induced reaction layer formation, GBDIREAC, low temperature processing could be reached.

In order to get the magnetically favourable $L1_0$ phase, post annealing of the disordered A1-FePt phase [151], growing at high temperature on suitable substrates [152], can be used. Additionally the grain size and crystal orientation (texture) should

likewise be controlled for applications. In order to overcome these challenges several methods have been developed, like annealing in different atmospheres or adding a third element, like Ag [153][154][155][156][157][158][159], Au [153][160][161] or Cu [162][163][164][165][166][149][167]. In all these cases the stress effects (created either by substitution or by diffusion and segregation) are supposed to be the common reason of the decrease of ordering temperature, or the increased ordering at a given temperature [160][168].

Investigation of these processes at low or moderate temperatures can open new pathways for ordered structure formation and can also help understanding the main effects in enhancing the ordering process.

In the past years different structures of Fe/Pt, Fe/Ag/Pt and Fe/Au/Pt thin films have been investigated at low temperatures. In [169] Pt/Fe/SiO_2 and Pt/Ag/Fe/SiO_2 thin films were created by dc magnetron sputtering, and the Pt and Fe layers were 15nm thick, while the Ag layer was 10 nm, when present. These films were then annealed for different times (few hours) at 593K and 613 K. At these temperatures the bulk diffusion could be certainly excluded. The samples were analysed by depth profiling of components using secondary neutral mass spectrometry (SNMS), transmission electron microscopy (TEM) and x-ray diffraction (XRD). The concentration profiles of the Fe/Pt bilayers (Fig. 10.1.3.1) showed that heat treatment at 613K resulted in mixing of the Fe and Pt layers. At longer annealing times the atomic fractions were even higher and the final state was an almost homogeneous FePt layer with about 50-50 at% composition (Fig. 10.1.3.1d.).

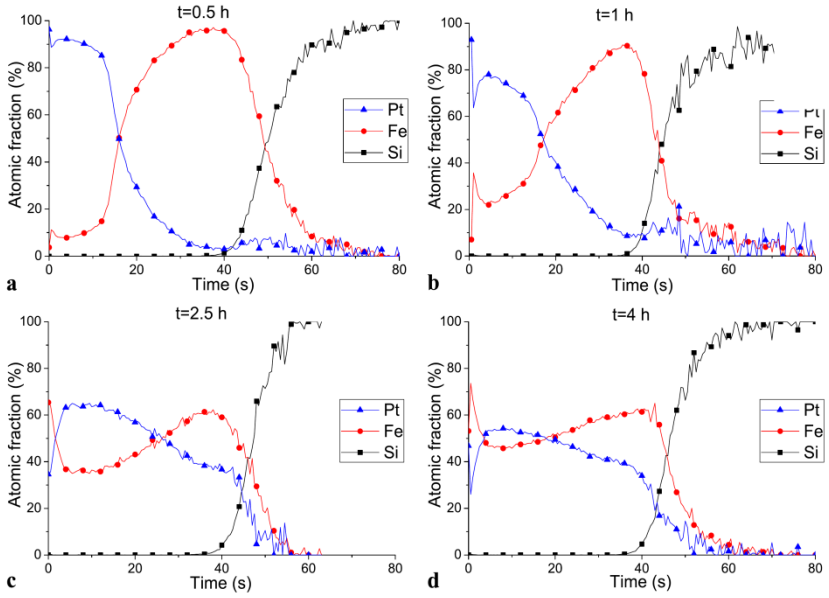

Figure Fig. 10.1.3.1 Composition profiles of Pt(15 nm)/Fe(15 nm)/SiO2 samples annealed at 613 K for different times of (a) 0.5 h, (b) 1 h, (c) 2.5 h, and (d) 4 h ([169])

The same annealing steps were performed on the Pt/Ag/Fe samples (Fig. 10.1.3.2). First the mixing of the Ag and Pt layer was observed, while some Pt appeared in the Fe layer. Further annealing first increased the mixing between the Ag and Pt layers and penetration of Pt into the Fe layer. The final state however was a bi-layer structure with a pronounced almost pure Ag layer at the surface (in place of the original Pt layer) and a homogeneous FePt layer at the substrate (Fig. 10.1.3.2e.). The FePt phase in both cases was at least partially ordered. In case of the Pt/Ag/Fe sample the XRD pattern of the final state showed clear reflexion from Ag which corresponds well to the structure seen in the depth profiles. Notice that the Ag plateau inside the FePt layer in Fig. 10.1.3.2e corresponds to Ag present in the GBs, which can be advantageous in improving the magnetic properties. For more details we refer to [169].

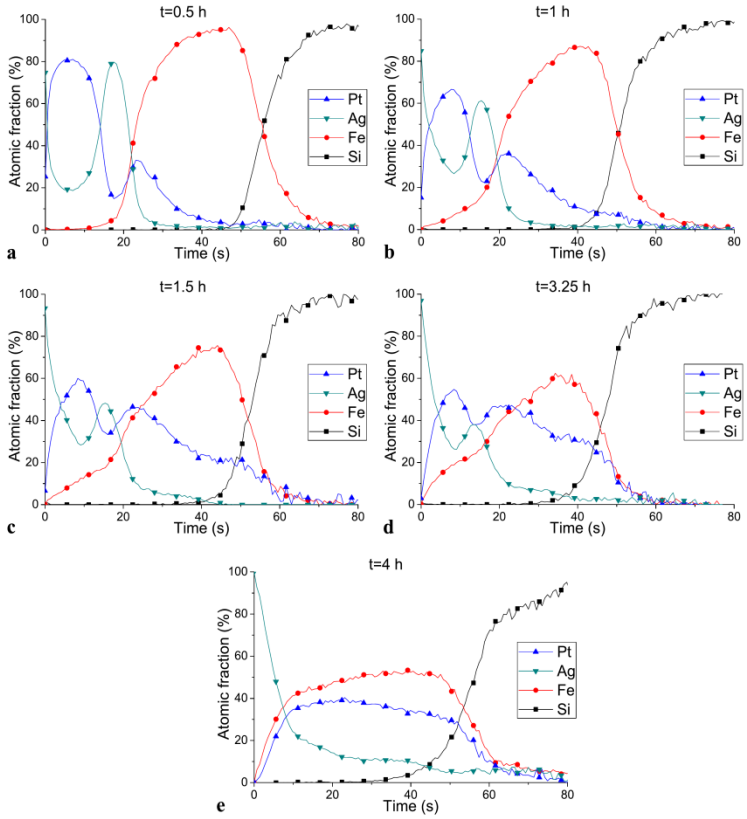

Figure 10.1.3.2 Composition profiles of Pt(15 nm)/Ag(10 nm)/Fe(15 nm)/SiO2 samples annealed at 613 K for different times of (a) 0.5 h, (b) 1 h, (c) 1.5, (d) 3.25 h, and (e) 4 h. ([169])

In [170] Fe/Ag/Pt/SiO_2 samples, having the opposite sequence than the one shown in Fig. 10.1.3.2a, was similarly investigated at both low ($245-390$ °C) and high ($600-900$ °C) temperatures. The samples were analysed in a similar way as in the previous case. The observed process was similar for the two sequences: first the Ag and Pt layers mixed. The Pt content in the Ag layer reached about 30-40 at%, while there is also about 20 at% Ag in the Pt layer after 2.5 h at 300°C (Fig. 10.1.3.3). These values are well above what could be expected from the filling up of grain boundaries only and indicate the formation of the AgPt phase. Up to 2.5h at 300°C this Ag-Pt mixing is the dominant effect, only small penetration of Pt into the Fe layer was detected.

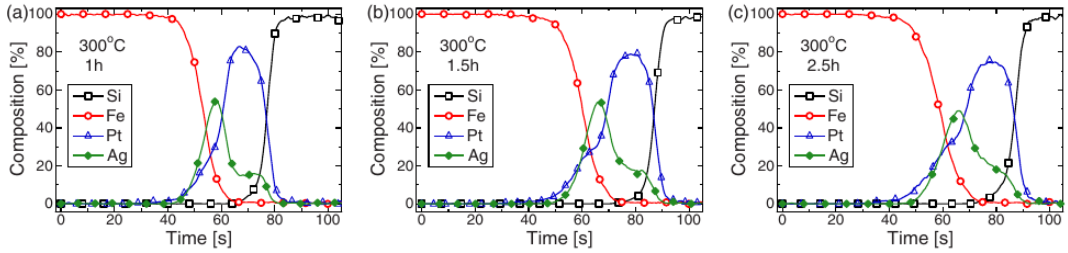

Fig. 10.1.3.3 Composition profiles of the Fe/Ag/Pt films obtained after (a) 1 h, (b) 1.5 h, and (c) 2.5 h at 300 °C. The symbols are for identification of the curves [170].

The more intensive mixing between the Pt and Fe layers started at longer annealing times at 340°C (Fig. 10.1.3.4). The Pt diffuses into the Fe layer, leaving the previously formed AgPt phase, reacting more and more with the Fe, and the Ag layer shifted to the substrate. The resulting structure after annealing at 390°C for 9.5h (Fig. 10.1.3.5) is an almost homogeneous FePt layer at the surface (in place of the original Fe layer) and an Ag layer at the substrate with some Fe and Pt content. The Fe and Pt ratio in the Ag layer is also equiatomic, suggesting the formation of FePt phase in the Ag layer. XRD patterns confirmed the formation of the partially ordered FePt phase, with well detectable Ag peak.

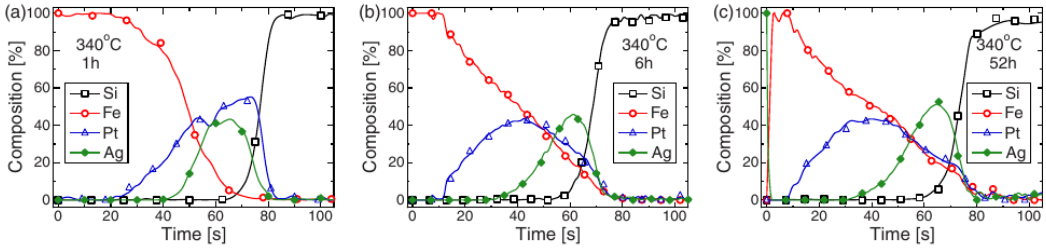

Fig. 10.1.3.4 Composition profiles of the Fe/Ag/Pt films obtained after (a) 1 h, (b) 6 h, and (c) 52 h at 340 °C. The symbols are for identification of the curves [170].

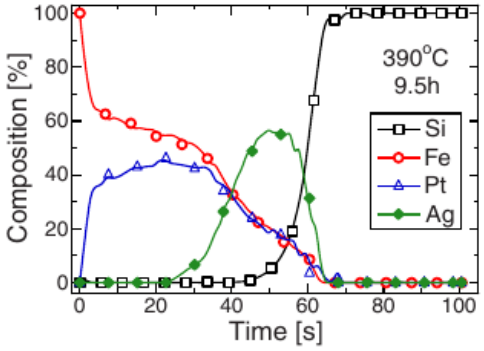

Fig. 10.1.3.5 Composition profiles of the Fe/Ag/Pt film obtained after 9.5 h at 390 °C. The symbols are for identification of the curves [170].

Similar investigations were carried out in Pt/Au/Fe/Al_2O_3(0001) system at 330°C up to 62h [47]. The annealing first resulted in the penetration of Fe into the Au layer and later into the Pt layer. Also Au diffusion into the Fe layer can be seen in Fig. 10.1.3.6a-c. It can also be seen that there is some segregation of Fe at the Pt/Au interface and of Au at the Fe/substrate interface. After 24h annealing there is pronounced mixing between the Au and Fe layer (about 30 at% Fe in Au) and also Fe is present in the Pt layer with more than 20 at% composition (Fig. 10.1.3.6d). Further annealing results in a drastic change of the sample structure, the Au layer shifted to the substrate (in place of the original Fe layer), while the FePt layer formed at the surface. XRD patterns confirmed the formation of FePt (partially ordered) compound layer and the presence of Au layer.

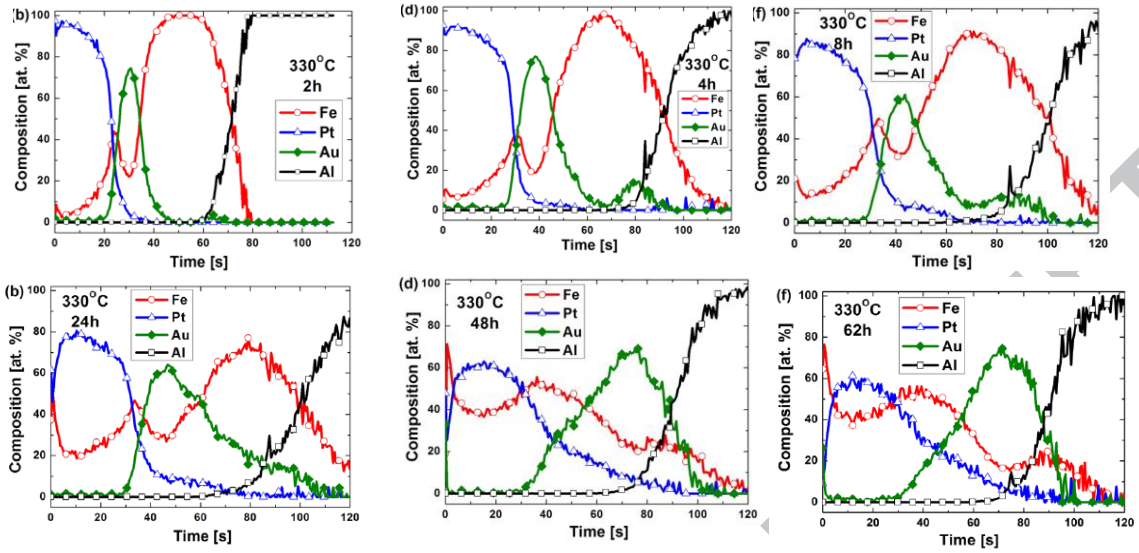

Fig. 10.1.3.6 Composition profiles of the Pt /Au /Fe films after annealing at 330 °C for different times [47].

The above presented results were interpreted with DIGM and GBDIREAC. The obtained depth profiles were similar in both systems (with Ag and Au) in the sense, that there was no phase formation at the original interfaces, supporting that the intermixing and reactions took place by GB diffusion induced effects. First the Fe grain boundaries were filled up by Ag/Au and at the same time the Fe and Pt appeared in the Ag/Au layer. This suggested the formation of FePt along the Ag/Au grain boundaries, which further thickened by the shift of the new FePt/Ag or FePt/Au boundaries. In both cases the Ag as well as the Au layers finally, like markers, were also shifted. The schematic picture shown in Fig. 10.1.3.7 illustrates the details on the example of Pt/Au/Fe samples.

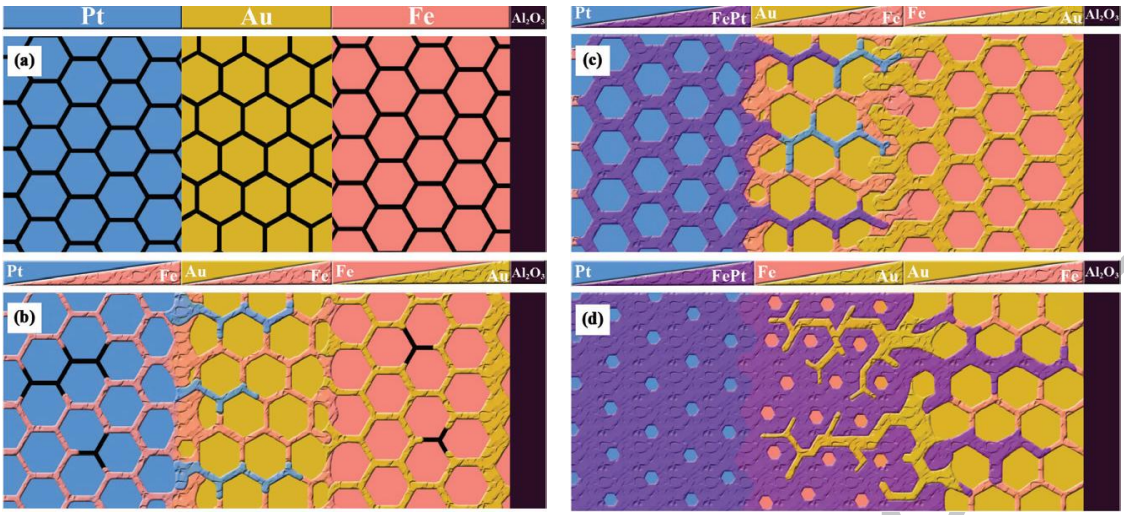

Fig. 10.1.3.7 Schematic view of the structural changes in the Pt /Au /Fe sample developing during annealing at 330 °C: (a) as-deposited, (b) after 4 –8 h (see Figs. 10.1.3.6 (a) and (c)), (c) after 24 h (see Fig. 10.1.3.6e), (d) final state after 62 h of annealing (see Fig. 10.1.3.6f). The colours of the elements are indicated in (a), while the FePt phase is coloured in purple [47].

10.2. Nanoscale sintering processes in binary powder mixtures

It is well known that nanocrystalline materials show increased strength, high hardness, and extremely high diffusion rates [130][171][172]. Many of advanced materials with precisely tailored set of properties for demanding applications can be fabricated by sintering of nanosized powders. The sintering of nano-powders can occur at relatively low temperatures, and this is the main advantage compared to powders of micrometer sizes, which require much higher temperatures for sintering and structural modifications of the compacts. Nanocrystalline materials have been synthesized by a number of techniques, such as the inert gas condensation [173], electro-deposition, plasma processing [174], and mechanical alloying (MA) [175]. The advantage of MA lies in its power to make mass amounts of solid state materials at room temperature using relatively simple equipment [175].

In all these techniques the materials are synthesized in a non-equilibrium state. This departure from equilibrium, as well as the extremely small size of the grains, results in a large fraction of the atoms in the grain boundaries, allow producing enhanced combinations of physical, mechanical, and magnetic properties (compared to materials with a more conventional grain size). To produce such materials, as a rule, a mixture of two or several metals, together with some additions introduced for dispersion hardening or segregation at GBs, is used for sintering and thus data on interdiffusion between these materials and accompanying phenomena become very important for optimization of the process.

We consider here some structural and composition variations caused by interdiffusion in binary (*A* and *B*) nano-powder compacts at low enough temperatures when bulk diffusion is completely frozen out. Two types of objects will be discussed: (i) compacts of nano-powder mixture and (ii) compacts consisting of *A/B* multilayers.

For demonstration of the main regularities, we present, as an example, the experimental results of [21] and [176] obtained at 300^{o}C for 50:50 Cu and Ni nano-powder mixture (powder size of 8-12 nm) and at 400^{o}C for particles with multi-layered Cr-Ni samples, produced by MA of 18 at % Cr and 82 at % Ni powder mixture, having alternating Cr and Ni layers of ~ 5 and 20 nm thick, respectively. The Cu-Ni system is characterized by mutual unlimited solubility of components, whereas the Cr-Ni system has an asymmetric miscibility gap (up to ~35 at.% Cr in Ni). The solid solution formation in the powder mixture compacts and multilayers was detected with standard methods of X-ray phase analysis on the asymmetric shape of diffraction maximum for the solvent component. The samples were annealed at isothermal regime and the duration of annealing was restricted by the condition $(D_v t)^{1/2} \leq a$ (D_v is the bulk diffusion coefficient, a is the lattice parameter).

It was observed that in the Cu-Ni nano-powder mixture with identical sizes of Cu and Ni powders, the solutions were formed on the Cu side. The shape of the Ni diffraction line remained practically symmetric. From the asymmetry of Cu diffraction lines and their variation in the sintering time the average concentration as well as the volume fraction of the solid solutions $\chi(t)$, were determined.

As it is seen from the time dependencies of $C(t)$ and $\chi(t)$ (Fig. 10.2.1), the process of sintering occurs in two stages. At the first stage the volume fraction of the solution rapidly grows ($t \leq 10^3$ s). According to data on the structural evolution, active grain growth occurs at this stage, with the velocity of GB migration of about $V_b \approx 10^{-11}$ m/s. At the second stage ($t > 10^3$s) the volume fraction of solid solution grew slowly with practically constant average concentration ($C \approx 0.2$). The first rapid stage was described by interdiffusion along moving GBs due to recrystallization in nano-compacts, caused by heterogeneous stresses produced by pressing or rolling of the powder mixture, as well as capillary forces. The slower second stage was caused by DIGM when the stresses were produced by the inequality of GB diffusion coefficients (see Section 3). Moving GBs leave solution behind independently of the nature of stresses.

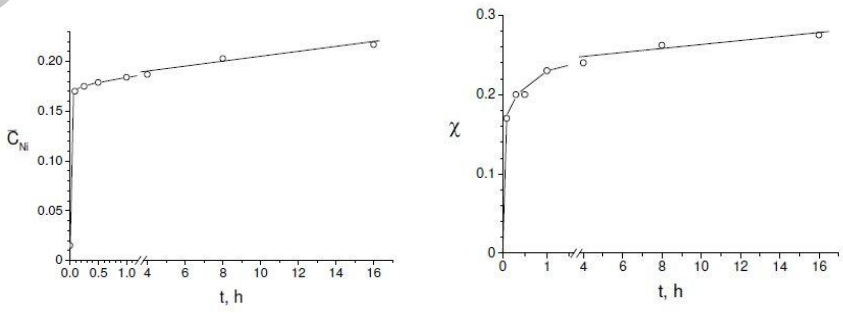

Fig. 10.2.1 Plots C_{Ni} (t) and $\chi(t)$ for Cu-Ni nano-powder compacts at 300°C (from [176]).

A comprehensive model of the above low temperature homogenization in *A-B* nano-powder mixture, available for semi-quantitative kinetic estimations are given in [21]. It is presumed that the disordered A-B powder mixtures can be regarded as being composed of the A and B broken lines (chains) consisting of grains of the same form and surrounded by grains of some other sort. Each GB in the chain can move with the probability 0.5 in one of the two possible directions. Using this scheme of homogenization, the volume fraction of the solution was calculated as a function of time.

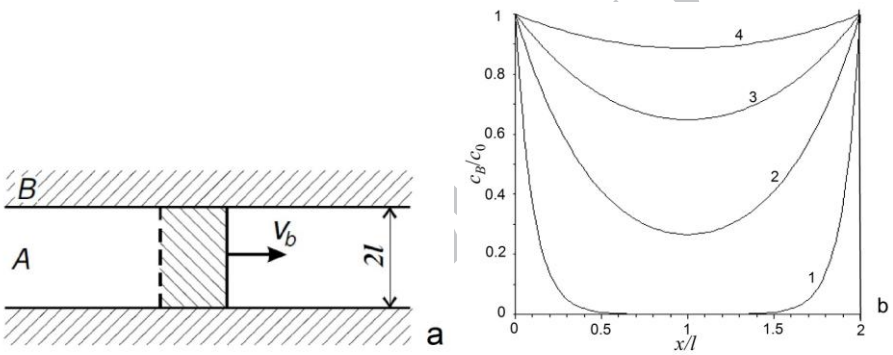

Fig. 10.2.2 a - Scheme of the plate *A* with the GB moving with the velocity $V_b(\equiv v)$. Atoms *B* diffusing into moving GB stay in the grain interior behind the GB.

b – Steady state concentration distribution of atoms *B* in the moving GB calculated for various l/λ: 1 - 0.1; 2 - 0.5; 3 – 1; 4 – 10 [21].

In order to estimate the kinetics at early stages, one can analyze the concentration distribution in the GB migrating with velocity *v*, inside the plate of *2l* width (see Fig.10.2.2a). The diffusion sources of *B* atoms are located at both surfaces of *A* plate. The *B* atoms diffusing along GBs are captured by the bulk after GB displacement for distance δ during time $\tau \approx \delta/v$ and solid solution is formed behind

migrating boundary in the swept region. The diffusion equation (3.3) describing this process can be rewritten in the form:

$$\frac{\partial c_B}{\partial t} = D_B \frac{\partial^2 c_B}{\partial y^2} - \frac{q_B c_B}{\delta} v \qquad (10.2.1)$$

where c_B is concentration of B atoms in the GB and q_B is the parameter explained in Section 3. The second term in (10.2.1) accounts for the leakage of diffusing atoms from moving GB into the grain. With $\partial c_B/\partial t = 0$ steady state condition and $c_B(0) = c_B(2l) = c_0$ boundary conditions the solution of Eq. (10.2.1) is:

$$c_B(y) = c_0\left(\cosh\frac{y}{\lambda} - \tanh\frac{l}{\lambda}\sinh\frac{y}{\lambda}\right) \qquad \lambda = \left(\frac{D_B\delta}{q_B v}\right)^{1/2} \qquad (10.2.2)$$

The parameter λ has the meaning of the characteristic diffusion length. The ratio l/λ controls the diffusion distribution of diffusing atoms inside the GBs and correspondingly the averaged concentration of the solution formed behind the migrating GBs. In Fig. 10.2.2b the diffusion profiles $c_B(y)/c_0$ are presented, which were calculated for different l/λ values using Eq.(10.2.2). Using the reasonable value, $l/\lambda \le 0.1$, the concentration c_B slightly varies along the GB length and the solid solution with practically constant concentration (about $q_B c_0$) is formed behind the migrating GB.

Under the assumption that two adjacent GBs in the chain move in opposite directions, the increase of the average concentration with sintering time was found to be in good agreement with the experiments [21].

It is worth to note that by size variation of the Cu and Ni powders, one can "reverse" the process of solution formation [177]. When the Ni particle size became one order of magnitude smaller than the Cu grains, the solution was formed on the Ni base, in spite of lower GB diffusivity of the Ni-atoms.

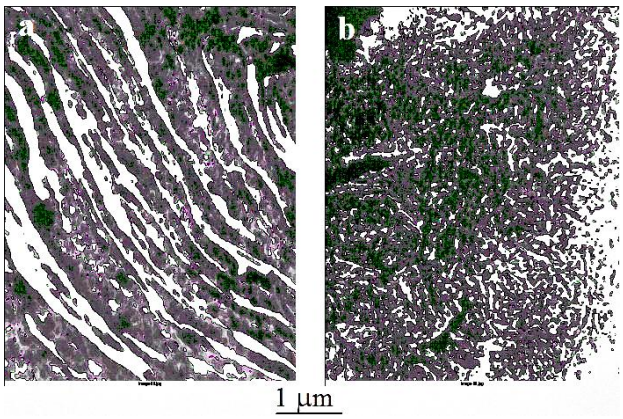

Fig.10.2.3. Decay of layered structure in a compact of MA Ni and Cr powders. a - before sintering; b - after sintering during 30 h at 400°C [178] .

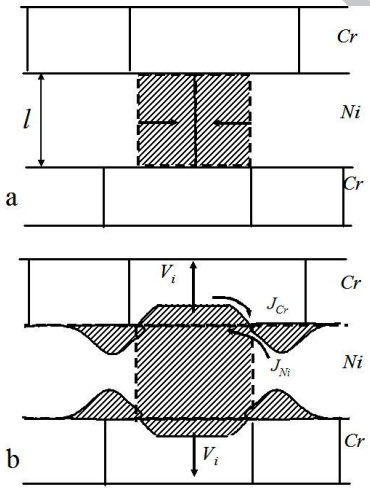

Fig. 10.2.4. Scheme of the decay of layered Cr-Ni structure: a – the solid solution is formed in the hatched grain as a result of motion of two adjacent GBs to one another; b – the interdiffusion fluxes J_{Ni} and J_{Cr} along the interfaces "solution-Cr" and "solution-Ni"

The kinetics in the multilayered Cr-Ni system [178] was similar to that described above (Fig. 10.2.1) for Cu-Ni powder mixtures. At 400°C, with $D \approx 2 \times 10^{-25}$ m^2/s [22] and t = 30 h, the bulk penetration into the grain interior is $(Dt)^{1/2} \approx 1.5 \times 10^{-10}$ m, i.e. smaller than the lattice parameter, and thus the solutions were formed without the participation of bulk diffusion. The increase of the average solution concentration and

the volume fraction with the sintering time took also place in two stages, similarly as it was discussed above. SEM study of microstructure evolution showed that the formation of the solid solution by migrating GBs is accompanied by the decay of the layered structure and by its transformation into homogeneous one (Fig.10.2.3).
to the decay of the layers [178].

In Fig. 10.2.4 the scheme is presented, which explains the mechanism of this phenomenon. Due to the interdiffusion of Cr and Ni along two adjacent GBs inside Ni-layer (Fig. 10.2.4a) the GBs move towards one another, forming the grain of Cr/Ni solution between two Ni-grains. The further growth of this grain is possible due to interdiffusion along the interfaces between the solution formed and the adjacent Cr and Ni layers (Fig. 10.2.4b). Interdiffusion of Cr and Ni atoms in the opposite directions along these interfaces results in their migration with solution formation behind them. The interfaces between solution and Cr layers move outside of solution grains and they become wider. The interfaces in the vicinity of the Ni grains move towards one another leading to separation of solution grain from adjacent Ni-grains. It results in the decay of layered structure with further transformation into a globular one. This process is similar to the well-known decay of thin rods or films under capillary forces [179]. In contrast to that, the decay of the layered structure is in fact caused by chemical force responsible for solution formation. As the solution is formed by DIGM mechanism the degradation of nanolayered structure can be considered as diffusion-induced decay.

Sometimes the degradation of layered structures can essentially lower their functional characteristics, and thus the stability at elevated temperatures becomes an extremely important problem. One of the effective ways for stabilization is doping by nanocrystalline insoluble inclusions embedded between the layers. Nano-inclusions act

as pinning points for moving interfaces, hindering the decay of the layers. For example, the Y_2O_3 particles hindered the decay of multilayered Cr-Ni system [180], as well as the kinetics.

11. Open questions

In this chapter we expose some problems of the low temperature GB interdiffusion and cold homogenization, which in our opinion are still not fully understood or are related to open questions.

11.1. Is the steady state reached or not?

As it was pointed out in Chapter 3.1.1.5 an order of magnitude estimation showed that the saturation by cold homogenization, in films with grain sizes less than about 40 nm, can be reached even before the steady state is established. This indicated that one has to be cautious if the above estimations for the steady state bulk compositions are compared with experimental data, since the expressions proposed for the compositions of the alloyed regions are based on the steady state assumption. Till now, although e.g. in [60] these were used for the discussion of experimental data, there are no experimental investigations directly addressing this point.

11.2. GB velocity decreases with time

It was observed already in 1982 that the migration distance versus the time showed a decaying function [38] (see also Fig. 9.2.1.7), illustrating that at longer annealing times the GB velocity decreases and goes to zero. This behavior still calls for further investigations. In [38] it was also shown that the above function was not considerably different in thin Ag/Au film couples with and without solid substrate. Thus we have argued in Chapter 9.2.1 that the constraint due to the influence of the substrate is less important than the stresses of different sign rising on the Ag and Au sides of the diffusion couple and present in both high and low constrained cases. In addition to the effects of stress accumulation constraints due to finite-size effects can also be important as possible reasons of slowing down. For thin films, the second derivative of the

concentration along the GBs should gradually decrease (because of the reflections from the film boundaries) and thus the interface velocity can also gradually decay, since it is proportional to the second derivative of the concentration (see also Eq. (3.9.)).

11.3. DIR at low temperatures

It is quite a usual observation that a thin alloyed layer forms near to the initial interface (in the near-surface region if the source of diffusant is vapor) and have a fine-grained structure [181][182][183]. This DIR phenomenon was mostly observed at high temperatures, although ~~in the explanation offered by~~ Kajihara [86] ~~he~~ argued that the volume diffusion was frozen out. This model was based on a chemical driving force model, while in [26] the determining role of the coherency strain was proven. In addition, in a next paper from the Kajihara group [183] on high temperature DIR in Cu(Pd) (where the bulk diffusion certainly can not be neglected) the authors argued that the chemical driving force model (with an assumption on the maximum driving force) provided an acceptable explanation. Note that, in contrast to the maximum driving force, in [26] the "selection by fastest growth rate" was favoured. Apart from the above contradictions, it is important to emphasize here the presence of a thin alloyed layer formed near the initial interface. There are some indications (see e.g. [86],[94], [123],[122],[184] and see also Fig. 10.2.1.3) that such a thin layer can also be formed, when other parts of the thin films are homogenized by DIGM or DBDIREAC. Hence the doubt arises: is it possible that the GB diffusion induced stresses alone can lead to nucleation of new grains (free of stresses) and thus lead to relaxation? It is clear from the treatment of [26] that, even with the contribution of the formation of a coherently stressed bulk zone, there exists a certain stress level necessary to break the coherency.

Probably a similar threshold value should exist for DIR initiated clearly by GB diffusion induced stresses alone (if it indeed can be observed).

11.4. Stop and go motion of GBs (meaning of "average" velocity)

It is well known that the GB motion during DIGM has a jerky character [27][58][181][86][185][186]. Note that this is not typical for DIR [86], most probably because of different mode(s) of stress relaxation. Thus, there is a clear problem regarding the meaning of experimentally determined GB velocities in DIGM or GBDIREAC and of course the meaning of the velocities appearing in the theoretical equations. Further complication can be related to the experimentally observed fact that the GB velocity decreases with increasing time. Thus these can only be used in average sense. On the other hand their values, of course with the above restrictions, can provide useful information on the rate of cold homogenization (at least in the initial stage: see e.g. Fig. 9.2.2.7).

11.5. Determination of miscibility gaps in binary phase diagram

It is well known that the diffusion couple technique can be widely used for the determination of the equilibrium phases, or miscibility gaps in the equilibrium phase diagram at fixed high temperatures, where the overwhelming role of bulk diffusion warrants the requested equilibrium in the final state. The question arises: whether thin film couples, implementing cold homogenization at low temperatures, can also be applied similarly as bulk diffusion couples or not? This can be important for the determination of low temperature parts of the phase diagrams. As we argued in Chapter 9.2.2 during GBDIREAC the zone left behind the moving interface always had a composition, corresponding to one of the phases present in the equilibrium phase diagram. This indicates that a positive answer could exist for the above question.

However, regarding the solubility limit (the composition at which a given compound is in equilibrium with the corresponding solid solution) there could be a problem. For example, during solid state reaction in Sn/Ag/Sn diffusion couple (between 433 and 473K) it was observed that although the two compound layers observed were the stable intermetallic compounds in the binary Ag-Sn system, in the region alloyed with Sn by DIR, the Ag phase adjacent to the ς phase-Ag interface the cocentration was smaller than the corresponding solubility of Sn in the Ag phase [86][184] (see y_s in Fig. 2 of [86]). A similar observation was published in nearly ideal Ni/Cu/Ni system [182]. In addition, it follows directly from the model of DIR published in [26] that the solute content in the DIR zone is determined by the critical composition, necessary for the accumulating stress to exceed the theoretical maximum strength of the material and not by the solubility limit.

There are two further facts which can raise further doubts. First, there is a general observation, for systems in which DIR and DIGM were simultaneously observed, that the concentration of the solute is usually greater in the DIR than in the DIGM region, respectively [86][181][187]. Thus, it is not surprising that even at high temperatures in DIGM experiments the concentration of the DIGM zone was always lower than the concentration of the parent phase richer in the solvent (or lower than that corresponding to the activity of the volatile element if the experiment was carried out in the vapour of the fast diffusing component) [182] [179]. The concentration in the alloyed zone is even more clearly different from the solubility limit in case of low temperature DIGM: it is determined by kinetic constraints and the role of finite size effects can also be important.

12. Acknowledgements

The work was supported by the GINOP-2.3.2-15-2016-00041 project. The project was co-financed by the European Union and the European Regional Development Fund.

References

[1] den Broeder FJ. INTERFACE REACTION AND A SPECIAL FORM OF GRAIN DIFFUSION IN THE Cr-W SYSTEM. Acta Metall 1972;20:319–32. doi:10.1016/0001-6160(72)90024-7.

[2] Balluffi RW, Cahn JW. Mechanism for diffusion induced grain boundary migration. Acta Metall 1981;29:493–500. doi:10.1016/0001-6160(81)90073-0.

[3] Hillert M, Purdy GR. Chemically induced grain boundary migration. Acta Metall 1978;26:333–40. doi:10.1016/0001-6160(78)90132-3.

[4] Shewmon PG. Diffusion in Solids. Switzerland: Springer; 2016.

[5] Mittemejer EJ. Fundamentals of Materials Science. Heidelberg: Springer; 2010. doi:10.1007/978-3-642-10500-5.

[6] Yoon D. Theories and observations of chemically induced interface migration. Int Mater Rev 1995;40:149–79. doi:10.1179/imr.1995.40.4.149.

[7] Blendell JE, Handwerker CA, Shen CA, Dang N-D. Diffusion Induced Interface Migration in Ceramics. In: Pask JA, Evans AG, editors. Ceram. Microstruct. '86 Role Interfaces, Boston, MA: Springer US; 1987, p. 541–8. doi:10.1007/978-1-4613-1933-7_55.

[8] Rabkin E, Ma CY, Gust W. Diffusion-induced grain boundary phenomena in metals and oxide ceramics. Mater Sci Monogr 1995;81:353–69. doi:10.1016/S0166-6010(06)80013-5.

[9] Smith DA, Grovenor CRM. Chemical effects on grain-boundray migration in Si and Ge. Trans Japan Inst Met Suppl 1986;27:969–78. doi:https://ora.ox.ac.uk/objects/uuid:25ca3d2c-1700-4636-996e-1cd822be6b9a.

[10] Mittemeijer, EJ., Beers AM. DISLOCATION WALL FORMATION DURING INTERDIFFUSION IN THIN BIMETALLIC FILMS. Thin Solid Films 1978;48:356–76.

[11] Mittemeijer, EJ, Beers AM. RECRYSTALLIZATION AND INTERDIFFUSION IN THIN BIMETALLIC FILMS. Thin Solid Films 1980;65:125–35.

[12] Kasen MB. An alternative view of diffusion-induced grain boundary motion. Philos Mag A Phys Condens Matter, Struct Defects Mech Prop 1986;54:493-L35. doi:10.1080/01418618608242875.

[13] Handwerker CA, Blendell JE, Interrante C, Ahn T. The potential role of diffusion-induced grain-boundary migration in extended life prediction. Mat. Res. Soc. Symp. Proc., vol. 294, 1993, p. 625–35.

[14] Handwerker CA, Cahn JW. Microstructural Control Through Diffusion-Induced Grain Boundary Migration. Mat. Res. Soc. Symp. Proc., vol. 106, 1988, p. 127–33.

[15] Doherty R. Grain Boundary Motion, Diffusion-Induced. In: Cahn RW, editor. Encycl. Mater. Sci En., Suppl. Vol. 3, Prgamon Press, Oxford; 1992, p. 1695–8.

[16] King AH. Diffusion induced grain boundary migration. Int Mater Rev 1987;32:173–89. doi:10.1179/095066087790150304.

[17] Handwerker CA. Diffusion-induced grain boundary migration in thin films. In: Gupta D, Ho P, editors. Diffus. Phenom. Thin Film Microelectron. Mater., Noyes, Park Rigde, NJ; 1989, p. 245–322.

[18] Shewmon PG. Role of moving boundaries in surface alloying. Trans Japan Inst Met Suppl 1986;27:443–8.

[19] Tu KN. Ch.18 Interdiffusion in Thin Films. Ann Rev Mater Sci 1985;15:147–76.

doi:10.4028/www.scientific.net/MSF.1.133.
[20] Beke DL, Langer GA, Molnár G, Erdélyi G, Katona GL, Lakatos A, et al. Kinetic pathways of diffusion and solid-state reactions in nanostructured thin films. Philos Mag 2013;93:1960–70. doi:10.1080/14786435.2012.732712.
[21] Geguzin YaYe, Kaganovskiy YS, Paritskaya LN. Cold homogenization diring interdiffusion in dispersed media. Phys Met Met 1982;54:120–30.
[22] Kaur I, Mishin Y, Gust W. Fundamentals of Grain and Interphase Boundary Diffusion. Chichester: John Wiley & Sons; 1995.
[23] Van Landuyt J. (Monographs on the Physics and Chemistry of Materials. vol. 32. Clarendon Press; 1997. doi:10.1016/S0025-5408(96)00172-9.
[24] Hillert M. On the driving force for diffusion induced grain boundary migration. Scr Metall 1983;17:237–40. doi:10.1016/0036-9748(83)90105-9.
[25] Doherty R. Diffusive Phase Transformations in the solid state. In: Cahn RW, Haasen P, editors. Phys. Metall., Elsevier Science BV; 1996, p. 1461–8.
[26] Schmitz G, Baither D, Kasprzak M, Kim TH, Kruse B. The hidden link between diffusion-induced recrystallization and ideal strength of metals. Scr Mater 2010;63:484–7. doi:10.1016/j.scriptamat.2010.05.011.
[27] den Broeder FJA. Diffusion-induced grain boundary migration and recrystallization, exemplified by the system CuZn. Thin Solid Films 1985;124:135–48. doi:10.1016/0040-6090(85)90256-1.
[28] Stephenson GB. Deformation During Interdiffusion. Acta Metall 1988;36:2663–83. doi:org/10.1016/0001-6160(88)90114-9.
[29] Beke DL, Szabó IA, Erdélyi Z, Opposits G. Diffusion-induced stresses and their relaxation. Mater Sci Eng A 2004;387–389:4–10. doi:10.1016/j.msea.2004.01.065.
[30] Harrison LG. Influence of dislocations on diffusion kinetics in solids with particular reference to the alkali halides. Trans Faraday Soc 1961;57:1191–9.
[31] Beke DL. Introduction. In: Beke DL, editor. Diffus. Semicond. Non-Metallic Solids, Subvolume A, Diffusion in Semiconductors., Heidelberg: Landolt-Börnstein New Series, Springer; 1998, p. 1-1–21.
[32] Rhines, FN, Montgomery AM. A New Type of Structure in the alfa-Copper-Zink alloys. Nature 1938;141:413. doi:10.1038/141413a0.
[33] Tu KN. Kinetics of thin-film reactions between Pb and the AgPd alloy. J Appl Phys 1977;48:3400–4. doi:10.1063/1.324182.
[34] Cahn JW, Pan JD, Balluffi RW. Diffusion induced grain boundary migration. Scr Metall 1979;13:503–9. doi:10.1016/0036-9748(79)90078-4.
[35] Yoon DN, Huppmann WJ. Chemically driven growth of tungsten grains during sintering in liquid nickel. Acta Metall 1979;27:973–7. doi:10.1016/0001-6160(79)90185-8.
[36] Sulonen MS. On the driving precipitation force of discontinuous and dissolution. Acta Metall 1964;12:749–53.
[37] Penrose O. On the elastic driving force in diffusion-induced grain boundary motion. Acta Mater 2004;52:3901–10. doi:10.1016/j.actamat.2004.05.004.
[38] Pan JD, Balluffi RW. Diffusion induced grain boundray migration in Au/Cu and Ag/Au thin films. Acta Metall 1982;30:861–370. doi:10.1016/0001-6160(82)90084-0.
[39] Chung YH, Shin MC, Yoon DY. The effect of external stress on the discontinuous precipitation in an Al□Zn alloy at high and low temperatures. Acta Metall Mater 1992;40:2177–84. doi:10.1016/0956-7151(92)90135-2.

[40] Beke DL, Erdélyi Z. Resolution of the diffusional paradox predicting infinitely fast kinetics on the nanoscale. Phys Rev B - Condens Matter Mater Phys 2006;73:35426. doi:10.1103/PhysRevB.73.035426.
[41] Smith DA, King AH. On the mechanism of diffusion-induced boundary migration. Philos Mag A 1981;44:333–40. doi:10.1080/01418618108239536.
[42] Jahn RJ, King AH. Vacancy deposition during diffusion-induced grain boundary migration. Philos Mag A 1986;54:L3–7. doi:10.1080/01418618608242872.
[43] Shenouda SS, Katona GL, Langer GA, Daróczi L, Beke DL. Nanoscale Kirkendall porosity formation during grain boundary intermixing in Au/Ag thin film system. Mater Lett 2015;145:67–9. doi:10.1016/j.matlet.2015.01.044.
[44] Klinger L, Rabkin E. Theory of the Kirkendall effect during grain boundary interdiffusion. Acta Mater 2011;59:1389–99. doi:10.1016/j.actamat.2010.10.070.
[45] Shewmon P. Diffusion driven grain boundary migration. Acta Metall 1981;29:1567–72. doi:org/10.1016/0001-6160(81)90038-9.
[46] Schmeltzle R, Giakupian B, T. M, Gust W, Fournelle RA. DIFFUSION INDUCED GRAIN BOUNDARY MIGRATION OF SYMMETRIC AND ASYMMETRIC (011) {011} TILT BOUNDARIES DURING THE DIFFUSION OF Zn INTO Cu. Acta Metall Mater 1992;40:997–1007. doi:.org/10.1016/0956-7151(92)90077-R.
[47] Vladymyrskyi IA, Gafarov AE, Burmak AP, Sidorenko SI, Katona GL, Safonova NY, et al. Low-temperature formation of the FePt phase in the presence of an intermediate Au layer in Pt /Au /Fe thin films. J Phys D Appl Phys 2016;49:35003. doi:10.1088/0022-3727/49/3/035003.
[48] Molnár GY, Katona GL, Langer GA, Csík A, Chen YC, Beke DL. Low temperature homogenization in nanocrystalline PdCu thin film system. Mater Res Express 2015;2:105012-1–8. doi:10.1088/2053-1591/2/10/105012.
[49] Klinger L, Rabkin E. The effect of stress on grain boundary interdiffusion in a semi-infinite bicrystal. Acta Mater 2007;55:4689–98. doi:10.1016/j.actamat.2007.04.039.
[50] Hwang JCM, Pan JD, Balluffi RW. Measurement of grain boundary diffusion at low temperature by the surface accumulation method. II. Results for gold-silver system. J Appl Phys 1979;50:1349–59.
[51] Bokstein BS, Schwindlerman LS. Osmotic effect during interdiffusion in metals. Solid State Phys 1974;16:2381–5.
[52] Herring C. Diffusional viscosity of a polycrystalline solid. J Appl Phys 1950;21:437–45. doi:10.1063/1.1699681.
[53] Geguzin YE, Krivoglaz MA. Migration of macroscopic inclusions in solids. New York-London: Consultant Bureau; 1973. p74-77
[54] Gao H, Zhang L, Nix WD, Thompson CV, Arzt E. Crack-like grain-boundary diffusion wedges in thin metal films. Acta Mater 1999;47:2865–78. doi:10.1016/S1359-6454(99)00178-0.
[55] Daruka I, Szabó IA, Beke DL, Cserháti C, Kodentsov A, Van Loo FJJ. Diffusion-induced bending of thin sheet couples: Theory and experiments in Ti-Zr system. Acta Mater 1996;44:4981–93. doi:10.1016/S1359-6454(96)00099-7.
[56] Brokman A, King AH, Vilenkin AJ. Role of segregation in diffusion-induced grain boundary migration. Acta Mater 2001;49:1–11. doi:10.1016/S1359-6454(00)00320-7.
[57] Rabkin E, Gust W, Estrin Y. On dynamic segregation in the discontinuous precipitation reaction. Scr Mater 1997;37:119–24. doi:10.1016/S1359-

6462(97)00056-0.
[58] Grovenor CRM. Diffusion Induced Grain Boundary Migration in Thin Gold / Copper Films. Acta Metall 1985;33:579–86. doi:org/10.1016/0001-6160(85)90022-7.
[59] Li JCM, Rath BB. A mechanism for the diffusion induced grain boundary motion. Scr Metall 1985;19:689–93. doi:10.1016/0036-9748(85)90027-4.
[60] Molnár GY, Shenouda SS, Katona GL, Langer GA, Beke DL. Determination of the compositions of the DIGM zone in nanocrystalline Ag/Au and Ag/Pd thin films by secondary neutral mass spectrometry. Beilstein J Nanotechnol 2016;7:474–83. doi:10.3762/bjnano.7.41.
[61] Parthasarathy TA, Shewmon PG. Diffusion induced grain boundary migration in NiC alloys. Scr Metall 1983;17:943–6. doi:10.1016/0036-9748(83)90267-3.
[62] Tseng D, Long QY, Tangri K. Hydrogen Induced Grain Boundary Migration. Scr Metall 1986;20:1423–6. doi:10.1017/CBO9781107415324.004.
[63] Rabkin EI, Shvindlerman LS, Gust W. Theory of grain boundary motion during high-temperature DIGM. Interface Sci 1993;1:133–7. doi:10.1007/BF00203602.
[64] Handwerker CA, Cahn JW, Yoon DN, Blendell JE. N. In: Murch GE, Dayananda MA, editors. "Diffusion Solids Recent Dev., Warrendale, PA, PA: TIMS-AIME; 1985, p. 275–92.
[65] Hirth JP, Pond RC. Steps, dislocations and disconnections as interface defects relating to structure and phase transformations. Acta Mater 1996;44:4749–63. doi:10.1016/S1359-6454(96)00132-2.
[66] Nam HS, Srolovitz DJ. Molecular dynamics simulation of Ga penetration along grain boundaries in Al: A dislocation climb mechanism. Phys Rev Lett 2007;99:1–4. doi:10.1103/PhysRevLett.99.025501.
[67] Joseph B, Picat M, Barbier F. Liquid metal embrittlement: A state-of-the-art appraisal. Eur Phys J Appl Phys 1999;5:19–31. doi:10.1051/epjap:1999108.
[68] Bokstein BS, Klinger LM, Apikhtina IV. Liquid grooving at grain boundaries. Mater Sci Eng A 1995;203:373–6. doi:10.1016/0921-5093(95)09830-5.
[69] Glickman EE. Fast penetration of Ga in Al : liquid metal embrittlement near the threshold. Zeitschitft Für Met 2005;96:1204–10.
[70] Rabkin E. Coherency strain energy as a driving force for liquid grooving at grain boundaries. Scr Mater 1998;39:685–90. doi:10.1016/S1359-6462(98)00229-2.
[71] Cahn JW. The kinetics of cellular segregation reactions. Acta Metall 1959;7:18–28. doi:10.1016/0001-6160(59)90164-6.
[72] Tashiro K, Purdy GR. OBSERVATIONS OF CHEMICALLY INDUCED GRAIN BOUNDARY MIGRATION IN SEVERAL "NEW" SYSTEMS. Scr Metall 1987;21:361–4. doi:org/10.1016/0036-9748(87)90229-8.
[73] Rhee WH, Yoon DN. The grain boundary migration induced by diffusional coherency strain in MoNi alloy. Acta Metall 1989;37:221–8. doi:10.1016/0001-6160(89)90280-0.
[74] Baik YJ, Yoon DN. The effect of curvature on the grain boundary migration induced by diffusional coherency strain in Mo-Ni alloy. Acta Metall 1987;35:2265–71. doi:10.1016/0001-6160(89)90280-0.
[75] Cahn JW. On spinodal decomposition in cubic crystals. Acta Metall 1962;10:179–83. doi:10.1016/0001-6160(62)90114-1.
[76] Khachaturyan A. Some questions concerning the theory of phase transformations in solids. Sov Phys Solid State 1967;8:2163–8.
[77] Hilliard J. Phase Transformations. In: Aronson H, editor., Metals Park, Ohio:

ASM; 1970, p. 497–560.
[78] Larche FC, Cahn JW. The effect of self-stress on diffusion in solids. Acta Metall 1982;30:1835–45. doi:10.1016/0001-6160(82)90023-2.
[79] Tashiro K, Purdy GR. The role of volume diffusion in DIGM, a reappraisal. Scr Metall 1983;17:455–8. doi:10.1016/0036-9748(83)90330-7.
[80] Rabkin E. Gradient and coherency strain energies as driving forces for DIGM. Scr Metall Mater 1994;30:1443–8. doi:10.1016/0956-716X(94)90243-7.
[81] Fournelle RA. A Theory for Diffusion Induced Grain Boundary Migration Based on Vacancy Diffusion. Mater Sci Forum 1993;126–128:383–6. doi:10.4028/www.scientific.net/MSF.126-128.383.
[82] Baither D, Kim TH, Schmitz G. Diffusion-induced recrystallization in silver-palladium layers. Scr Mater 2008;58:99–102. doi:10.1016/j.scriptamat.2007.09.030.
[83] Kasprzak M, Baither D, Schmitz G. Diffusion-induced recrystallization in nickel/palladium multilayers. Acta Mater 2011;59:1734–41. doi:10.1016/j.actamat.2010.11.040.
[84] Kruse B, Baither D, Schmitz G. Concentration characteristics of diffusion-induced recrystallization in Cu/CuAu multilayers of varying lattice mismatch. Scr Mater 2010;62:144–7. doi:10.1016/j.scriptamat.2009.10.012.
[85] Hartung F, Schmitz G. Interdiffusion and reaction of metals: The influence and relaxation of mismatch-induced stress. Phys Rev B 2001;64:245418-1-245418–13. doi:10.1103/PhysRevB.64.245418.
[86] Kajihara M. Chemical driving force for diffusion-induced recrystallization or diffusion-induced grain boundary migration in a binary system consisting of nonvolatile elements. Scr Mater 2006;54:1767–72. doi:10.1016/j.scriptamat.2006.01.035.
[87] Kosevich VM, Gladkikh AN, Karpovskyi M V. Klimenko VN. Interdiffusion in two-layer Pd/Ag films II. “Cold” homogenization mechanisms. Interface Sci 1995;2:261–70. doi:10.1007/BF00215172.
[88] Suryanarayana C, Norton M. X-Ray Diffraction: A Practical Approach. New York: Plenum press; 1998.
[89] McCandlish LE, Seegopaul P, Wu L. Determination of the average WC grain size in nanostructured WC-Co powders by Fourier analysis of x-ray diffraction peak shapes. In: Kneringer G, Rodhammer P, editor. 14th Int. Plansee Semin. vol. 4, Reutte, Tyrol, Austria: Plansee AG; 1997, p. 363–75.
[90] Lönnberg B. Characterization of milled Si3N4 powder using X-ray peak broadening and surface area analysis. J Mater Sci 1994;29:3224–30. doi:10.1007/BF00356667.
[91] Aymard L, Delahaye-Vidal A, Portemer F, Disma F. Study of the formation reactions of silver-palladium alloys by grinding and post-milling isothermal annealing. J Alloys Compd 1996;238:116–27. doi:10.1016/0925-8388(95)02174-4.
[92] Scherrer P. Estimation of the size and internal structure of colloidal particles by means of röntgen. Göttinger Nachrichten Gesell 1918;2:96–100.
[93] Sheng J, Welzel U, Mittemeijer EJ. Interdiffusion and stress development in Ni-Cu thin film diffusion couples. Zeitschrift Fur Krist Suppl 2009;30:247–52. doi:10.1524/zksu.2009.0036.
[94] Shenouda SS, Langer GA, Katona GL, Daróczi L, Csik A, Beke DL. Production of NiSi phase by grain boundary diffusion induced solid state reaction between

Ni2Si and Si(100) substrate. Appl Surf Sci 2014;320:627–33. doi:10.1016/j.apsusc.2014.09.071.
[95] Karpovskii M, Kosmachev S, Dudkin V. Apparatus for measuring the anisotropy of specific resistivity of thin films during condensation. Prib Tekh Eksp (in Russ 1983;2:214–22.
[96] Oechsner H. Formation of sputtered molecules. In: Popović M, Krstić P, editors. Phys. Ioniz. Gases, Singapore: World Scientific; 1985, p. 571.
[97] Lakatos A, Erdelyi G, Makovec A, Langer GA, Csik A, Vad K, et al. Investigation of diffusional intermixing in Si/Co/Ta system by Secondary Neutral Mass Spectrometry. Vacuum 2012;86:724–8. doi:10.1016/j.vacuum.2011.07.017.
[98] Lakatos A, Langer GA, Csik A, Cserhati C, Kis-Varga M, Daroczi L, et al. Nanoscale investigations of shift of individual interfaces in temperature induced processes of Ni-Si system by secondary neutral mass spectrometry. Appl Phys Lett 2010;97:233103. doi:10.1063/1.3524491.
[99] Molnár G, Erdélyi G, Langer GA, Beke DL, Csik A, Katona GL, et al. Evolution of concentration profiles in Pd-Cu systems studied by SNMS technique. Vacuum 2013;98:70–4. doi:10.1016/j.vacuum.2013.04.015.
[100] Tynkova A, Katona GL, Langer GA, Sidorenko SI, Voloshko SV, Beke DL. Formation of CuxAu1-x phases by cold homogenization of Au/Cu nanocrystalline thin films. Beilstein J Nanotechnol 2014;5:1491–500. doi:10.3762/bjnano.5.162.
[101] Oechsner H, Getto R, Kopnarski M. Quantitative characterization of solid state phases by secondary neutral mass spectrometry. J Appl Phys 2009;105:63523. doi:10.1063/1.3099595.
[102] Müller K, Oechsner H. Quantitative Secondary Neutral Mass Spectrometry Analysis of Alloys and Oxide-Metal-Interfaces. Microchim Acta 1983;10:51. doi:10.1007/978-3-7091-3943-1_4.
[103] Glodán G, Cserháti C, Beke DL. Temperature-dependent formation and shrinkage of hollow shells in hemispherical Ag/Pd nanoparticles. Philos Mag 2012;92:3806–12. doi:10.1080/14786435.2012.687841.
[104] den Broeder FJA, Nakahara S. Diffusion induced grain boundary migration and recrystallization in the CuNi system. Scr Metall 1983;17:399–404. doi:10.1016/0036-9748(83)90181-3.
[105] Rabkin E, Klinger LM, Izyumova T, Semenov VN. Diffusion induced grain boundary porosity in NiAl. Scr Mater 2000;42:1031–7.
[106] Garbovitskaya T, Geguzin Y, Paritskaya L. Mutual diffusion in thin-films of face plane tape with overlappiing (Ag-Au system). Fiz Met I Met (in Russ 1979;47:1244–51.
[107] Garbovitskaya T, Geguzin Y, Paritskaya L. Study of Frenkel and Kirkendall effects in thin polycsytalline films (Cu-Ni system). Fiz Met I Met (in Russ 1976;42:1214–20.
[108] Geguzin Y. On the ffect of pressure on the interdiffusion in metals in relation to the formation of diffusional porosity. Dokl Akad Nauk SSSR (in Russ 1956;5:839–43.
[109] d'Heurle FM, Gas P. Kinetics of formation of silicides: A review. J Mater Res 1986;1:205–21. doi:10.1557/JMR.1986.0205.
[110] Gusak A. Duiffusion-Controlled Solid State Reactions. Weiheim, Gemany: WILEY-VCH Verlag GmbH&Co; 2010.
[111] Zaporozhets TV, Storozhuk NV, Gusak AM. Competition of Voiding and

Kirkendall Shift during Compound Growth in Reactive Diffusion–Alternative Models. Metallofiz I Noveishie Tekhnologii 2016;38:1279–92. doi:10.15407/mfint.38.10.1279.
[112] Beke DL, Erdélyi Z, Katona GL. Anomalous Kinetics and Regimes of Growth of Intermetallic Phases during Solid State Reactions in Nanosystems. Diffus Found 2014;2:107–39. doi:10.4028/www.scientific.net/DF.2.107.
[113] Ogunseitan O. Public health and environmental benefits of adopting lead-free solders. Jom 2007;59:12–7. doi:10.1007/s11837-007-0082-8.
[114] Tu KN, Zeng K. Tin-lead (SnPb) solder reaction in flip chip technology. Mater Sci Eng R Reports 2001;34:1–58. doi:10.1016/S0927-796X(01)00029-8.
[115] Laurila T, Vuorinen V, Kivilahti JK. Interfacial reactions between lead-free solders and common base materials. Mater Sci Eng R Reports 2005;49:1–60. doi:10.1016/j.mser.2005.03.001.
[116] Ho CE, Yang SC, Kao CR. Interfacial reaction issues for lead-free electronic solders. Lead-Free Electron Solder A Spec Issue J Mater Sci Mater Electron 2007:155–74. doi:10.1007/978-0-387-48433-4_10.
[117] Wierzbicka-Miernik A, Wojewoda-Budka J, Litynska-Dobrzynska L, Kodentsov A, Zieba P. Morphology and chemical composition of Cu/Sn/Cu and Cu(5 at-%Ni)/Sn/Cu(5 at-%Ni) interconnections. Sci Technol Weld Join 2012;17:32–5. doi:10.1179/1362171811Y.0000000075.
[118] Lau J. Flip Chip Technology. 1st ed. New York: McGraw Hill; 1996.
[119] Poate JM, Tu KN, Mayer JW. Thin Films Interdiffusion and Reactions. New York: John Wiley & Sons; 1978.
[120] Farrell H, Gilmer G. Grain boundary diffusion and growth of intermetallic layers: Nb3Sn. J Appl Phys 1974;45:4025–9. doi:org/10.1063/1.1663907.
[121] Corcoran YL, King AH, de Lanerolle N, Kim B. Grain boundary diffusion and growth of titanium silicide layers on silicon. J Electron Mater 1990;19:1177–83. doi:10.1007/BF02673330.
[122] Zaka H, Shenouda SS, Fouad SS, Medhat M, Katona GL, Csik A, et al. Formation of Cu6Sn5 phase by cold homogenization in nanocrystalline Cu-Sn bilayers at room temperature. Microelectron Reliab 2016;56:85–92. doi:10.1016/j.microrel.2015.10.018.
[123] Samy N, Shenouda SS, Fadel M, Talaat H, Katona GL, Langer GA, et al. Investigation of solid-state reaction in Ag/Sn nanostructured thin films at room temperature. Philos Mag 2015;95:2990–3001. doi:10.1080/14786435.2015.1083135.
[124] Xu H, Vuorinen V, Dong H, Paulasto-Kröckel M. Solid-state reaction of electroplated thin film Au/Sn couple at low temperatures. J Alloys Compd 2015;619:325–31. doi:10.1016/j.jallcom.2014.08.245.
[125] Paritskaya LN, Bogdanov VV, Kaganovskii Y. Size-dependent kinetics of reactive diffusion in nano-grained Ag-Sn thin films. Mater Lett 2017;193:292–4. doi:10.1016/j.matlet.2017.01.117.
[126] Tu KN, Thompson RD. Kinetics of interfacial reaction in bimetallic CuSn thin films. Acta Metall 1982;30:947–52. doi:10.1016/0001-6160(82)90201-2.
[127] Bhedwar HC, Ray KK, Kulkarni SD, Balasubramanlan V. Kirkendall Effect Studies in Copper-Tin Diffusion Couples. Scr Met 1972;6:919–22. doi:org/10.1016/0036-9748(72)90145-7.
[128] Onishi M, Fujibuchi H. Reaction-Diffusion in the Cu-Sn System. J Chem Inf Model 1975;16:539–47. doi:10.1017/CBO9781107415324.004.

[129] Kaganovskii Y, Paritskaya LN, Bogdanov VV. Lateral diffusion spreading of two competitive intermetallic phases over free surface. Defect Diffus Forum 2008;277:9–20. doi:10.4028/3-908451-55-8.9.
[130] Gleiter H. Nanocrystalline materials. Prog Mater Sci 1989;33:223–315. doi:10.1016/0079-6425(89)90001-7.
[131] Ciccariello JC, Poize S, Gas P. Lattice and grain boundary self-diffusion in Ni2Si: Comparison with thin-film formation. J Appl Phys 1990;67:3315–22. doi:10.1063/1.345367.
[132] Lis A, Park MS, Arroyave R, Leinenbach C. Early stage growth characteristics of Ag3Sn intermetallic compounds during solid-solid and solid-liquid reactions in the Ag-Sn interlayer system: Experiments and simulations. J Alloys Compd 2014;617:763–73. doi:10.1016/j.jallcom.2014.08.082.
[133] Kaganovskii Y, Paritskaya LN, Bogdanov VV. Grain boundary induced lateral propagation of intermetallic phases in nano-grained Cu-Sn thin film couples. J Nano Res 2009;7:59–68. doi:10.4028/www.scientific.net/JNanoR.7.59.
[134] Huang W, Zhang L, Gao Y, Jin H. Effect of a thin W, Pt, Mo, and Zr interlayer on the thermal stability and electrical characteristics of NiSi. Microelectron Eng 2007;84:678–83. doi:10.1016/j.mee.2006.11.006.
[135] Qu XP, Jiang YL, Ru GP, Lu F, Li BZ, Detavernier C, et al. Thermal stability, phase and interface uniformity of Ni-silicide formed by Ni-Si solid-state reaction. Thin Solid Films 2004;462–463:146–50. doi:10.1016/j.tsf.2004.05.091.
[136] Gregoire M, Beneyton R, DelMedico S, Zoll S. Gate shadowing effect on Ni(Pt)Si abnormal diffusion for sub-45 nm technologies. Microelectron Eng 2011;88:548–52. doi:10.1016/j.mee.2010.07.017.
[137] O'Neill A, Agaiby R, Olsen S, Yang Y, Hellstrom PE, Ostling M, et al. Reduced self-heating by strained silicon substrate engineering. Appl Surf Sci 2008;254:6182–5. doi:10.1016/j.apsusc.2008.02.172.
[138] Zhang Z, Zhang SL, Yang B, Zhu Y, Rossnagel SM, Gaudet S, et al. Morphological stability and specific resistivity of sub-10 nm silicide films of Ni1-x Ptx on Si substrate. Appl Phys Lett 2010;96:9–11. doi:10.1063/1.3323097.
[139] De Keyser K, Van Bockstael C, Van Meirhaeghe RL, Detavernier C, Verleysen E, Bender H, et al. Phase formation and thermal stability of ultrathin nickel-silicides on Si(100). Appl Phys Lett 2010;96:4–6. doi:10.1063/1.3384997.
[140] Zhang Z, Yang B, Zhu Y, Gaudet S, Rossnagel S, Kellock AJ, et al. Exploitation of a self-limiting process for reproducible formation of ultrathin Ni1-x Ptx silicide films. Appl Phys Lett 2010;97:1–4. doi:10.1063/1.3529459.
[141] Putero M, Ehouarne L, Ziegler E, Mangelinck D. First silicide formed by reaction of Ni(13%Pt) films with Si(1 0 0): Nature and kinetics by in-situ X-ray reflectivity and diffraction. Scr Mater 2010;63:24–7. doi:10.1016/j.scriptamat.2010.02.040.
[142] Gas P, d'Heurle FM. Formation of silicide thin films by solid state reaction. Appl Surf Sci 1993;73:153–61. doi:10.1016/0169-4332(93)90160-D.
[143] Barge T, Gas P, d'Heurle FM. Analysis of the diffusion controlled growth of cobalt silicides in bulk and thin film couples. J Mater Res 1995;10:1134–45. doi:10.1557/JMR.1995.1134.
[144] Hummada K, Magnelinck D, Portavoce A. Kinetic of formation of Ni and Pd silicide: determination of interfacial mobility and interdiffusion coefficient by in-situ tehcniques. Solid State Phenom 2011;172–74:640–5. doi:10.4028/www.scientific.net/SSP.172-174.640.

[145] Nemouchi F, Mangelinck D, Bergman C, Gas P, Smith U. Differential scanning calorimetry analysis of the linear parabolic growth of nanometric Ni silicide thin films on a Si substrate. Appl Phys Lett 2005;86:41903. doi:10.1063/1.1852727.
[146] Piramanayagam S, Chong T, editors. Developments in Data Storage: Materials Perspective. New York: John Wiley & Sons; 2011. doi:10.1002/9781118096833.
[147] Lyubina L, Rellinghaus B, Gutfleisch O, Albrecht M. Structure and magnetic properties of L10-ordered Fe–Pt alloys and nanoparticles. In: Buschow K, editor. Handb. Magn. Mater. Vol. 19. 1st ed., Amsterdam: North Holland; 2011, p. 291–395.
[148] McCallum AT, Krone P, Springer F, Brombacher C, Albrecht M, Dobisz E, et al. L10FePt based exchange coupled composite bit patterned films. Appl Phys Lett 2011;98:2011–4. doi:10.1063/1.3599573.
[149] Brombacher C, Grobis M, Lee J, Fidler J, Eriksson T, Werner T, et al. L1 $_0$ FePtCu bit patterned media. Nanotechnology 2012;23:25301. doi:10.1088/0957-4484/23/2/025301.
[150] Makarov D, Lee J, Brombacher C, Schubert C, Fuger M, Suess D, et al. Perpendicular FePt-based exchange-coupled composite media. Appl Phys Lett 2010;96:1–4. doi:10.1063/1.3309417.
[151] Yan ML, Powers N, Sellmyer DJ. Highly oriented nonepitaxially grown L10 FePt films. J Appl Phys 2003;93:8292–4. doi:10.1063/1.1556257.
[152] Farrow RFC, Weller D, Marks RF, Toney MF, Cebollada a., Harp GR. Control of the axis of chemical ordering and magnetic anisotropy in epitaxial FePt films. J Appl Phys 1996;79:5967. doi:10.1063/1.362122.
[153] Platt CL, Wierman KW, Svedberg EB, Van De Veerdonk R, Howard JK, Roy AG, et al. L-10 ordering and microstructure of FePt thin films with Cu, Ag, Au additive. J Appl Phys 2002;92:6104–9. doi:10.1063/1.1516870.
[154] Chen C, Kitakami O, Okamoto S, Shimada Y. Ordering and orientation of CoPt/SiO2 granular films with additive Ag. Appl Phys Lett 2000;76:3218. doi:10.1063/1.126634.
[155] Tokuoka Y, Seto Y, Kato T, Iwata S. Effect of Ag addition to L10 FePt and L10 FePd films grown by molecular beam epitaxy. J Appl Phys 2014;115:1–4. doi:10.1063/1.4864251.
[156] Kitakami O, Shimada Y, Oikawa K, Daimon H, Fukamichi K. Low-temperature ordering of L10-CoPt thin films promoted by Sn, Pb, Sb, and Bi additives. Appl Phys Lett 2001;78:1104–6. doi:10.1063/1.1346628.
[157] You CY, Takahashi YK, Hono K. Particulate structure of FePt thin films enhanced by Au and Ag alloying. J Appl Phys 2006;100:1–4. doi:10.1063/1.2335600.
[158] Wei DH, Yuan FT, Chang HW, You KL, Liou Y, Yao YD, et al. Magnetization reversal and microstructure of FePt-Ag (001) particulate thin films for perpendicular magnetic recording media. J Appl Phys 2008;103:1–4. doi:10.1063/1.2829022.
[159] Zhang L, Takahashi YK, Hono K, Stipe BC, Juang JY, Grobis M. L10-ordered FePtAg-C granular thin film for thermally assisted magnetic recording media (invited). J Appl Phys 2011;109:23–6. doi:10.1063/1.3536794.
[160] Feng C, Zhan Q, Li B, Teng J, Li M, Jiang Y, et al. Magnetic properties and microstructure of FePt/Au multilayers with high perpendicular magnetocrystalline anisotropy. Appl Phys Lett 2008;93:10–3. doi:10.1063/1.3001801.

[161] Feng C, Li B-H, Liu Y, Teng J, Li M-H, Jiang Y, et al. Improvement of magnetic property of L1[sub 0]-FePt film by FePt/Au multilayer structure. J Appl Phys 2008;103:23916. doi:10.1063/1.2828148.
[162] Yu YS, Li H-B, Li WL, Liu M, Zhang Y-M, Fei WD. Structure and magnetic properties of magnetron-sputtered [(Fe/Pt/Fe)/Au]n multilayer films. J Magn Magn Mater 2010;322:1770–4. doi:10.1016/j.jmmm.2009.12.027.
[163] Brombacher C, Schletter H, Daniel M, Matthes P, Jöhrmann N, Maret M, et al. FePtCu alloy thin films: Morphology, L10 chemical ordering, and perpendicular magnetic anisotropy. J Appl Phys 2012;112:0–8. doi:10.1063/1.4757038.
[164] Kai T, Maeda T, Kikitsu A, Akiyama J, Nagase T, Kishi T. Magnetic and electronic structures of FePtCu ternary ordered alloy. J Appl Phys 2004;95:609–12. doi:10.1063/1.1635978.
[165] Maeda T, Kai T, Kikitsu A, Nagase T, Akiyama JI. Reduction of ordering temperature of an FePt-ordered alloy by addition of Cu. Appl Phys Lett 2002;80:2147–9. doi:10.1063/1.1463213.
[166] Maret M, Brombacher C, Matthes P, Makarov D, Boudet N, Albrecht M. Anomalous x-ray diffraction measurements of long-range order in (001)-textured L10 FePtCu thin films. Phys Rev B 2012;86:24204. doi:10.1103/PhysRevB.86.024204.
[167] Gilbert DA, Wang LW, Klemmer TJ, Thiele JU, Lai CH, Liu K. Tuning magnetic anisotropy in (001) oriented L10 (Fe 1-xCux)55Pt45 films. Appl Phys Lett 2013;102:1–5. doi:10.1063/1.4799651.
[168] Hsu YN, Jeong S, Laughlin DE, Lambeth DN. Effects of Ag underlayers on the microstructure and magnetic properties of epitaxial FePt thin films. J Appl Phys 2001;89:7068–70. doi:10.1063/1.1360683.
[169] Katona GL, Vladymyrskyi IA, Makogon IM, Sidorenko SI, Kristály F, Daróczi L, et al. Grain boundary diffusion induced reaction layer formation in Fe/Pt thin films. Appl Phys A Mater Sci Process 2014;115:203–11. doi:10.1007/s00339-013-7949-z.
[170] Katona GL, Safonova NY, Ganss F, Mitin D, Vladymyrskyi IA, Sidorenko SI, et al. Diffusion and solid state reactions in Fe/Ag/Pt and FePt/Ag thin-film systems. J Phys D Appl Phys 2015;48:165001 (9p). doi:10.1088/0022-3727/48/17/175001.
[171] Koch CC. The synthesis and structure of nanocrystalline materials produced by mechanical attrition: A review. Nanostructured Mater 1993;2:109–29. doi:10.1016/0965-9773(93)90016-5.
[172] Suryanarayana C. Nanocrystallline materials. Int Mater Rev 1995;40:41–64. doi:doi.org/10.1179/imr.1995.40.2.41.
[173] Suryanarayana C, Norton M. Chapter 4 Mechanical alloying. Pergamon Mater Ser 1999;2:49–85. doi:10.1016/S1470-1804(99)80050-9.
[174] Upadhya K, editor. Plasma synthesis and processing of materials. Warrendale, PA, TMS; 1993.
[175] Suryanarayana C. Mechanical alloying and milling. Prog Mater Sci 2001;46:1–184. doi:10.1016/S0079-6425(99)00010-9.
[176] Paritskaya LN. Diffusion processes in dispersed systems (review). Sov Powder Metall Met Ceram 1990;29:893–904. doi:10.1007/BF00794024.
[177] Novikov V, Trusov L, Lopovok V, Geileshvili TP. Mechanism of low temperature diffusion activated by boundary migration. Fiz Tverd Tela (in Rusiian) 1983;25:3696–9.
[178] Bogdanov VV, Lisenko VV, Paritskaya LN. Diffusion-induced decomposition of

dispersed layered structures in the process of low-temperature homogenization. Phys Met Metallogr 1990;69:115–21.
[179] Geguzin Y, Kaganovskiy Y. Diffusion Processes on a Crystal Surface. Moscow: Energoatomizdat; 1984.
[180] Paritskaya L, Bogdanov V. The Effect of Dispersion-Hardening Dopants on Low Temperature Homogenization in Dispersed Powder Systems. Sci Sinter 1994;26:259–69.
[181] Chongmo L, Hillert M. A metallographic study of diffusion-induced grain boundary migration in the Fe-Zn system. Acta Metall 1981;29:1949–60. doi:10.1016/0001-6160(81)90032-8.
[182] Yamamoto Y, Uemura S, Yoshida K, Kajihara M. Kinetic features of diffusion induced recrystallization in the Cu(Ni) system at 873 K. Mater Sci Eng A 2002;333:262–9. doi:10.1016/S0921-5093(01)01847-0.
[183] Inomata S, O M, Kajihara M. Diffusion-induced recrystallization in the Cu(Pd) system at complete solid-solution temperatures. J Mater Sci 2011;46:2410–21. doi:10.1007/s10853-010-5087-y.
[184] Takenaka T, Kajihara M. Fast penetration of Sn into Ag by diffusion induced recrystallization. Mater Trans 2006;47:822–8. doi:10.2320/matertrans.47.822.
[185] Chen F Sen, King AH. Misorientation effects upon diffusion induced grain boundary migration in the copper-zinc system. Acta Metall 1988;36:2827–39. doi:10.1016/0001-6160(88)90129-0.
[186] Sivaiah B, Gupta SP. Diffusion induced grain boundary migration in the Cu – Zn system. Mater Charact 2008;59:1141–51. doi:10.1016/j.matchar.2007.08.031.
[187] Goukon N, Ikeda T, Kajihara M. Growth behavior of fine grains formed by diffusion induced recrystallization in the Cu(Zn) system. Acta Mater 2000;48:2959–68. doi:10.1016/S1359-6454(00)00096-3.
[188] Kajihara M, Gust W. Chemical composition of regions alloyed by DIGM or DIR. Acta Metall Mater 1991;39:2565–74. doi:10.1016/0956-7151(91)90071-8.

Contact: Prof. Dr. Dezső L. Beke

Department of Solid State Physics
University of Debrecen
Bem ter 18/b
4026 Debrecen, Hungary
tel.: +3630228571
e-mail: dbeke@science.unideb.hu

Education:

Secondary school: 1960-64, Debrecen, University: 1964-69, at L. Kossuth University, Debrecen; Master Degree: 1969 Physicist

Scientific degrees:

1975: Doctor. Univ. on Physics (L. Kossuth Univ. Debrecen). 1981: Candidate on Physics (degree of the Hungarian Academy of Sciences). 1992: DSC

Positions:

1969-75 Young Assistant Professor,; 1975-83 Assistant Professor; 1983-93 Associate Professor; 1993-2015 Full Professor (all at Department of Solid State Physics, L. Kossuth University Debrecen): 1987-90 Vice Dean of Faculty of Natural Sciences; 1990-2008 Head of Department of Solid State Physics; 1998-2000 Vice Rector for Research,; 2000-2010 Director of PhD School on Physics, University of Debrecen. 2000-2015 Leader of "Solid State Physics and Materials Science" in the PhD school. From 15.09.2015 professor emeritus

Teaching Activities

Basic lectures and seminars on solid state physics and materials science. Special courses on "Point defects and diffusion", and "Nanostructured materials". Leader of the PhD. subproject on "Solid State Physics and Materials Science" in the PhD School "Physics" at University, Debrecen, 1970- at present: supervisor of more than 50 diploma works and of 24 PhD theses.

Research activities

Research field: solid state physics, materials science. Special fields: diffusion in solids; grain-boundary segregation and diffusion; stresses and diffusion; solid state reactions in nano-materials, shape memory alloys, magnetic and acoustic noises

Publications:

- editor of five conference proceedings and reviews (e.g. "Nanodiffusion", J of metastable and nanocrystalline materials, Vol. 19 (2014), "Diffusion and Stresses" Defect and Diffusion Forum, vol. 129-130 (1996)); author of 18 chapters in books (three of them in Landolt-Börnstein, New Series, Vol. III/33a-b)

- volume editor of Landolt-Börnstein, New Series, Vol. III/33a and Vol. III/33b as well as editor of „Nanodiffusion" and „Materials Science of Nanostructures" books.

Conferences, memberships:

- organiser of nine international conferences, invited lecturer and member of the scientific boards of numerous conferences on diffusion, nanocrystalline materials and shape memory alloys.

- editor of the International Journal “Defect and Diffusion Forum”

- member of the Editorial Board of the “Materials Science Forum” “Materials Transactions”, “Diffusion fundamentals.com” and “Optoelectronics and Advanced Materials-Rapid Communications”

- Doctor honoris causa of National University of Uzgorod, Ukraine, 2005

- Doctor honris causa of University of Miskolc, Hungary 2017

Functions:

-1970- member of the R. Eötvös Physical Society, Hungary, 1973- individual member of the European Physical Society,

Secretary (1976-80) and chairman (1989-92) of the Metal Physics Group of the R. Eötvös Phys. Soc., Vice president (1995-98) and vice secretary (1992-95) of the Hungarian Physical Society, 1996-2002 secretary and 2003-2008 chairman of the “Committee of Solid State Physics” of the Hungarian Academy of Sciences, 2008-2014 chairman of the “Engineering and Sciences Panel” of the Hungarian Scientific Research Found, 2014- chairman of the Jury for international applications of the Hungarian Scientific Research Found, Hungarian delegate in the EU Domain Committee Materials, Physics and Nanosciences Cost Committee on “Physics and Nanomaterials” 2012-2015

Scientific publications and citations: more than 380 papers, 1900 independent citations, h-factor 29.